creative commons
COMMONS DEED

저작자표시-비영리-변경금지 2.0 대한민국

이용자는 아래의 조건을 따르는 경우에 한하여 자유롭게

- 이 저작물을 복제, 배포, 전송, 전시, 공연 및 방송할 수 있습니다.

다음과 같은 조건을 따라야 합니다:

저작자표시. 귀하는 원저작자를 표시하여야 합니다.

비영리. 귀하는 이 저작물을 영리 목적으로 이용할 수 없습니다.

변경금지. 귀하는 이 저작물을 개작, 변형 또는 가공할 수 없습니다.

- 귀하는, 이 저작물의 재이용이나 배포의 경우, 이 저작물에 적용된 이용허락조건을 명확하게 나타내어야 합니다.
- 저작권자로부터 별도의 허가를 받으면 이러한 조건들은 적용되지 않습니다.

저작권법에 따른 이용자의 권리는 위의 내용에 의하여 영향을 받지 않습니다.

이것은 이용허락규약(Legal Code)을 이해하기 쉽게 요약한 것입니다.

Disclaimer

dCollection

공학박사 학위논문

Development of spleen targeting H_2S donating liposome for therapeutic immunomodulation of inflammatory bowel disease

대장염의 치료적 면역조절을 위한 비장 표적 황화수소 공여 리포좀의 개발

2023년 2월

서울대학교 융합과학기술대학원

응용바이오공학과

오 치 우

Development of spleen targeting H_2S donating liposome for therapeutic immunomodulation of inflammatory bowel disease

지도 교수 임 형 준

이 논문을 공학박사 학위논문으로 제출함
2023년 1월

서울대학교 융합과학기술대학원
응용바이오공학과
오 치 우

오치우의 공학박사 학위논문을 인준함

2022년 12월

위 원 장 이 윤 상 (인)

부위원장 임 형 준 (인)

위 원 이 재 규 (인)

위 원 최 홍 윤 (인)

위 원 정 경 오 (인)

Abstract

Development of spleen targeting H_2S donating liposome for therapeutic immunomodulation of inflammatory bowel disease

Chiwoo Oh

Department of Applied Bioengineering

Graduate School of Convergence Science & Technology

Seoul National University

Nanoparticles systemically administrated are mostly ingested by immune cells of mononuclear phagocyte system (MPS) related organs. Among MPS related organs, the spleen filters the pathogens and is involved in systemic immunity. Thus, there have been studies to develop spleen targeting nanoparticles for systemic immune modulation of tumor or inflammatory diseases. Inflammatory bowel disease (IBD) is characterized by chronic inflammation in the gastrointestinal tract and is considered incurable despite many treatment options including immunomodulators. Hydrogen sulfide (H_2S), one of gasotransmitters, involved in various anti-inflammatory related processes, and have shown therapeutic potential in various

inflammatory disease models including IBD. However, systemically injected hydrogen sulfide donors have high reactivity and are difficult to deliver specifically.

Herein, we developed H_2S donor delivering liposome for spleen targeting (ST-H_2S lipo) and studied its immune modulation and therapeutic potential in dextran sulfate sodium (DSS) induced colitis model. In part 1 (chapter 2), we compared liposomes with different polyethylene glycol (PEG) types and ratios to find the liposome which has high loading efficiency, stability, and the ability of spleen targeting. In in vitro studies, H_2S lipo showed significantly higher H_2S release ability and immune modulatory effect than those of unloaded H_2S donor. In in vivo studies, ST-H_2S lipos demonstrated substantial splenic accumulation and potent immune modulatory effects. In part 2 (chapter 3), ST-H_2S lipo and conventional long-circulating liposomes loaded with H_2S donors (LC-H_2S lipo) could reduce the inflammation degree of colitis model whereas unloaded H_2S donors could not. Moreover, ST-H_2S lipo showed significantly higher therapeutic effects than LC-H_2S lipo, which can be attributed to the systemic immunomodulatory effect of ST-H_2S lipo. Our results illustrate that spleen targeting H_2S lipo may be a new treatment option for IBD.

Keyword: Nanoparticle, Spleen targeting, H_2S, IBD, Anti-inflammation, Systemic immune modulation
Student Number: 2018-21910

Table of Contents

List of Figures

List of Tables

List of Abbreviation

Full name	*Abbreviations*
%ID/g	Percentage of the injected dose per tissue weight
(p-SCN-Bn)-NOTA	2-(p-Isothiocyanatobenzyl)-1,4,7-triazacyclononane-N,N',N'-triacetic acid trihydrochloride
^{64}Cu-H_2S lipo	^{64}Cu radiolabeled H_2S lipo
Ag	Antigen
$AgNO_3$	Silver nitrate
AgS	Silver sulfide
AHR	Air hyperresponsiveness
AmB	Amphotericin B
ANOVA	One-way analysis of variance
APCs	Antigen presenting cells
APCs	Antigen presenting cells
APOA1	Apolipoprotein A1
AUC	Area under curve
CBS	Cystathionine-beta-synthase
CNP	Chitosan nanoparticle

COVID-19	Coronavirus disease 2019
COX-2	Cyclooxygenase-2
CRP	C-reactive protein
CTH	Cystathionine-gamma-lyase
CTL	Cytotoxic T lymphocyte
DC	Dendritic cells
DC-SIGN	Dendritic cell-specific intercellular adhesion molecule-3-grabbing non-integrin
DDAB	Dimethyldioctadecylammonium
DIPEA	N,N-Diisopropylethylamine
DIPEA	N,N-Diisopropylethylamine
DiR	1,1’-dioctadecyl-3,3,3',3’-tetramethyl-indotricarbocyanine iodide
DLS	Dynamic scattering light
DMG-PEG	PEGylation of myristoyl diglyceride
DMPC	1,2-dimyristoyl-sn-glycero-3-phosphocholine
DODAP	1,2-dioleoyl-3-dimethylammonium-propane
DOPE	Dioleoylphosphatidylethanolamine

DOTAP	1,2-Dioleoyl-3-trimethylammoniumpropane
DSPC	Distearoyl phosphatidylcholine
DSPE-PEG2k	1,2-Distearoyl-sn-glycero-3-phosphoethanolamine (methoxy(polyethylene glycol)-2000)
DSPE-PEG2K-NH_2	1,2-Distearoyl-sn-glycero-3-phosphoethanolamineN-[amino(polyethylene glycol)-2000]
DSS	Dextran sulfate sodium
EAE	Encephalomyelitis
FITC	Fluorescein 5(6)-isothiocyanate
FOXP3	Forehead box P3
H_2S	Hydrogen sulfide
H_2S lipo	H_2S donor, GYY4137, loaded liposome
HEPC	Hydrogenated egg phosphatidylcholine
HMOXs	Ham oxygenases
IBD	Inflammatory bowel disease
IFN-γ	Interferon-γ

IL	Interleukin
IL-10	Interleukin-10
iNOS	Inducible nitric oxide synthase
JAK	Janus kinase
LC-H_2S lipo	Conventional long-circulating liposomes with H_2S donors
LNPs	Lipid nanoparticles
MHPC	1-myristoyl-2-hydroxy-sn-glycero-phosphocholine
MI	Myocardial infarct
MPS	Mononuclear phagocyte system
MPST	3-mcaptopyruvate sulfurtransferase
mTOR	Rapamycin
MTT	3-[4,5-dimethylthiazol-2-yl]-2,5-diphenyltetrazolium bromide reagent
MZ	Marginal zone
NF-κB	Nuclear factor-κB
NOSs	NO synthases
NPSCs	Nanoparticle-stabilized nanocapsules
NSAIDs	Nonsteroidal anti-inflammatory drugs

O.D	Optical density
PBS	Phosphate buffered saline
pDNA	Plasmid DNA
PEG	Polyethlyene glycol
PEG-bl-PPS	poly(ethylene glycol)-bl-poly(propylene sulfide)
PET	Positron emission tomography
PFA	Paraformaldehyde
PHPC	1-palmitoyl-2-hydroxy-sn-glycero-3-phosphocholine
PLA	Poly(DL-lactide)
PLG-H	Poly(DL-lactide-co-glycolide) with high molecular weights
PLGA	Poly(lactide-coglycolide)
POPC	1-palmitoyl-2-oleoyl-sn-glycero-3-phosphocholine
PPARγ	Peroxisome proliferator-activated receptor gamma
PS	Phosphatidylserine
RBC	Red blood cell
RNA-LPX	RNA-lipoplex
ROI	Region of interest

ROS	Reactive oxygen species
RP	Red pulp
S6K1	S6 kinase-1
SCNPs	4-sulfated N-acetyl galactosamine conjugated chitosan nanoparticles
siRNA	Short interfering RNA
sLNPs	Solid lipid nanoparticles
SORT	Selective organ targeting
SPF	Specific pathogen free
ST-H_2S lipo	H_2S donor delivering liposome for spleen targeting
SUV	Standard uptake value
SUV	Standard uptake value
TEM	Transmission microscopy
TET	Ten-eleven translocation protein
TLC	Thin layer chromatography
TNF	Tumor necrosis factor
TPP	Sodium tripolyphosphate
T_{reg}	Regulatory T cells
UC	Ulcerative colitis
WP	White pulp
αGC	α-galactosylceramide

Chapter 1.

Introduction

1.1 Inflammatory bowel diseases (IBD)

IBD, which consists of ulcerative colitis and Crohn's disease, is characterized by a chronic incurable inflammatory process in the gastrointestinal tract with an uncertain pathophysiology (1, 2). IBD is one of the growing global health problems with 6.8 million cases in 2017 globally, and its prevalence rate is increasing from 79.5 among 100,000 in 1990 to 84.3 among 100,000 in 2017 (**Figure 1.1A**) (3). Although the mechanism of IBD has not been clearly identified, it is reported that abnormalities in immune regulation, genetic susceptibility, changes in the intestinal microflora, and environmental factors are associated with its pathophysiology (4, 5). Therapeutic options for IBD include conventional anti-inflammatory agents such as 5-aminosalicylate, steroids, newer immunomodulatory agents such as tumor necrosis factor (TNF)-alpha antagonist, anti-interleukin (IL) 23 and IL12 agents, and Janus kinase (JAK) inhibitors (**Figure 1.1B**) (6). These newer immunomodulatory agents have shown an efficacy in patients who did not respond to the conventional agents; however, the response rates have widely varied from 16~70% and 10~15% in patients who eventually underwent a colectomy due to refractory disease (**Table 1**) (7). Furthermore, these immunomodulatory agents can

increase the probability of opportunistic infections due to immune suppression (6, 8-10).

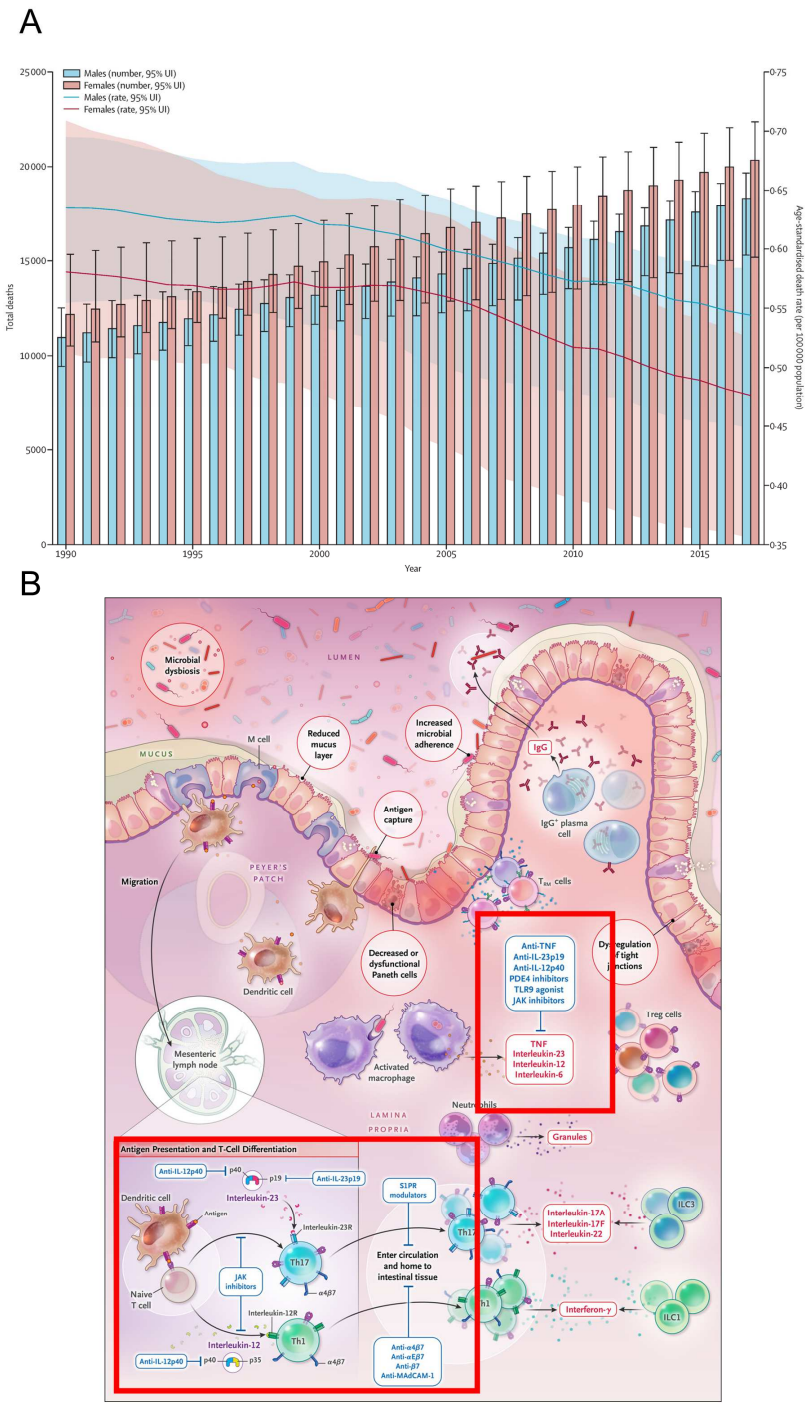

Figure 1.1 Inflammatory Bowel Disease (IBD) A. Increase of the IBD related deaths. From reference (3). B. Pathophysiology of IBD. From reference (5).

Drugs	Target	Efficacy(%)
Infliximab	TNF-α	69.4
		45.5
Adalimumab	TNF-α	18.5
		16.5
		17.3
Golimumab	TNF-α	51
Vedolizumab	Adhesion-molecules	47.1
		44.8
Etrolizumab	Adhesion-molecules	21
Tofacitinib	JAK	78

Table 1 Varied response rate of newer immunomodulators.

From reference (7)

1.2 Hydrogen sulfide (H_2S)

Hydrogen sulfide (H_2S) is one of the endogenous gasotransmitters that involves various physiological processes (11, 12). Because H_2S has a crucial role in the homeostasis of multiple physiological functions, abnormally decreased or increased H_2S levels are associated with multiple diseases including hypertension (13), atherosclerosis (14), diabetes (15), and gastrointestinal disorders (16) (**Figure 1.2**). In particular, H_2S has pronounced anti-inflammatory and cytoprotective effects in the gastrointestinal tract; therefore, H_2S donors are considered promising treatment agents in various gastrointestinal diseases. Additionally, several studies have demonstrated that a H_2S donor that escalates the H_2S level in tissues elicited notable therapeutic effects in a gastritis or colitis model (17-19). However, in previous studies, H_2S donors were administered directly as an experiment to demonstrate proof-of-concept for H_2S treatment, and studies on the development drug delivery systems for H_2S donors are lacking. An adequate drug delivery system for a H_2S donor is needed because direct administration has the following limitations: 1) it may not be suitable for clinical translation because local administration needs an expansive and cumbersome procedure such as endoscopy; 2) H_2S donors are not stable after they are dissolved in solution, and 3) a systemic

immunomodulation effect is less likely when it is administered locally (**Table 2**).

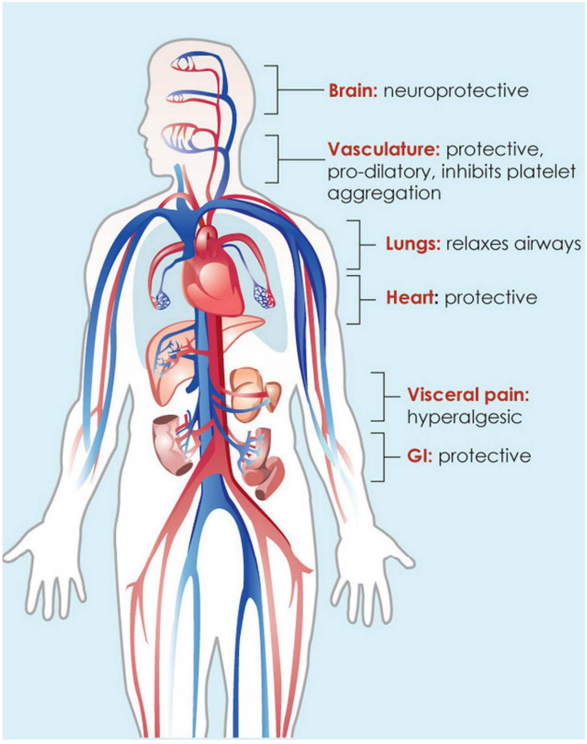

Figure 1.2 Hydrogen sulfide (H_2S) involving various physiological processes. From reference (11)

Disease model	Administration	Drugs	Inflammatory processes	References
Gastric ulcer	Intragastric	ATB-429	Not mentioned	(19)
Colitis	Intracolonic	Diallyl disulfide	Not mentioned	(17)
Colitis	Intracolonic	NaHS or Lawesson's reagent	COX-2	(18)
Acute joint inflammation	Intraperitoneal	GYY4137	IL-1β/6/8, TNF-α	(20)
Asthma	Intraperitoneal	NaHS	IL-5/13	(21)
Myocardial infarction	Intraperitoneal	NaHS	M2 macrophage	(22)
Obesity-induced kidney injury	Intraperitoneal	NaHS	IL-6/10, MCP-1	(23)
Acute lung injury	Intraperitoneal	NaHS	IL-6/8/10	(24)
Diaphragm dysfunction	Intraperitoneal	NaHS	NF-κB, ROS	(25)

Table 2 Treatment studies using H_2S donors

1.3 Spleen targeting nanoparticles

The majority of nanoparticles that are systematically injected are captured by immune cells including macrophages, dendritic cells, and lymphocytes (26-28). Therefore, nanoparticles are considered highly suitable drug delivery vehicles for immunomodulation in various types of diseases. In particular, there have been studies utilizing spleen-targeting nanoparticles for immunomodulation (29) because the spleen is the largest lymphatic organ and modulates immune responses locally and systemically in the body (**Table 3**) (30). For example, Zhai et al. developed a spleen targeting cancer nano-vaccine based on the damaged membrane of red blood cells (29). Kranz et al. developed RNA-lipoplex (RNA-LPX) with a net charge suitable for DCs targeting (31). LoPresti et al. studied the lipid types of lipid nanoparticles (LNPs) suitable for spleen targeting. It was identified that LNP using phosphatidylserine (PS) is 24-fold higher spleen accumulation than that of using dioleoylphosphatidylethanolamine (DOPE) (32). Schmid et al. reported that anti-CD8 antibody labeled nanoparticles can be used as immune cell targeting delivery vehicles for cancer immunotherapy (33). Sago et al. identified ratios and compositions of LNP suitable for spleen targeting among over 250 compositions of LNPs using a high throughput method which is selectively read functional mRNA delivery (34). Kimura et

al. demonstrated high loading efficiency of plasmid DNA (pDNA) and spleen targeting efficiency by using a certain ratio of 1,2-dioleoyl-3-dimethylammonium-propane (DODAP), an ionizable lipid, and DOPE, a helper lipid (35). Kimura et al. reported double coating method using a specific ratio of pH-responsive ionizable lipid and octaarginine peptide as a spleen targeting strategy (36). Cheng et al developed selective organ targeting (SORT), a strategy to target specific organ by adding supplementary components to LNPs. They demonstrated the higher the molar percentage of 1,2-Dioleoyl-3-trimethylammoniumpropane (DOTAP), the more it accumulates in spleen than in liver (37). Alvarez-benedicto et al. reported that the more negatively charged LNPs were, the more they accumulated in the spleen than the liver (38). Ye et al. developed a solid lipid nanoparticles (sLNPs) for passive spleen targeting. sLNPs with specific ratios of stearic acid, soya lecithin, and poloxamer 188 has characteristics of high spleen targeting efficiency (39). Li et al. identified the appropriate PEG length for spleen targeting glabridin loaded nanoparticles by comparing various PEG lengths (40). Yi et al. reported the polymersome as the most suitable form for spleen targeting through a comparison of morphological structures composed of poly(ethylene glycol)-bl-poly(propylene sulfide) (PEG-bl-PPS) block copolymers (41). Several

studies have studied the ratio of composition of nanoparticles suitable for spleen targeting. In addition, various spleen targeting strategies including appropriate PEG length, lipid type, surface charge, and morphological structure have been reported.

Among spleen targeting strategies, there have been studies to develop nanoparticles targeting specific splenic immune cells for immune modulation (**Table 4**). Shimizu et al. reported that a large amount of antigen (Ag) encapsulated in PEGylated liposome (PL) was delivered to splenic B cell in marginal zone by pre-injecting empty PL (42). Fenton et al. reported that mRNA encapsulated in LNPs was successfully delivered to splenic B cells using organ-specific degradability of ionizable lipid including degradable linkages (43). Jeught et al. synthesized a hybrid mRNA nanoparticle (lipopolyplex) with a trimannose sugar tree and demonstrated that the nanoparticle induced antitumor T-cell immunity by delivering mRNA to splenic dendritic cells (DC) without causing an inflammatory response (44). Maldonado et al. reported dendritic cell targeting through intravenously injecting tolerogenic nanoparticles which improve immune tolerance (45). Stead et al. developed porous silicon nanoparticles containing c-type lectin, dendritic cell-specific intercellular adhesion molecule-3-grabbing non-integrin (DC-SIGN), and CD11c antibody to

deliver immunosuppressive drugs to DC (46). Leuschner et al. developed LNPs carrying CCR2-silencing short interfering RNA (siRNA). the LNP suppressed CCR2 expression by targeting inflammatory monocytes, resulting in blocking localization to inflammatory sites (47). Tripathi et al. developed 4-sulfated N-acetyl galactosamine conjugated chitosan nanoparticles (SCNPs) for targeting splenic macrophage (48). Jiang et al. developed the nanoparticle-stabilized nanocapsule for cytosolic siRNA delivery to splenic macrophages. After intravenously injection of the NPSCs, inflammation in mice was alleviated by silencing TNF-αexpression (49). Van leent et al. delivered rapamycin (mTOR) inhibitor and ribosomal protein S6 kinase-1 (S6K1) inhibitor to myeloid cell using apolipoprotein A1 (APOA1) based nanobiologics. As a result, the inflammatory response of macrophages in the plaque was reduced (50). Saito et al developed a drug-free biodegradable nanoparticle targeting inflammatory monocytes and neutrophils. The nanoparticle composed of 50:50 poly(DL-lactide-co-glycolide) with high molecular weights (PLG-H) alleviated the inflammation by monocyte and neutrophil after intravenously injection (51). To summarize, several studies developed nanoparticles with targeting moieties for splenic immune cells and showed therapeutic potential in various diseases, including inflammatory diseases and tumors.

Nanoparticles	Targeting strategies	Preparation methods	Composition	Size	Zeta potential	Spleen targeting efficiency (%)	Ref
iPSC@RBC Mlipo	Including damaged RBC membrane	Extrusion	DPPC, cholesterol, DDAB, mannose lipid, α-tocopherol, DSPE-PEG_{2000}	184	4.7	160	(29)
RNA-LPX	Negatively charged LNP	Pipetting or vortex-mixing	Cationic lipid: DOTMA, helper lipid: DOPE, cholesterol	200-320	- 30	N/M	(31)
Anionic LNP	Using the anionic helper lipid	Vortex-mixing	Lipidoid, PS, cholesterol, C_{14}-PEG_{2000}	N/M	- 6	300	(32)
7C3 LNP	Fining the ideal composition and ratio	Microfluidic-mixing	7C3, DOPE, cholesterol C_{14}-PEG_{2000}	Around 60	NM	50	(34)
DODAP-LNP	Lipid combination	Vortex-mixing	DODAP, DOPE, cholesterol, DMG-PEG	221 ± 27.8	- 30 ± 11.5	69	(35)
MEND	Double coating	Sonication	DOPE, DOTAP, YSK05, STR-R8, DMG-PEG	201 ± 32	- 21.5 ± 4.2	170	(36)
SORT LNP	Adding a supplementary molecule	Ethanol dilution method	18PA, 5A2-SC8, DOTAP, DOPE, DMG-PEG	142.1	- 2.11	150	(37)
SORT LNP	Selecting the appropriate phospholipid	Pipetting	BMP,4A3-SC8, DOPE, DMG-PEG	Around 140	Around -4	488	(38)

Nanoparticles	Targeting strategies	Preparation methods	Composition	Size	Zeta potential	Spleen targeting efficiency (%)	Ref
Actarit loaded SLNs	Passive targeting to RES organs	Modified solvent diffusion-evaporation	Stearic acid, soya lecithin, poloxamer 188	241 ± 23	−17.14 ± 1.6	120	(39)
Gla-loaded nanoparticle	Ideal PEG size	Double emulsion	DSPE-PEG_{5000}	80.67 ± 5.71	-3.57 ± 0.12	150	(40)
PS	Changing the nanostructure morphology	Controlled self-assembly	PEG-bl-PPS	113.7	- 0.2 ± 1.68	16.7	(41)

Table 3 Various spleen targeting strategies. Spleen targeting efficiency (%) is calculated by the (spleen uptake of the nanoparticle/ the liver uptake of the nanoparticle) × 100. iPSC@RBC-Mlipo: iPSCs encapsulated in coalescent erythrocyte-liposome, DPPC: The phospholipid 1,2-dihexadecanoyl-snglycero-3-phosphocholine, DDAB: Dimethyldioctadecylammonium, DSPE: 1,2- Distearoyl-sn-glycero-3-phosphoethanolamine, PEG: polyethylene glycol, RNA-LPX: RNA-lipoplexes, DOTMA: N-[1-(2,3-Dioleyloxy)propyl]-N,N,N-trimethylammonium, PS: phosphatidylserine, SORT: selective oragn targetingDOPE: dioleoylphosphatidylethanolamine, DOTAP: 1,2-Dioleoyl-3-trimethylammoniumpropane, DMG-PEG: PEGylation of myristoyl diglyceride, Gla: glabridin, PEG-bl-PPS: poly(ethylene glycol)-bl-poly(propylene sulfide).

Targeted splenic immune cells	NP Type	Targeting composition of NP	Encapsulated reagents	Composition	Targeted disease	Spleen targeting efficiency (%)	Ref
B cells	liposome	DSPE-PEG_{2000}	αGC, OVA	HEPC, DSPE-PEG_{2000},	Tumor	Not mentioned	(42)
B cells	LNP	OF-Deg-Lin	mRNA	OF-Deg-Lin, DOPE, C_{14}-PEG_{2000}	N/A	81	(43)
DC	LNP	TriMan-Lip	mRNA/PEG-HpK polyplexs	TriMan-Lip, Lip1, Lip2	Tumor	Not mentioned	(44)
DC	PLGA	N/A	Rapamycin, $OVA_{323-339}$	PLGA, OVA	Encephalomyelitis Hemophilia A	128	(45)
DC	Silicon NP	CD11c DC-SIGN	Rapamycin, $OVA_{323-339}$	Silicon	N/A	52.1	(46)
Monocyte	LNP	N/A	CCR2-siRNA	C12-200, DSPC, DMG-PEG	Atherosclerosis Pancreatic islet transplantation Tumor	296	(47)
Macrophage	CNP	4-SO_4 GalNAc	AmB	Chitosan, TPP	Leishmaniasis	50.9	(48)

Targeted splenic immune cells	NP Type	Targeting composition of NP	Encapsulated reagents	Composition	Targeted disease	Spleen targeting efficiency (%)	Ref
Macrophage	NPSCs	N/A	si_TNF-α	Linoleic acid, Arg-AuNP	LPS induced inflammation	44	(49)
			si_GADPH				
Myeloid cells	Lipid based NP	APOA1	mTORi	MHPC, DMPC	Atherosclerosis	66.7	(50)
			S6K1i	POPC, PHPC			
Neutrophil	PLGA	PLG-H	N/A	PLA, PLG-H	Encephalomyelitis	14.3	(51)
Monocyte							

Table 4 Strategies for targeting nanoparticles to specific splenic immune cells. Spleen targeting efficiency (%) is calculated by the (spleen uptake of the nanoparticle/ the liver uptake of the nanoparticle) × 100. DPSE: phosphatidylethanolamine, PEG: Poly(ethylene glycol), αGC: α-galactosylceramide, HEPC: Hydrogenated egg phosphatidylcholine, LNP: lipid nanoparticle, OF-Deg-Lin: the ionizable lipid designed to include degradable linkages, DOPE: dioleoylphosphatidylethanolamine, TriMan-Lip: trimannosyl diether lipid. Lip1: O,O-dioleyl-N-[3N-(N-methylimidazolium iodide)propylene] phosphoramidate, Lip2: O,O-dioleyl-

N-histamine phosphoramidate, PLGA: poly(lactide-coglycolide), DC-SIGN: dendritic cell-specific intercellular adhesion molecule-3-grabbing non-integrin, DMG-PEG: PEGylation of myristoyl diglyceride, DPSC: 1,2-distearoyl-sn-glycero-3-phosphocholine, CNP: chitosan nanoparticle, 4-SO4 GalNAc: 4-sulfated N-acetyl galactosamine, AmB: amphotericin B, TPP: Sodium tripolyphosphate, NPSCs: nanoparticle-stabilized nanocapsules, APOA1: apolipoprotein A1, MHPC: 1-myristoyl-2-hydroxy-sn-glycero-phosphocholine, DMPC: 1,2-dimyristoyl-sn-glycero-3-phosphocholine, POPC: 1-palmitoyl-2-oleoyl-sn-glycero-3-phosphocholine, PHPC: 1-palmitoyl-2-hydroxy-sn-glycero-3-phosphocholine, PLG-H: 50:50 poly(DL-lactide-co-glycolide) with high molecular weights, PLA: poly(DL-lactide).

1.4 Research objectives

We developed H_2S donor, GYY4137, loaded spleen-targeting liposomes and tested their immunomodulatory properties in a dextran sulfate sodium induced mouse colitis model (**Figure 1.3**). Based on the anti-inflammatory effect of the H_2S donor and the intrinsic immune cell targeting ability of the nanoparticles, we hypothesized that 1) liposomal delivery of the H_2S donor would elicit a higher immunomodulation effect compared to the unloaded H_2S donor and that 2) delivery of the H_2S donor using spleen-targeting liposomes would show a better immunomodulatory effect compared to the conventional long circulating liposome loaded H_2S donor.

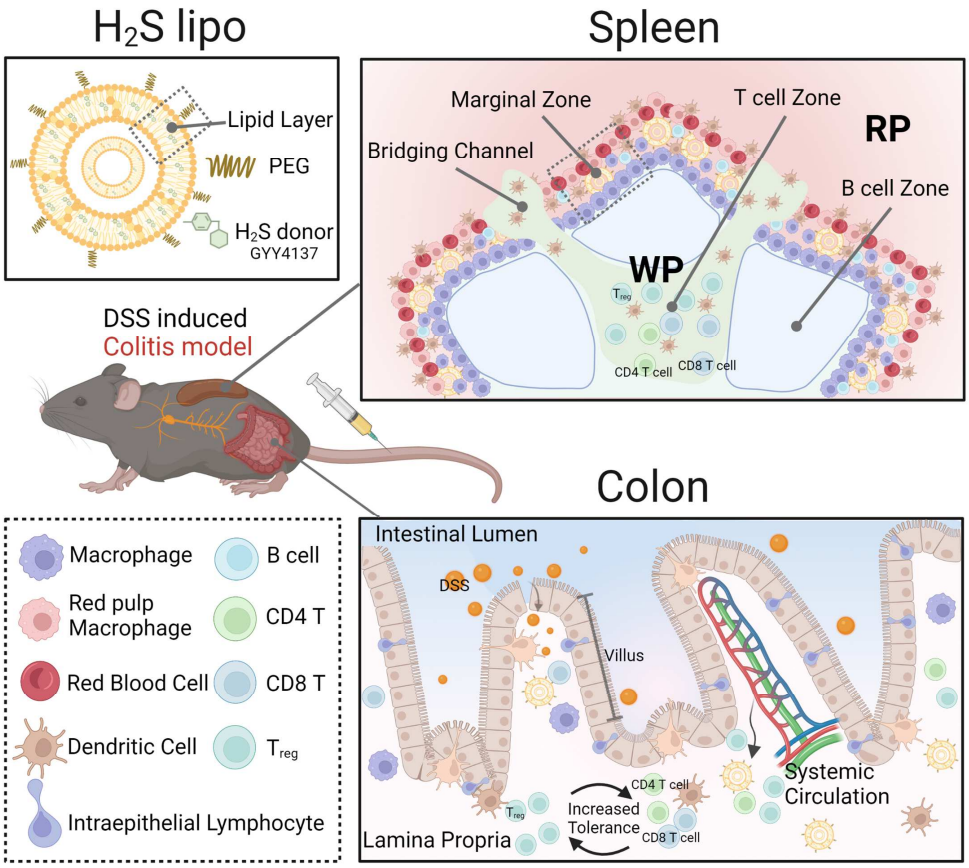

Figure 1.3 Schematic illustration of the H_2S lipo treatment in DSS induced colitis model. Immune responses according to H_2S lipo of spleen and colon are illustrated. DSS: dextran sulfate sodium, WP: white pulp, RP: red pulp. The figure is created with BioRender.com

Chapter 2.

Development of spleen targeting H_2S donating liposome

2.1 Backgrounds

H_2S has an anti-inflammatory activity in cardiovascular, respiratory, gastrointestinal systems in various pathological conditions (**Figure 1.1**) (20, 21, 52). H_2S is rapidly diffused into the cytoplasm without a specific transporter and involved in several anti-inflammatory processes (**Figure 2.1**) (12, 53-55). H_2S promotes T_{reg} differentiation, which is important for preventing autoimmunity. H_2S promotes the expression of ten-eleven translocation protein (TET1) and TET2 to maintain the demethylation of forehead box P3 (FOXP3), resulting in more T_{reg} differentiation and immune homeostasis(56, 57). H_2S also promotes the secretion of interleukin-10 (IL-10) associated with T_{reg} (23, 24, 58). In macrophage polarization, H_2S facilitates the production of peroxisome proliferator-activated receptor gamma (PPARγ) and PPARγ coactivator-1β, resulting in inducing anti-inflammatory M2 macrophage (22). In the inflammatory signaling pathway, The nuclear factor-κB (NF-κB) signaling pathway induces the expression of pro-inflammatory cytokines and chemokines such as IL-1/6/8/b, interferon-γ (IFN-γ), inducible nitric oxide synthase (iNOS), cyclooxygenase-2 (COX-2), and tumor necrosis factor- α (TNF-α). Several studies have been showed that H_2S inhibits the NF-κB signaling pathway,

resulting in alleviating inflammation (25, 59, 60). To sum up, hydrogen sulfide has anti-inflammatory activity in a wide range of ways, from signaling pathway to anti-inflammatory related immune cell differentiation.

A

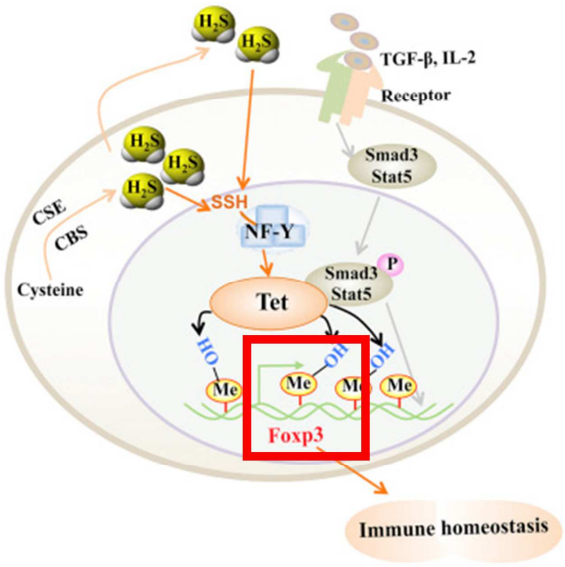

B

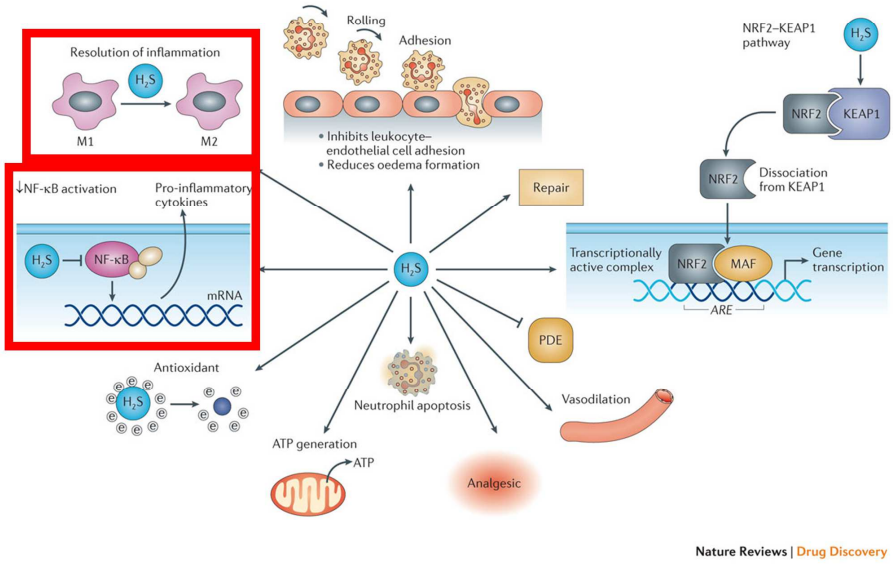

Figure 2.1 H_2S related anti-inflammatory processes. A. H_2S promotes T_{reg} differentiation by regulating expression of FOXP3, resulting in immune homeostasis. From reference (56). B. H_2S is involved in M2 polarization and NF-κB signaling pathway. From reference (61). FOXP3: forehead box P3

Several studies have demonstrated that treatment using H_2S donors alleviates symptoms in various disease models, resulting from facilitating anti-inflammatory responses (**Table 2**) (17-24). Li et al. reported that GYY4137 mitigated knee joints swelling by decreasing expressions of IL-1β/6/8 and TNF-α in the acute joint inflammatory model ($P< 0.05$) (20). Zhang et al. reported that NaHS diminished air hyperresponsiveness (AHR) by reducing activation of IL-5/13 in asthma model ($P< 0.05$) (21). Miao et al. reported that NaHS attenuated myocardial infarct (MI) size by promoting differentiation of M2 macrophage in MI model ($P< 0.01$) (22). Wu et al. reported NaHS relieved kidney dysfunction by increasing expression of IL-10 and decreasing expression of IL-6 and MCP-1 in obesity induced kidney injury model ($P< 0.05$) (23). Li et al. reported that NaHS alleviated degree of acute lung injury (ALI) by promoting expression of IL-10 and diminishing of IL-6/8 in ALI model ($P< 0.05$) (24). Zhang et al. reported that NaHS preserved diaphragmatic function and structure by inhibiting NF-κB signaling pathway and reactive oxygen species (ROS) in diaphragm dysfunction model (25). To sum up, versatile H_2S involved in several anti-inflammatory processes has shown therapeutic potential in various disease models.

The spleen, the largest lymphatic organ, is composed of various structures

and has different roles. Structurally, the spleen consists of red pulp (RP), white pulp (WP) and marginal zone (MZ) (**Figure 2.2A**). The spleen is a reservoir of various immune cells (**Figure 2.2B**). In the RP, monocytes, macrophages, and dendritic cells are abundant. The primary role of the RP is to filter blood borne pathogens and damaged erythrocytes. WP consists of B cells, T cells and dendritic cells, which are responsible for antigen specific immune responses to viral, bacterial, and fungal infections (62). Macrophages and metallophilic macrophages, B cells and dendritic cells are located in the MZ. Marginal zone macrophages can internalize blood borne pathogens and damaged molecules (63). Moreover, in the MZ, antigen presenting cells (APCs) ingest antigens and migrate into the white pulp for interaction with lymphocytes. The interaction between the lymphocytes of the white pulp and APCs could induce T_{reg} cell differentiation from naïve T cells (30, 64). The spleen has a crucial role in regulating immunological responses in various pathological states such as ischemic stroke (65), myocardial infarction (66) and infections including coronavirus disease 2019 (COVID-19) (30, 67). The progression of these pathological conditions is strongly associated with the regulation of immune cells in the spleen. For example, in ischemic myocardial injury, monocytes in the spleen are mobilized and recruited to the ischemic myocardium. The recruited

monocytes have critical roles in the regulation of inflammation and repair of damaged tissue (68). Therefore, spleen mediated immune modulation is gaining momentum as a therapeutic target in various pathologic conditions related to unregulated inflammation (29, 69, 70).

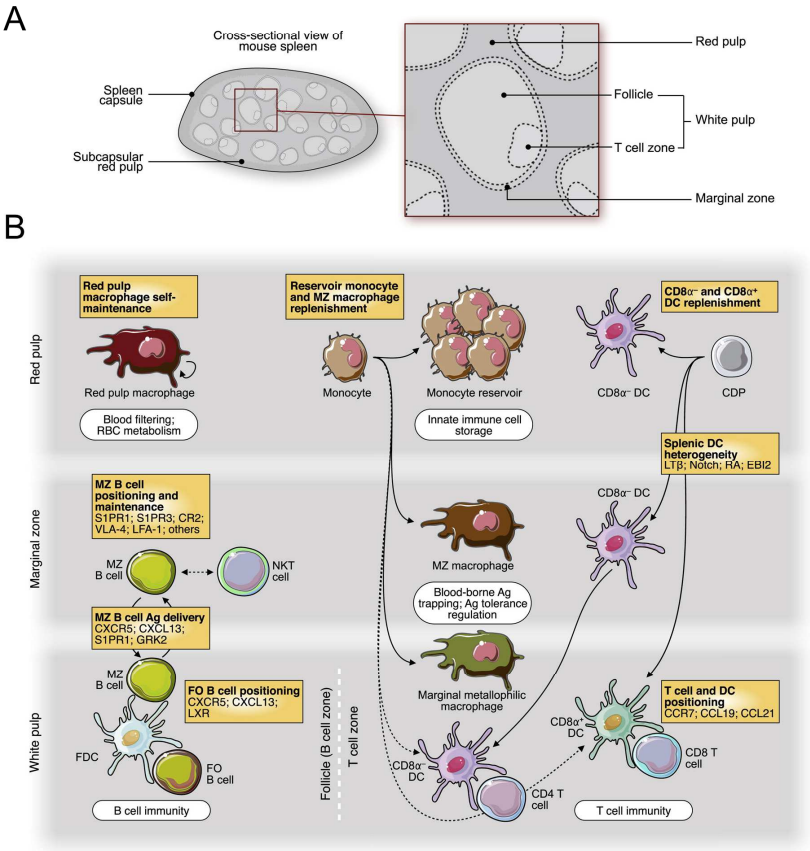

Figure 2.2 Spleen's structure and roles of various splenic immune cells. A. Spleen consists of RP, MZ, and WP. B. The scheme demonstrates roles of splenic immune cells. Orange boxes illustrates mechanism or the cell's origin. White boxes indicate various roles according to splenic structure. From reference (30)

RP: red pulp, MZ: marginal zone, WP: white pulp

The liver and spleen have a natural characteristic to clear nanoparticles from systemic circulation because they are a natural filter for blood borne pathogens and antigens which can have a similar size with nanoparticles (**Figure 2.3**). This characteristic can reduce the drug delivery efficiency to diseased tissue such as tumors or inflammatory lesions; therefore, long circulating nanoparticles have been developed to reduce and delay nanoparticle uptake in the liver and spleen. However, recently, studies on the re-direction of nanoparticles to target the spleen are gaining attention for immune modulative therapy (71). In an experiment on polystyrene nanoparticle biodistribution during systemic inflammation, nanoparticles with a 20, 100, and 500 nm size mostly accumulated in the marginal zone of the spleen. Particularly, the nanoparticles were more dramatically accumulated in the spleen when inflammation was induced in mice by lipopolysaccharide (72, 73).

Conventionally, one of the most effective strategies for a longer circulation was to modify the nanoparticle surface using polyethylene glycol (PEG). PEG helps nanoparticles to maintain a more stable condition, evade the immune system, and enhance the delivery efficacy to the target region (74). Considering spleen targeting, surface PEG does not appear to be an appropriate component of nanoparticles. Therefore, we tested various sizes

and ratios of PEG to achieve a high stability, high loading efficiency of GYY4137, and effective spleen targeting.

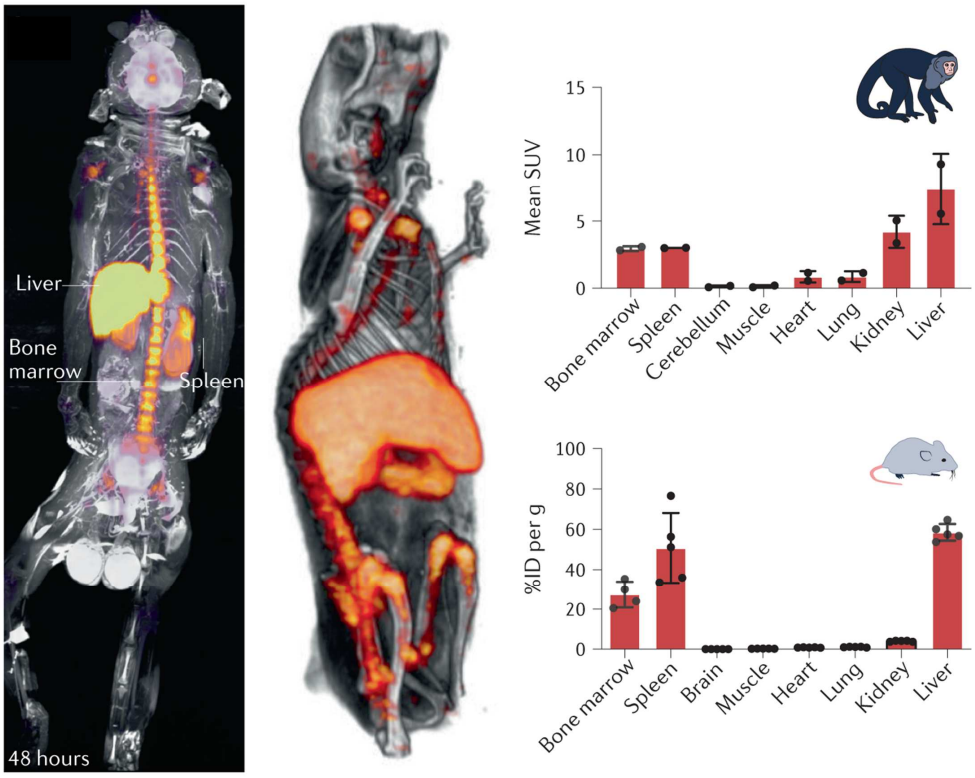

Figure 2.3 Mononuclear phagocyte system (MPS). MPS related organs capture NPs and rapidly excrete from the systemic circulation. Among MPS related organs, the liver and spleen make up a large portion of clearing systemically administrated nanoparticle. From reference (75)

2.2 Material and Methods

2.2.1 Materials

Raw 264.7 cell line was purchased from Korean Cell Line Bank (Seoul, Korea). Distearoyl phosphatidylcholine (DSPC) was purchased from Avanti Polar Lipids, Inc. (AL, USA). 1,2-Distearoyl-sn-glycero-3-phosphoethanolamine (methoxy(polyethylene glycol)-2000) (DSPE-PEG2k) and DSPE-PEG5k, and 1,2-Distearoyl-sn-glycero-3-phosphoethanolamineN-[amino(polyethylene glycol)-2000] (DSPE-PEG2K-NH2 were obtained from Creative PEGworks (NC, USA). Cholesterol, N,N-Diisopropylethylamine (DIPEA), Silver nitrate (AgNO3), GYY 4137 (SML0100), phosphate buffered saline (PBS) tablet, 3-[4,5-dimethylthiazol-2-yl]-2,5-diphenyltetrazolium bromide reagent (MTT), Triton X-100 were purchased from Sigma Aldrich (MO, USA).

Antibody: CD45 (23-0451-81), CD4 (11-0041-81), FOXP3 (41-5773-82 and 45-5773-82), F4/80 (53-4801-80), CD80 (12-0801-82), CD206 (53-2061-82), Fluorescein 5(6)-isothiocyanate (FITC), and Hoechst 33342 were purchased from Thermo Fisher Scientific (MA, USA). 2-(p-Isothiocyanatobenzyl)-1,4,7-triazacyclononane-N,N’,N’-triacetic acid

trihydrochlor ide ((p-SCN-Bn)-NOTA) was purchased from FUTURECHEM (Seoul, Korea). Hsip-1 was purchased from Dojindo (Kumamoto, Japan). Dextran sulfate sodium (DSS) salt, colitis grade (36000-50000) was purchased from MP Biomedicals (OH, USA). 4% paraformaldehyde (PFA) was purchased from Biosesang (Seongnam, Korea).

The PET images were acquired by GENISYS4, small PET scanner (Sofie Bioscience, CA, USA), The in vivo imaging system (IVIS, Perkin Elmer, MA, USA) was used to fluorescence images. The optical density was acquired by a microplate reader (SYNERGY H1, BioTek, VT, USA). The size distribution by dynamic light scattering (DLS) was performed to using the ZETASIZER Nano ZS (Malvern Instrument, Worcs, UK). The Cryo-TEM images were acquired by TALOS L120C (OR, USA).

2.2.2 Synthesis of H_2S lipo

Self-assembled H_2S lipo comprised DSPC, cholesterol, GYY4137, and DSPE-PEG (**Figure 2.6A**). GYY4137 has been studied in diverse fields (20, 76, 77). All experimental group comprised identical mass ratio of DSPC and cholesterol (6:1). 133.3 μM of H_2S donor was prepared for H_2S lipo. Additionally, 600 μM of H_2S donor was prepared for reducing

administration volume of DSS treatment. The composition of H_2S lipo was dissolved in organic solvent; chloroform/methanol (3:1 v/v) and evaporated. Dried lipids were vacuumed overnight for removing residual organic solvent. Dried lipids formed bilamellar vesicles through adding distilled water (DW) at 37℃. Then, H_2S lipo was formed with several cycles of ultrasonication.

2.2.3 Detection of H_2S release from H_2S lipo

H_2S released by H_2S donor or H_2S lipo was identified by precipitation reaction with silver nitrate ($AgNO_3$)(**Figure 2.4**) (78). Firstly, $AgNO_3$ was added to solution including H_2S donor or H_2S lipo. D.W with H_2S lipo added methanol to destroy liposomal structure. Released H_2S reacted with $AgNO_3$ and then the product, silver sulfide (AgS), was sedimented. AgS was detected through colorimetric assay. The optical density (O. D) of AgS was 405 nm. H_2S donor or H_2S lipo were quantitatively calculated by standard curve. When doing colorimetric assay, we added reagent, $AgNO_3$, and methanol as 1:1:3 ratio.

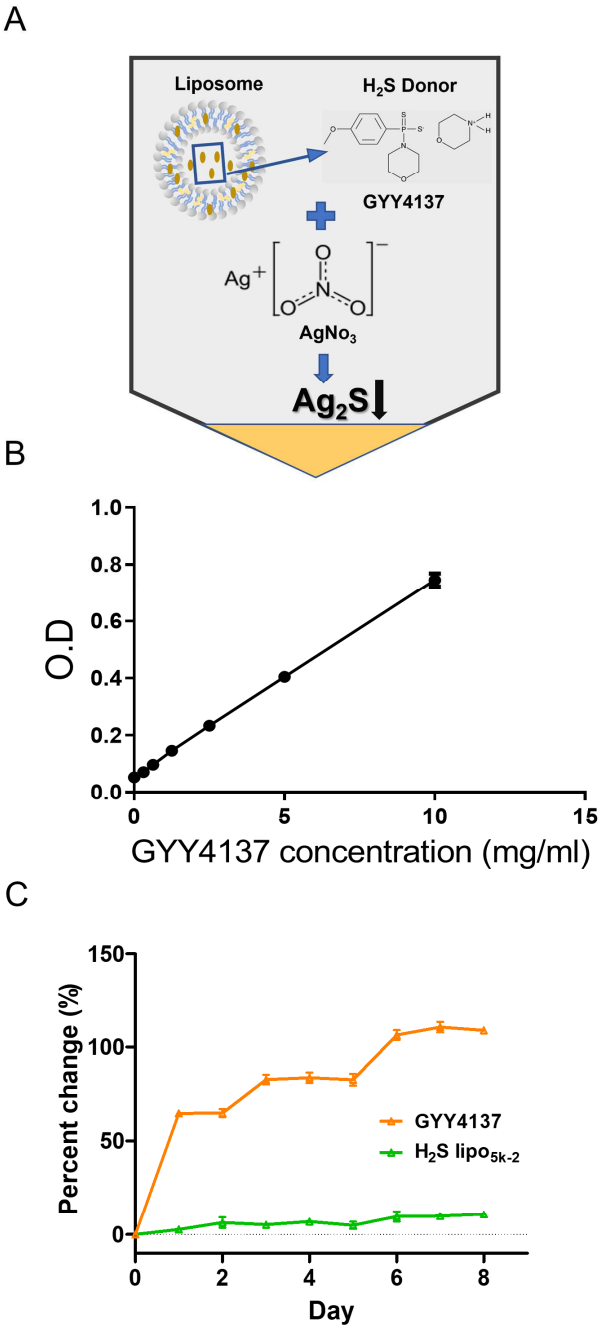

Figure 2.4 Released H_2S detection method. A. Schematic design of H_2S detection by $AgNO_3$ precipitation. When encapsulated H_2S donor,

GYY4137, was released, $AgNO_3$ reacted with H_2S and precipitation of Ag_2S occurred. B. The standard curve of serial diluted GYY4137 solution. The calculated O.D of GYY4137 concentration was 10 mg/ml, 5 mg/ml, 2.5 mg/ml, 1.25 mg/ml, 0.6125 mg/ml, and 0.30625. The equation is y= 0.0692x + 0.0559, R^2= 0.997. Conversion mass to mole used molar mass of GYY4137 which is 376. 47 g/mol. C. Loading stability test. GYY4137 and H_2S $lipo_{5k-2}$ were stored in 4℃. H_2S detection method repeatedly performed the same amount of stored samples every day. The graph indicated the percent change of O.D with reagents and $AgNO_3$ (N= 3). O.D: optical density, D.W: distilled water, $AgNO_3$: silver nitrate

2.2.4 Size stability and loading efficiency of H_2S lipos

The stability of H_2S lipos was investigated using size distribution profiles. Investigated H_2S lipo was suspended with DW and stored at room temperature. Size distribution profiles were acquired by dynamic scattering light (DLS). The acquisition time points were day 0, 3, 7 and 14. Loading efficiency of H_2S lipos was compared by colorimetric assay at 90 mins after precipitation reaction. Serial concentration group of GYY4137 were simultaneously performed for calculating the standard curve. Measured O.D value is converted into molar concentration using indicated GYY4137 molecular weight and the standard curve. Loading efficiency (%) of H_2S lipo was calculated using below formula: loading efficiency (%) = GYY4317 mass converted from measured O.D/ initial GYY4137 mass × 100%.

2.2.5 In vitro experiments using H_2S lipo

Macrophage cell line, RAW 264.7, was used to in vitro experiments. 10^5 cells were incubated in confocal dish. Next day, saline, GYY 4137, and fluorescent H_2S lipo were treated in RAW 264 cells respectively.

Fluorescent H_2S lipo was used for examining cell uptake of H_2S lipo. The FITC was mixed with DSPE-PEG2k-Amine in the same molecular weight. The mixture was dissolved in organic solvent when H_2S lipo was synthesized. The time point of cell uptake images was 0, 1, 2, and 3 hours. The fluorescence intensity is quantified using ImageJ. In cell differentiation study, we assessed ability of promoting anti-inflammatory (M2) macrophage differentiation. The 64.57 μM of GYY4137 and H_2S lipo were treated in RAW 264.7 cells. We observed elongated RAW 264.7 cells after 48 hours. The elongation factor (A.U) is used as assessment method of macrophage differentiation (79). The elongation factor is the number of dividing longitudinal cell length into cross-sectional cell length. It indicates M2 macrophage differentiation that the elongation factor is increased. Saline, bare lipo, GYY 4137, and H_2S lipo are used as the reagents respectively. All images are acquired by confocal scanning microscope.

2.2.6 The Comparison of in vitro H_2S release between various PEGylation strategies of H_2S lipo

In the H_2S release test, 10^5 cells of RAW 264.7 were incubated in confocal dish. Next day, cells were treated with reagents. The reagents are

saline, GYY 4137, and H_2S lipos. Various PEGylation strategies of H_2S lipo were used for comparing H_2S release ability depending on the mass ratio of DSPC/DSPE-PEG and the type of PEG. After 2 hours from treating the reagents H_2S detection probe, Hsip-1, was used to identify released H_2S (80). The fluorescence intensity of released H_2S was quantified using ImageJ. All images were acquired by confocal scanning microscope.

2.2.7 The cell viability assessment after treating H_2S lipo

RAW 264.7 cell line was treated with H_2S lipo in medium (DMEM with 5% fetal bovine serum). H_2S lipo serially diluted based molar concentration. After 24 hours treating with H_2S lipo, 0.5 mg/ml of 3-[4,5-dimethylthiazol-2-yl]-2,5-diphenyltetrazolium bromide reagent (MTT) was added and incubated at 37 ℃ for 3 hours. After reagent removal, 100 µl of DMSO was added. Absorbance at 540 nm was detected by microplate spectrophotometer (81).

2.2.8 Radiolabeling method of H_2S lipo

The Composite structure made of chelator and PEG was used to

synthesize radiolabeled H_2S lipo. Firstly, 2-(p-Isothiocyanatobenzyl)-1,4,7-triazacyclononane-N,N',N,'-triacetic acid trihydrochloride ((p-SCN-Bn)-NOTA) as chelator and PEG-amine were dissolved in methanol with same molar ratio. N,N-Diisopropylethylamine (DIPEA) was added in the mixture for inducing covalent bond. The mixture was reacted for overnight. Then, PEG conjugated chelator was added in H_2S lipo synthesis before evaporating process. Chelated H_2S lipo was mixed with radioisotope in pH 5 solution adjusted by 2 M sodium acetate. The final mixture was incubated at 37 ℃ for 30 minutes. In the end, serial size exclusion chromatography was proceeded for sorting purified radiolabeled H_2S lipo. The radiolabeling efficiency was assessed by radio-thin layer chromatography (TLC) which is iTLC plates with 50 mM EDTA solution.

2.2.9 In vivo PET images of radiolabeled H_2S lipo.

Compared compositions are H_2S $lipo_{5k-2}$, H_2S $lipo_{5k-6}$, and H_2S $lipo_{5k-12}$. 50 μCi of ^{64}Cu radiolabeled H_2S lipo (^{64}Cu-H_2S lipo) at saline was injected to normal C57/BL6N mouse intravenously. The chronological PET Images were acquired by PET scanner (GENESYS4). The acquisition time point of PET Images was 0, 2, 12, and 36 hours. Quantitative analysis was conducted

by MIM Encore (MIM software Inc., OH, USA). The calculated region of interest (ROI) was Bloodpool, spleen, liver, muscle. The time-activity curve of bloodpool was calculated by fit curve equation. The ROI was quantified as percentage of the injected dose per tissue weight (%ID/g). The standard uptake value (SUV) was calculated by (tissue radioactivity concentration)/ [(injected dose)/(bodyweight)]. A time activity curve was calculated by fitting equation (y=y0+a*e-b×) using SUVmean of Bloodpool at 0, 2, 12, and 36 hours.

2.2.10 Flowcytometry

Flow cytometry was conducted for assessing immune cell differentiation in spleen and bone marrow. $FOXP3^+$ and $CD4^+$ antibodies were used for T_{reg} markers. $CD80^+$ and $CD206^+$ antibodies were used for M1 and M2 macrophage respectively. The scheme of gating strategy was illustrated (**Figure 2.5**). Extracted spleen and bone marrow were homogenized. The PBS washing was performed between each procedure. All data is acquired by flow cytometer. All data is analyzed by Guava Incyte program.

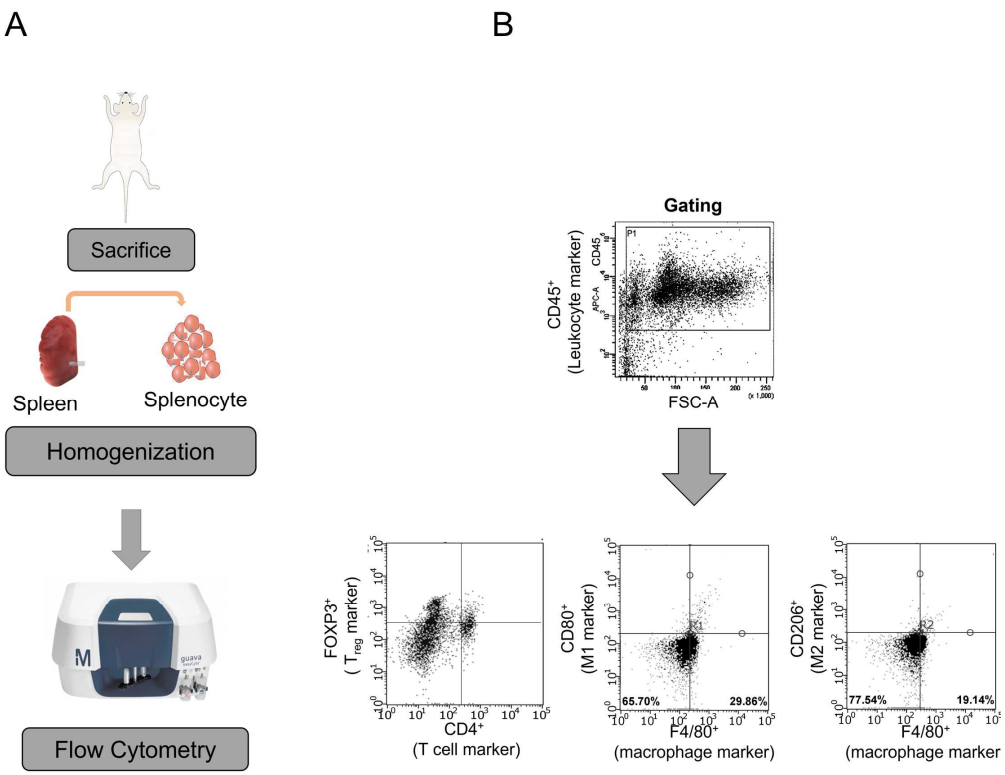

Figure 2.5 Gating Strategy of flow cytometry. A. Procedures of flow cytometry using splenocyte B. Gating strategy of flow cytometry analysis. CD45 antibody was used as leukocyte marker. CD4 and FOXP3 antibodies were used as regulatory T cell markers. CD80 and F4/80 antibodies were used as M1 macrophage markers. CD206 and F4/80 antibodies were used as M2 macrophage markers.

2.3 Results and Discussion

2.3.1 Identification of ideal composition of H_2S lipo

We synthesized a H_2S donor, GYY4137, loaded liposome (H_2S lipo) (**Figure 2.6A**). We tested various PEGylation strategies to develop the H_2S lipo with high stability and an efficient spleen targeting ability. Two types of 1,2- distearoyl-sn-glycero-3-phosphoethanolamine – polyethylene glycol (DSPE-PEG) (PEG: 2 kDa or 5kDa) and four different mass ratios of distearoyl phosphatidylcholine (DSPC) and DSPE-PEG (1:12, 1:6, 1:2, and 1:1) were tested in the synthesis of the H_2S lipo. The four different mass ratios using 2kDa PEG (1:12, 1:6, 1:2 and 1:1) were named H_2S $lipo_{2k\text{-}1}$, H_2S $lipo_{2k\text{-}2}$, H_2S $lipo_{2k\text{-}6}$ and H_2S $lipo_{2k\text{-}12}$, respectively. The four groups using 5 kDa PEG (1:12, 1:6, 1:2 and 1:1) were named H_2S $lipo_{5k\text{-}1}$, H_2S $lipo_{5k\text{-}2}$, H_2S $lipo_{5k\text{-}6}$ and H_2S $lipo_{5k\text{-}12}$, respectively. First, we tested the size stability of the various H_2S lipos in DW at room temperature for 14 days using dynamic light scattering (DLS). We calculated the size changes of the H_2S lipos between day 0 and day 14 to assess the degree of size stability, and the sizes of H_2S $lipo_{2k\text{-}1}$, H_2S $lipo_{2k\text{-}2}$, H_2S $lipo_{2k\text{-}6}$, H_2S $lipo_{2k\text{-}12}$, H_2S $lipo_{5k\text{-}1}$, H_2S $lipo_{5k\text{-}2}$, H_2S $lipo_{5k\text{-}6}$ and H_2S $lipo_{5k\text{-}12}$ were increased by 21.21%, 38.22%, 20.98%, 6.44%, 36%, 8.52%, 4.65%, and 12.53%,

respectively (**Figure 2.7, Table 5**). We considered H_2S lipo groups with over a 20% size change as unstable forms of H_2S lipo. Additionally, H_2S $lipo_{2k-12}$ was the only H_2S lipo with 2 kDa PEG left'; thus, we could not compare characteristics of the H_2S lipo with different 2 kDa PEG ratios. Therefore, H_2S $lipo_{5k-2}$, H_2S $lipo_{5k-6}$ and H_2S $lipo_{5k-12}$ were used in further characterization experiments. The H_2S donor loading efficiency was tested by a precipitation method using silver nitrate ($AgNO_3$) (**Figure 2.4A**) (78). The detected optical density (O.D) can be converted to the molar concentration using the weight concentration and molecular weight of GYY4137 calculated from the standard curve (**Figure 2.4B**). There was no significant difference in the loading efficiency between the various H_2S lipos (P = N.S.) (**Figure 2.6B**). Next, the surface net charge was analyzed (**Figure 2.6C**). The zeta potential (mV) of H_2S $lipo_{5k-2}$, H_2S $lipo_{5k-6}$, and H_2S $lipo_{5k-12}$ were -28.1±0.9, -24.8±0.8, and -23.2±0.2, respectively. The surface net charge of the H_2S lipo tended to increase as the mass of the PEG was increased (H_2S $lipo_{5k-2}$ vs. H_2S $lipo_{5k-6}$, $P < 0.01$; H_2S $lipo_{5k-2}$ vs. H_2S $lipo_{5k-12}$, $P < 0.001$ and H_2S $lipo_{5k-6}$ vs. H_2S $lipo_{5k-12}$, $P = 0.08$). Moreover, the loading stability test was confirmed with the H_2S detection method to identify whether the H_2S donor was well encapsulated and preserved in the H_2S lipo. We checked the percent change of the O.D of GYY4137 and H_2S

lipo$_{5k-2}$ in D.W for 8 days. The O.D of GYY4137 increased over time up to 100% and was saturated at day 7; however, the O.D of H_2S lipo$_{5k-2}$ was only increased less than 10%, which indicated GYY4137 was stably loaded in the liposome. We speculated that GYY4137 is loaded in the hydrophobic layer of the liposome because GYY4137 releases H_2S in aqueous solution and does not release H_2S in a hydrophobic environment (**Figure 2.4C**). Taken together, the H_2S lipo is a drug delivery vehicle that could stably encapsulate the H_2S donor without any unwanted H_2S release.

Additionally, cell viability after treatment with GYY4137 and H_2S lipo was tested by MTT assay in RAW 264.7 cells. GYY4137 and H_2S lipo were not cytotoxic up to 120 μM of GYY4137 (**Figure 2.8A**). In the cryogenic transmission microscopy (TEM) images, we identified that H_2S lipo$_{5k-2}$ are uniformly shaped bilamellar liposomes (**Figure 2.8B**).

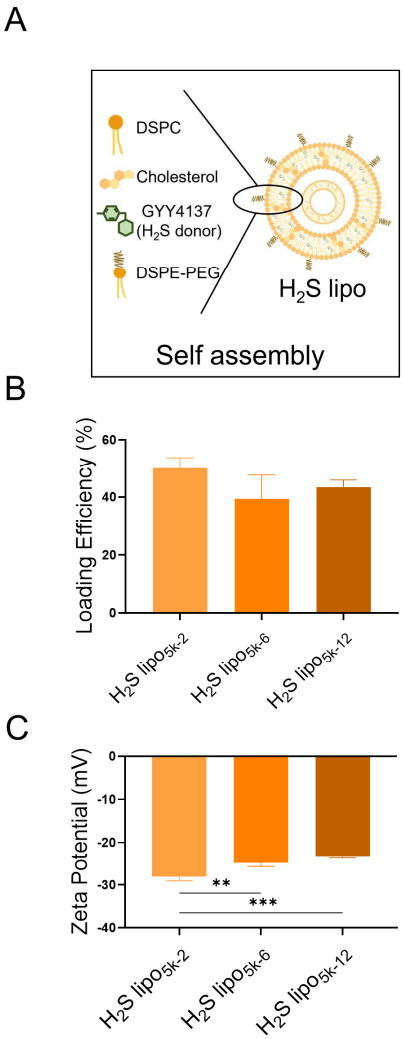

Figure 2.6 The scheme of H_2S lipo composition, the comparison of loading efficiency, and the comparison of surface net charge. A. The schematic design of H_2S lipo composition. B. The comparison of H_2S loading efficiency between different H_2S lipos using the H_2S detection method (n = 3). C. The comparison of surface net charge using zeta potential of DLS. **: $P < 0.01$, ***: $P < 0.001$.

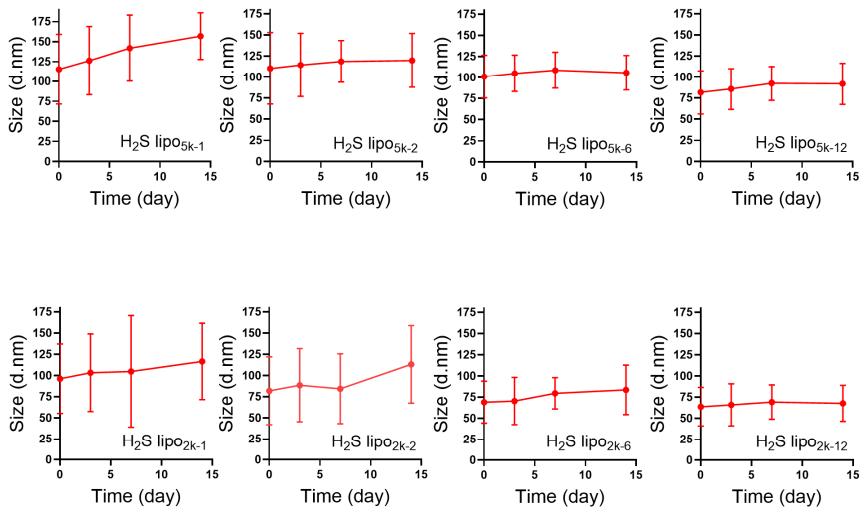

Figure 2.7 The stability test of H_2S lipo with different PEGylation strategies. A. The stability of H_2S lipo was analyzed using size distribution profiles of DLS. The size distribution of H_2S lipo was acquired up to 14 days. B. The table of H_2S lipo stability test. The data of size and PDI according to composition are filled in the table up to 14 days. PDI: polydispersity index.

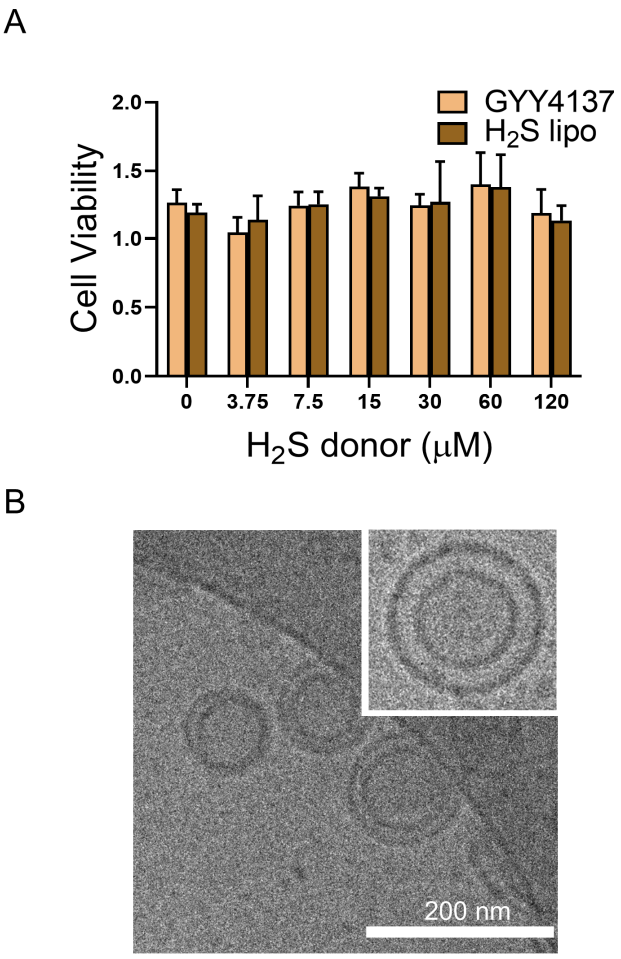

Figure 2.8 The cell viability test and Cryo-TEM images of H_2S lipo. A. The cell viability test of H_2S lipo and GYY4137 using colorimetric MTT assay. Raw 264.7 cell line was used for MTT assay. The range of H_2S donor or H_2S lipo concentration is 0 to 120 μM. B. Cryo-TEM images of H_2S lipo.

Composition	Measures	Time (day)			
		0	3	7	14
H_2S lipo$_{2k-1}$	Size (d.nm)	96.2±4	103.3±45.8	104.8±65.9	116.6±45
	PDI	0.262	0.259	0.251	0.252
H_2S lipo$_{2k-2}$	Size (d.nm)	81.9±40.1	88.6±43.2	84.4±41.3	113.2±45.8
	PDI	0.243	0.266	0.229	0.188
H_2S lipo$_{2k-6}$	Size (d.nm)	69.1±24.7	70.5±28	79.6±18.5	83.6±29.2
	PDI	0.162	0.145	0.148	0.151
H_2S lipo$_{2k-12}$	Size (d.nm)	63.7±22.8	66±24.6	69.2±20.2	67.8±21.4
	PDI	0.157	0.134	0.460	0.150
H_2S lipo$_{5k-1}$	Size (d.nm)	115.3±43.8	114.4±37.6	141.8±41.4	156.8±29.24
	PDI	0.193	0.22	0.207	0.200
H_2S lipo$_{5k-2}$	Size (d.nm)	110.3±42.4	114.4±37.6	118.6±24.74	119.7±32.1
	PDI	0.211	0.220	0.252	0.227
H_2S lipo$_{5k-6}$	Size (d.nm)	101±25.4	104.9±21.6	108.7±21.4	105.7±20.58
	PDI	0.076	0.060	0.073	0.089
H_2S lipo$_{5k-12}$	Size (d.nm)	81.6±25.7	85.8±24.3	92.3±20.1	91.83±24.48
	PDI	0.171	0.160	0.163	0.152

Table 5 The stability test of H_2S lipo with different PEGylation strategies. Table indicates size (d.nm) and PDI up to 14 days. PDI: polydispersity index.

2.3.2 In vitro H_2S releasing and immune modulatory effects of H_2S lipo

When RAW 264.7 cells were treated H_2S lipos, they were able to release H_2S. We found that the H_2S releasing ability of H_2S lipo is superior to that of the unloaded H_2S donor, GYY4137. Moreover, as the PEG composition included in the H_2S lipo was decreased, more H_2S release was detected (**Figure 2.9**). However, H_2S $lipo_{2k\text{-}1}$ and H_2S $lipo_{5k\text{-}1}$ were not used for further experiments because they were unstable in the size stability test (**Figure 2.7, Table 5**). Additionally, further studies were done using H_2S $lipo_{5k\text{-}2}$ because it has the highest degree of H_2S releasing ability among the stable H_2S lipos. In a cell uptake study, we found that a fluorescent H_2S lipo gradually was phagocyted by RAW 264.7 cells over time (**Figure 2.10**). To assess the immunomodulatory effect of the H_2S lipo in RAW 264.7 cells, we calculated the elongation factor of the cells which is a phenotypic marker for anti-inflammatory M2 macrophages (**Figure 2.11A**) (82). H_2S lipo was able to induce macrophage elongation, and the degree of elongation was higher in the H_2S lipo treated cells compared to the control, liposome, and unloaded H_2S donor treated cells ($P < 0.001$, $P < 0.01$, $P < 0.001$, respectively) (**Figure 2.11B, C**).

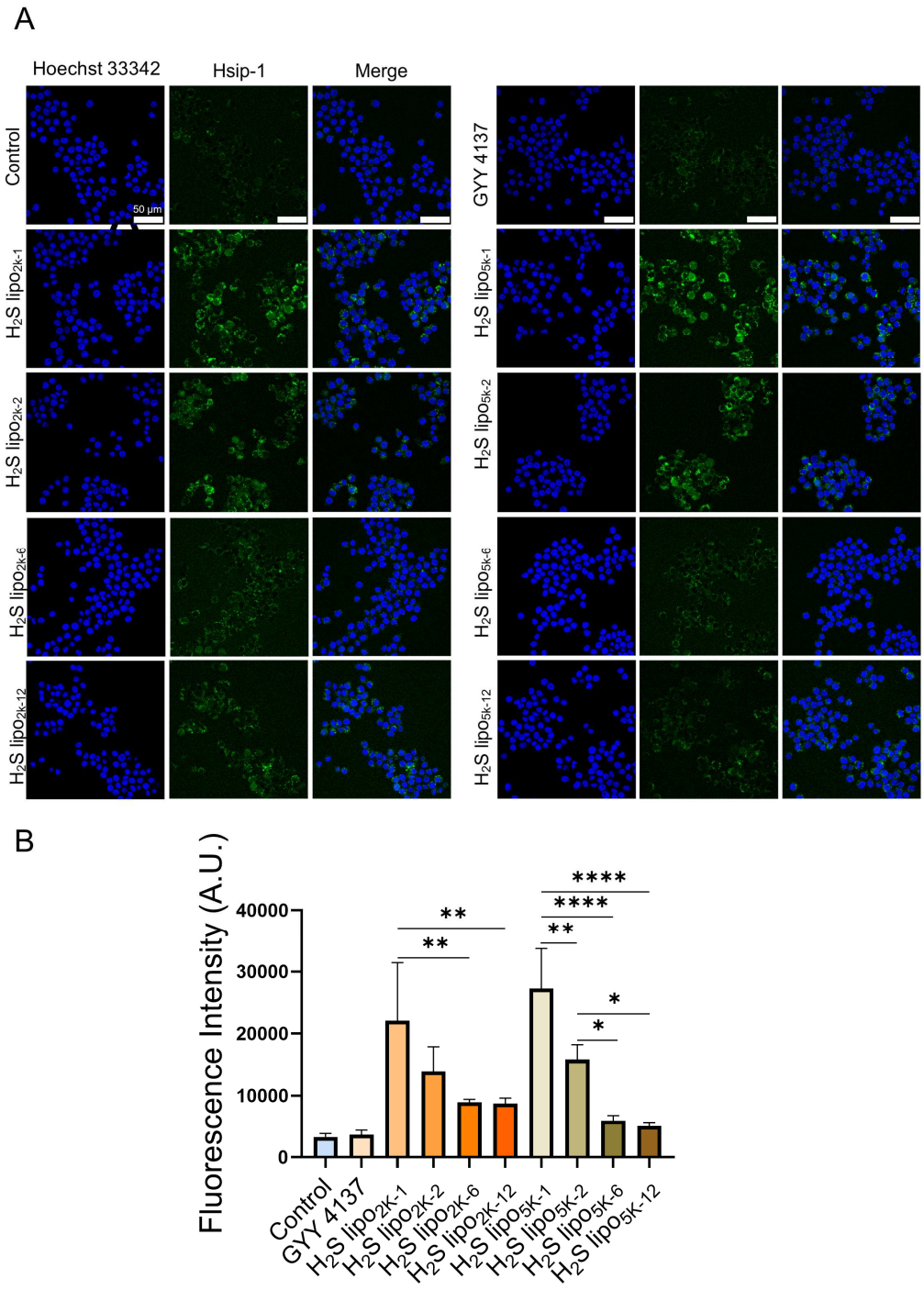

Figure 2.9 The fluorescence images of released H_2S by H_2S lipos. A. The fluorescence images of released H_2S by H_2S lipo after cell uptake. Hoechst

33342 was used for staining nucleic acid. Hsip-1 was used for detecting released H_2S by H_2S lipo after 1 hour from adding reagents (n = 4). B. The graph indicates the comparison of quantified fluorescence intensity between control, GYY 4137, and H_2S lipos. *: $P < 0.05$, **: $P < 0.01$, ****: $P < 0.0001$.

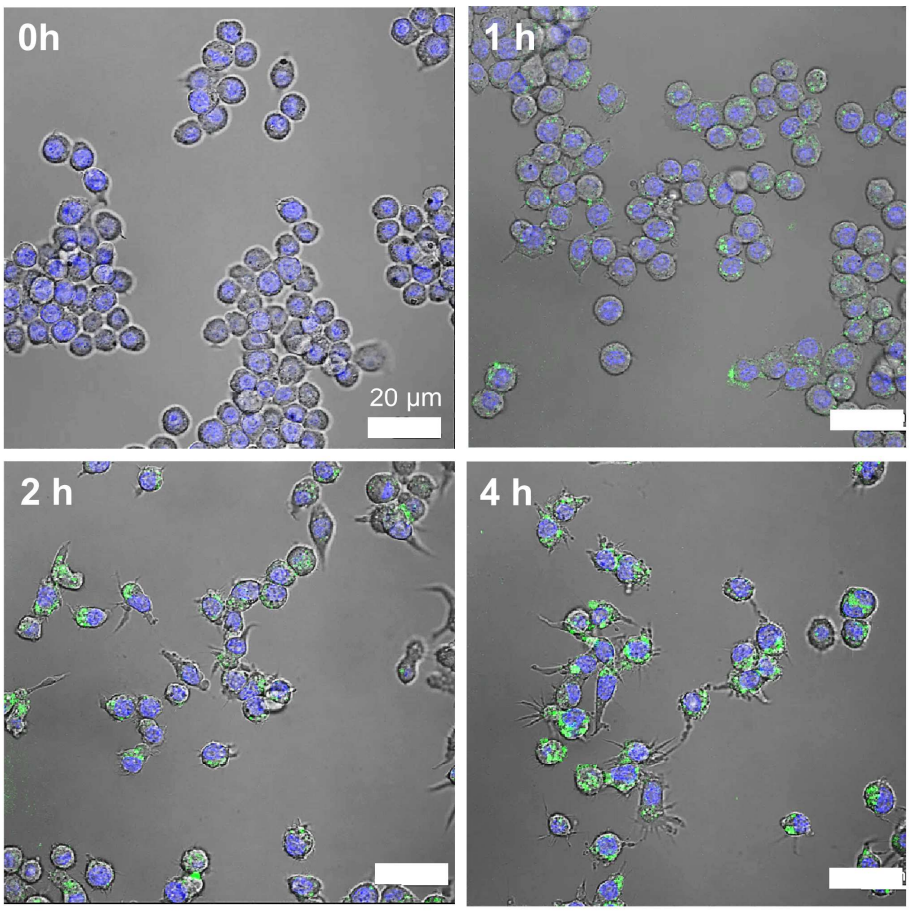

Figure 2.10 The cell uptake images of H_2S lipo. FITC labeled H_2S lipo is used (n = 6). The confocal images were acquired at 0, 1, 2, and 4 hours.

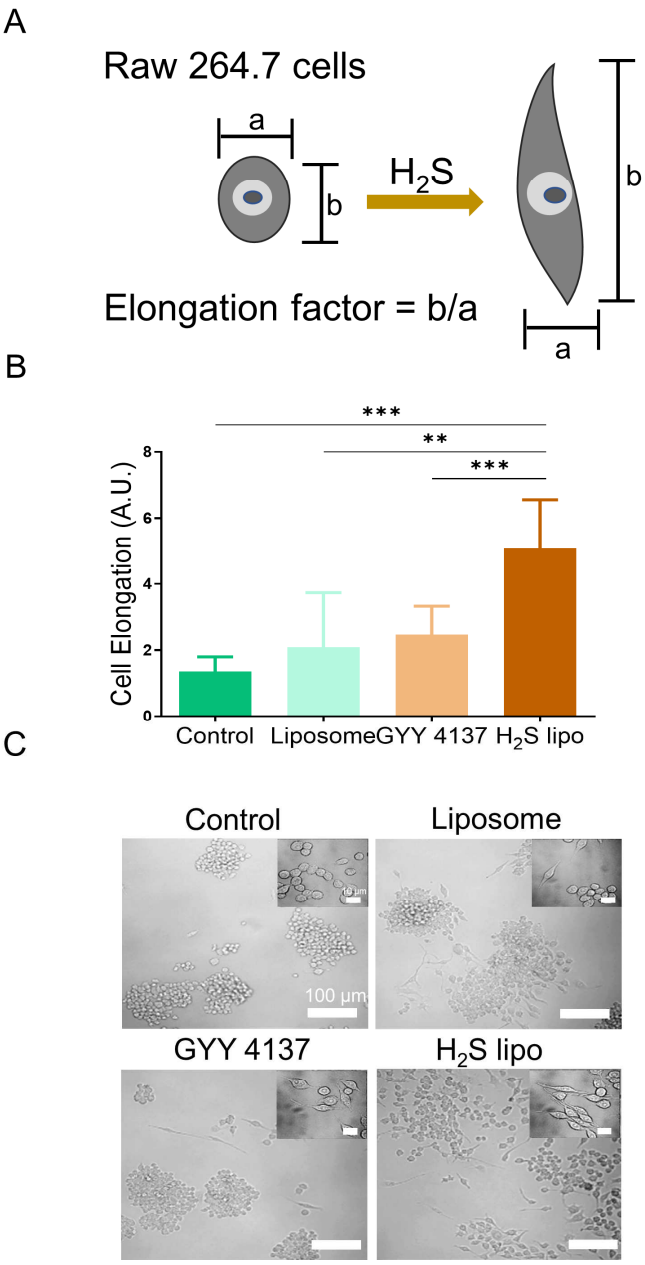

Figure 2.11 Morphological analysis of M2 macrophage differentiation. A. The schematic design of elongation factor analysis. B. The graph indicates the comparison of quantified cell elongation factor between control, liposome, GYY4137, and H_2S lipo (n = 8, respectively). C. The comparison of M2 macrophage differentiation between bare liposome, GYY4137, and H_2S lipo using morphological analysis. **: $P < 0.01$, ***: $P < 0.001$.

2.3.3 Assessment of the spleen targeting ability of H_2S lipo.

Positron emission tomography (PET) image based biodistribution analysis was done to assess the spleen targeting ability of H_2S lipo. We selected H_2S $lipo_{5k-2}$, H_2S $lipo_{5k-6}$ and H_2S $lipo_{5k-12}$ to assess the spleen targeting ability because 1) PEG 2 kDa included H_2S lipos were more unstable compared to the PEG 5 kDa included ones, and 2) H_2S $lipo_{5k-1}$ was unstable. PET has the advantage of showing the biodistribution of nanoparticles because it has excellent sensitivity and can detect an altered biodistribution by minor changes in the nanoparticles (83). To evaluate the appropriate PEGylation strategy for spleen targeting, we compared the in vivo biodistribution of ^{64}Cu radiolabeled H_2S $lipo_{5k-2}$, H_2S $lipo_{5k-6}$, and H_2S $lipo_{5k-12}$. First, we investigated the radiolabeling efficiency and radiochemical stability using thin layer chromatography (TLC). Even after 24 hours, the radiolabeling efficiency of H_2S $lipo_{5k-2}$, H_2S $lipo_{5k-6}$, and H_2S $lipo_{5k-12}$ remained 94.46%, 92.79%, and 95.74% in phosphate buffered solution (PBS), confirming successful radiolabeling (**Figure 2.12**). From the in vivo biodistribution shown on the PET image, it was identified that H_2S $lipo_{5k-2}$ rapidly accumulated in the spleen (**Figure 2.13**). The circulation half-life of H_2S $lipo_{5k-2}$, H_2S $lipo_{5k-6}$, and H_2S $lipo_{5k-12}$ was 4.4, 9.8, and 14.7

hours, respectively, making H_2S $lipo_{5k\text{-}12}$ suitable for a long circulating liposome loaded H_2S donor (**Figure 2.14, Table 6**). In the standard uptake value (SUV_{mean}) graph, which quantitatively calculated the H_2S lipos targeted to the spleen, the SUV_{mean} of H_2S $lipo_{5k\text{-}2}$ was significantly higher than that of H_2S $lipo_{5k\text{-}12}$. ($P < 0.001$). In the area under curve (AUC) of the SUV_{mean} graph, the AUC of H_2S $lipo_{5k\text{-}2}$ was significantly higher than that of H_2S $lipo_{5k\text{-}12}$ ($P < 0.001$). In the spleen to muscle ratio, H_2S $lipo_{5k\text{-}1}$ was significantly more accumulated than that of H_2S $lipo_{5k\text{-}6}$ and H_2S $lipo_{5k\text{-}12}$ ($P < 0.05$, $P < 0.05$, respectively) (**Figure 2.15**). We found a simple PEGylation strategy suitable for spleen-targeting by quantitatively analyzing the PET images and designated H_2S $lipo_{5k\text{-}2}$ as a spleen-targeting H_2S lipo (ST-H_2S lipo) and H_2S $lipo_{5k\text{-}12}$ as a long-circulating H_2S lipo (LC-H_2S lipo).

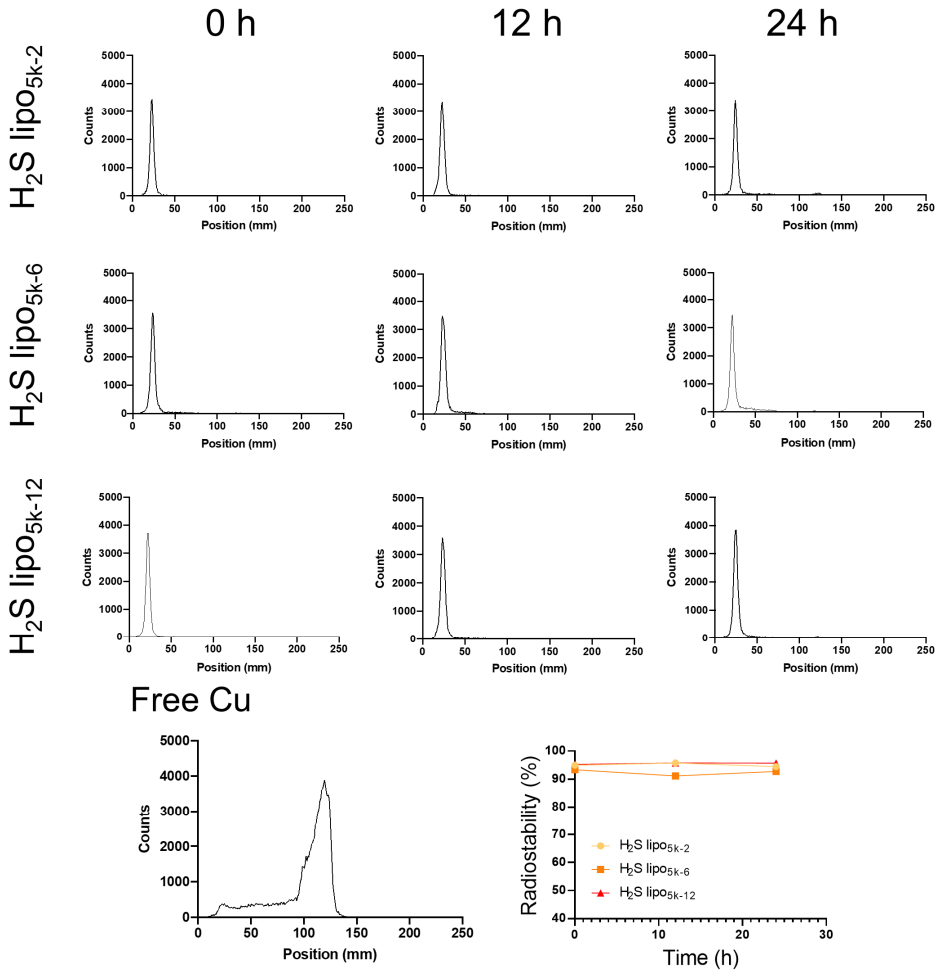

Figure 2.12 Radiochemical stability test of ^{64}Cu-H_2S lipo. ^{64}Cu radiolabeled H_2S lipo with 5k-1, 5k-3, 5k-6 and free ^{64}Cu were compared. The radiostability of compared group were calculated at 0h, 12h, and 24h. 5k: DSPE-PEG5k, 1: 1 mg, 3: 3 mg, 6: 6 mg.

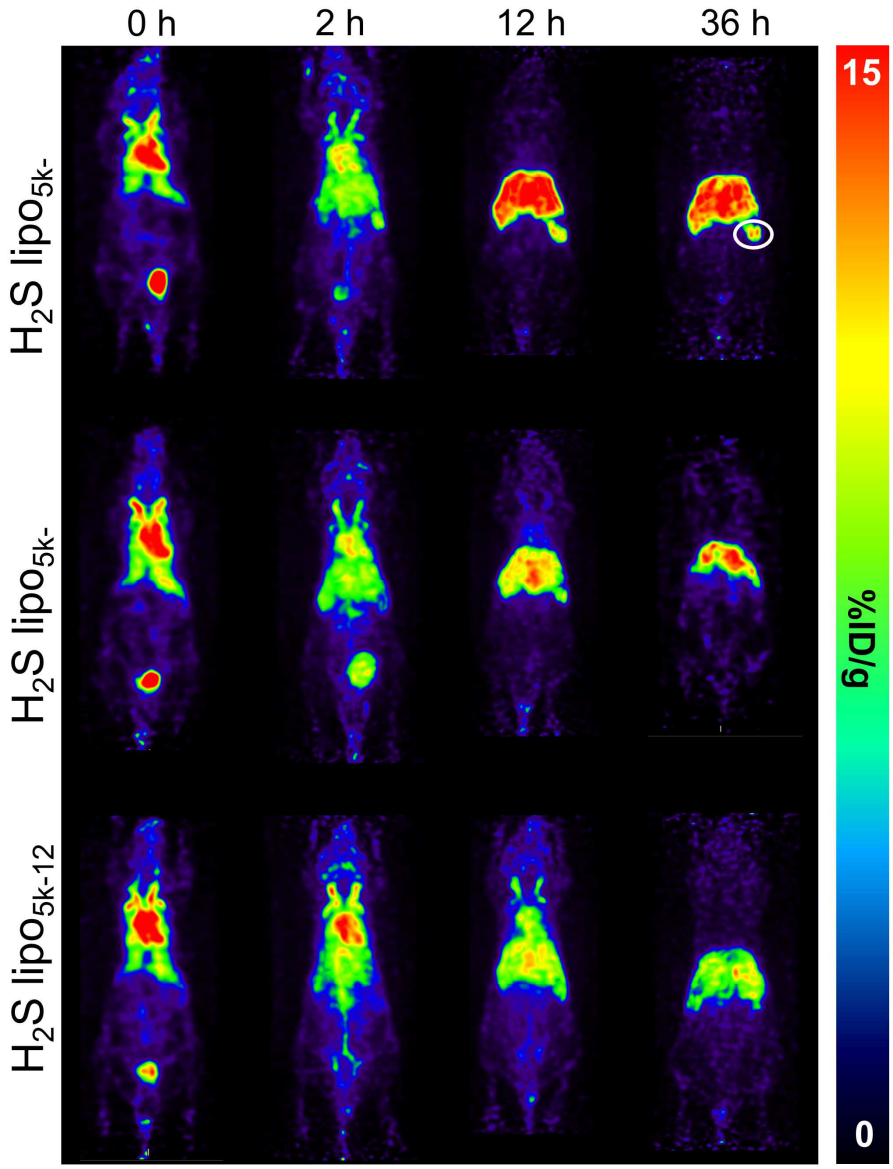

Figure 2.13 The in vivo PET images of ^{64}Cu radiolabeled H_2S lipo. The PET images were acquired using intravenously injected ^{64}Cu radiolabeled H_2S lipos which include H_2S lipo$_{5k\text{-}2}$, H_2S lipo$_{5k\text{-}6}$, and H_2S lipo$_{5k\text{-}12}$ (n = 3, respectively). The time points of image acquisition are 0, 2 hours, 12 hours, and 36 hours after injection. White circle indicates spleen.

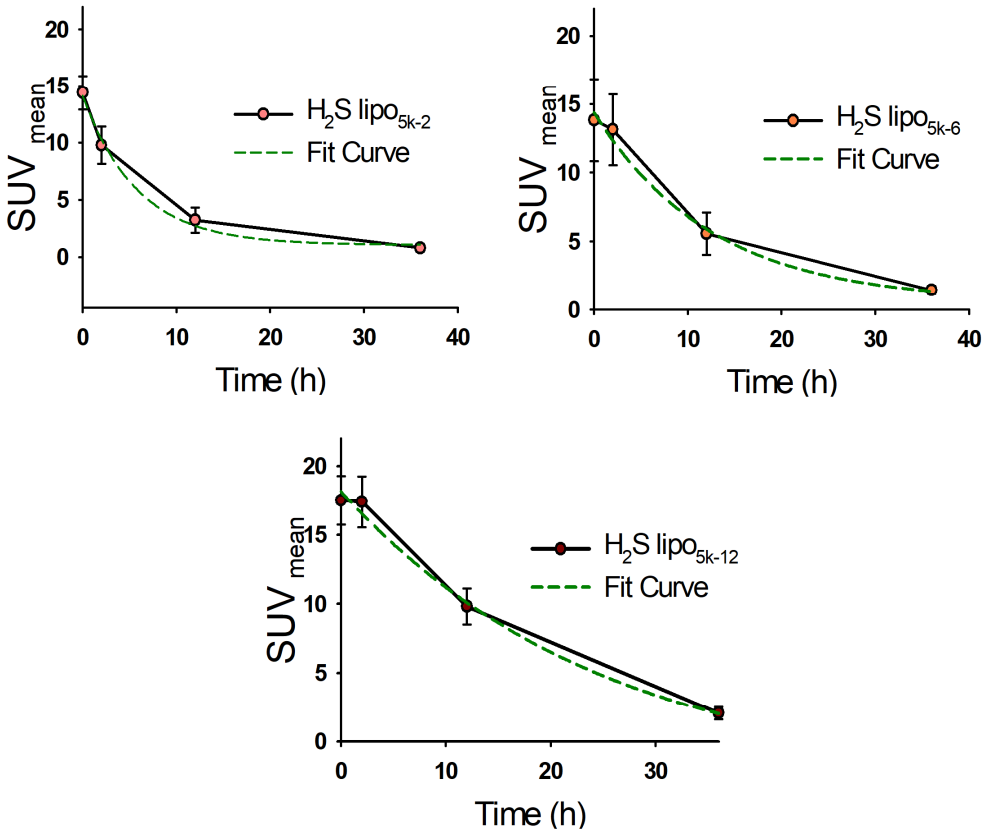

Figure 2.14 The time activity curve graphs of blood pool and indicate circulation half-life.

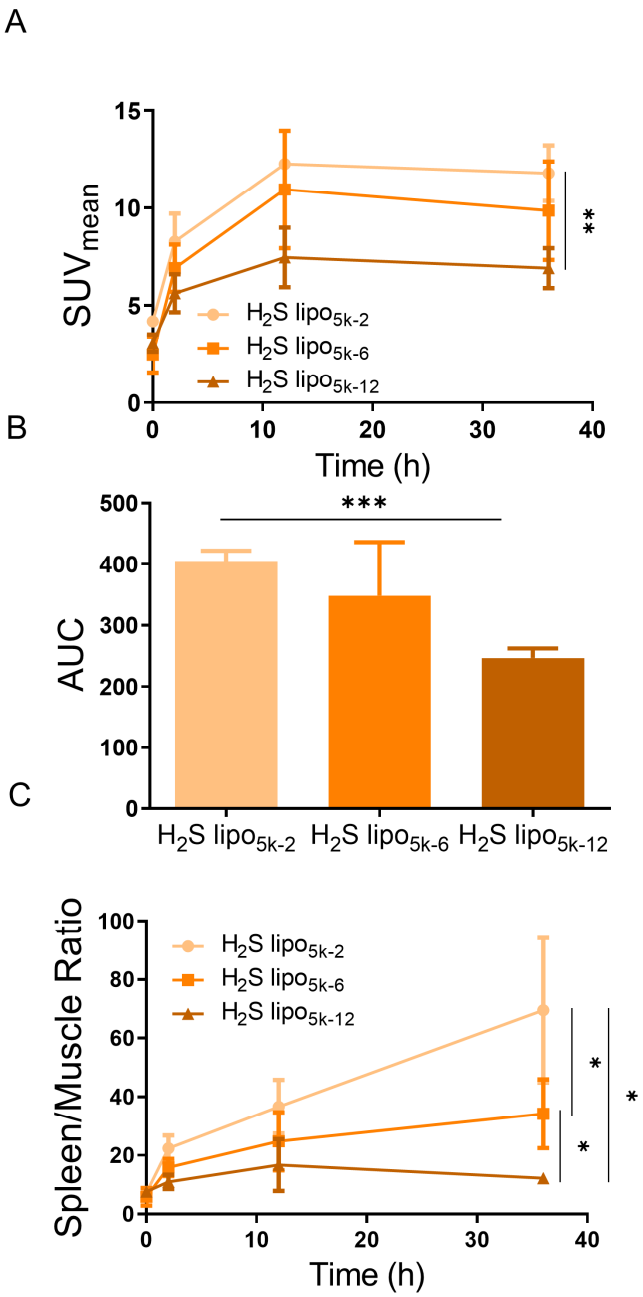

Figure 2.15 Quantitative analysis of in vivo PET images. The graph (A) indicates comparison of quantified spleen uptake. The graph (B) indicates comparison of quantified AUC of spleen uptake graph. The graph (C) indicates comparison of quantified spleen/muscle ratio. PET: Positron emission tomography *: $P < 0.05$, **: $P < 0.01$, ***: $P < 0.001$.

Group (PEG)	H_2S $lipo_{5k-2}$	H_2S $lipo_{5k-6}$	H_2S $lipo_{5k-12}$
Fitting equation $y=y_0+a*e^{-b\times}$ $R^2=c$	a: 13.0357 b: -0.0794 c: 0.997	a: 13.7958 b: -0.0794 c: 0.995	a: 21.0601 b: -0.0402 c: 0.996
Half-life ($t_{1/2}$)	4.4 hours	9.8 hours	14.7 hours

Table 6 The table of time activity curve data. The table includes fitting equation and half-life data

2.3.4 The in vivo analysis of splenic T_{reg} differentiation by ST-H_2S lipo

We also tested whether ST-H_2S lipo successfully delivers H_2S donors to the spleen (**Figure 2.16A**). We intravascularly injected saline, GYY4137, and ST-H_2S lipo each into mice. Next day, the mice were euthanized, and the spleens were collected. The extracted spleens were homogenized and reacted with $AgNO_3$. After the reaction, the spleen sample from the ST-H_2S lipo injected mice showed the darkest color and the highest O.D. among the compared groups (**Figure 2.16B, C**), which confirmed that ST-H_2S lipo can efficiently deliver H_2S donors to the spleen. Furthermore, we studied whether the delivered H_2S to the spleen affects the differentiation of immune cells using flow cytometry (**Figure 2.16A**). We observed changes in the differentiation of regulatory T cells (T_{reg}, $CD45^+FOXP3^+CD4^+$ T cells) among the splenocyte population. The ST-H_2S lipo injected group showed more T_{reg} differentiation than that of the saline and GYY4137 injected groups ($P < 0.01$ and $P < 0.001$, respectively) (**Figure 2.16B**).

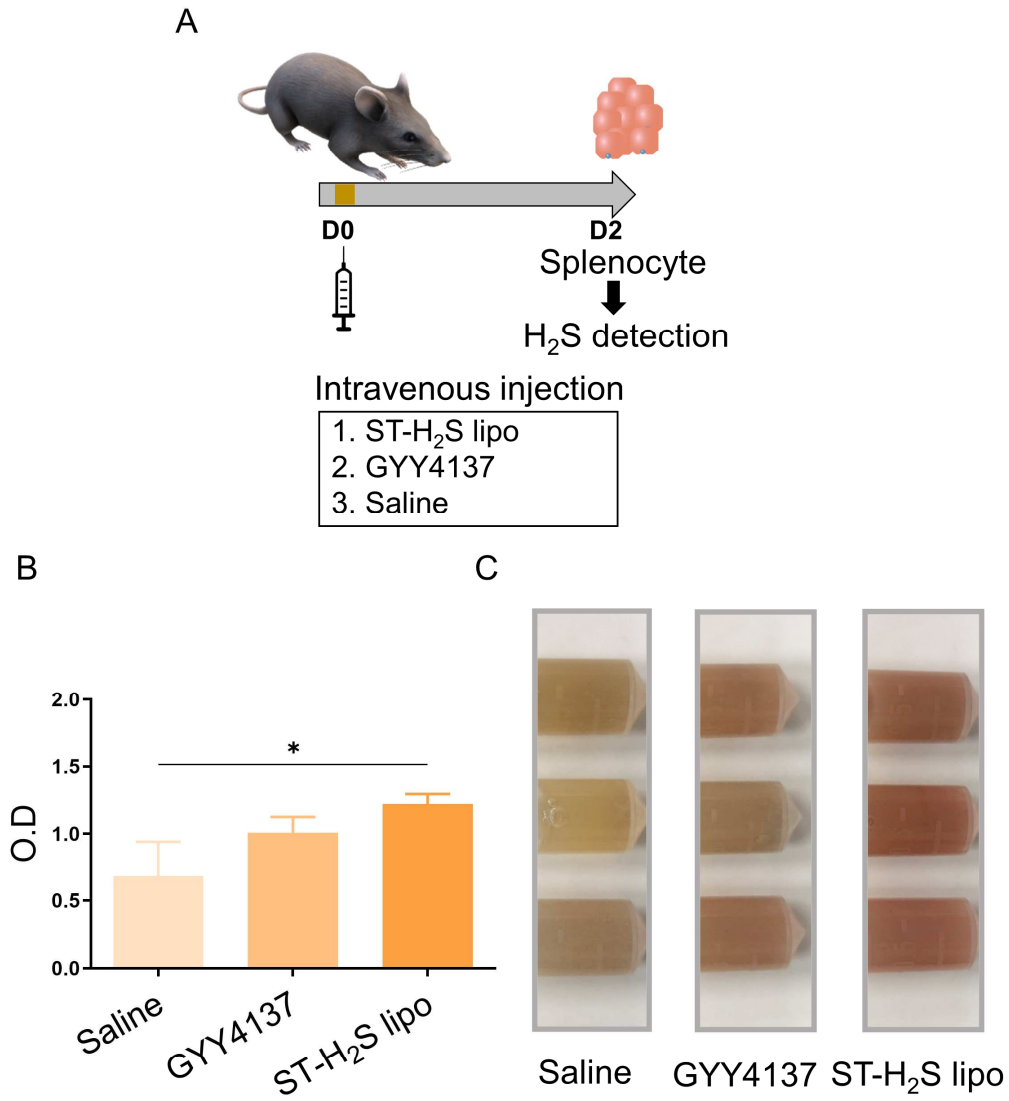

Figure 2.16 In vivo experiments of spleen targeting ability. A. The schematic design of spleen targeting ability of intravenously injected ST-H_2S lipo (N= 3). After 48 hours of intravenous injection, extracted spleen were homogenized to splenocytes. Splenocytes of saline, GYY 4137, and

ST-H_2S lipo were reacted with $AgNO_3$ then solution was calculated for O.D using 405 nm absorbance of microplate reader. B. The graph indicated that the optical density of saline, GYY4137, and ST-H_2S lipo C. The images were splenocytes with $AgNO_3$. Each tube is a spleen of each mouse.

*: $P < 0.5$.

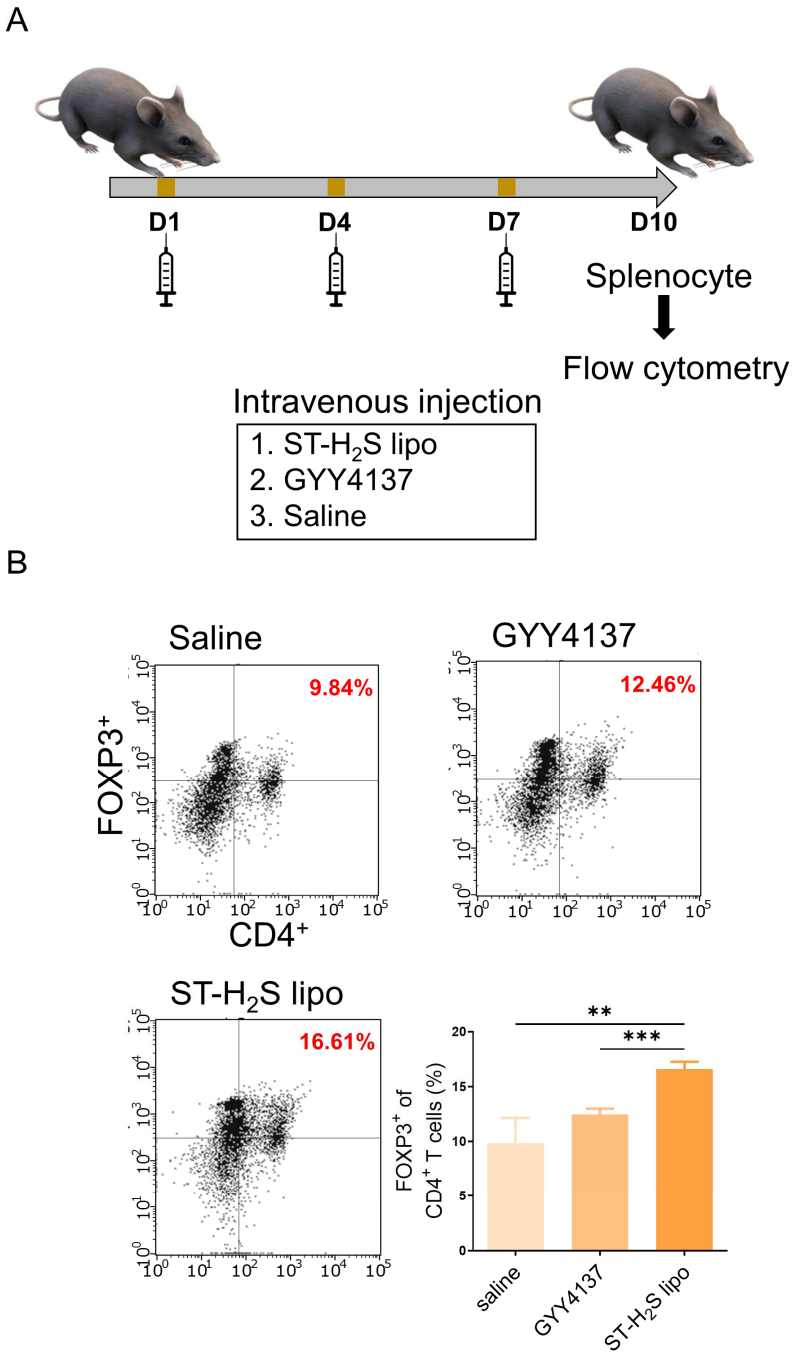

Figure 2.17 T_{reg} cell differentiation in spleen. A. The schematic design of comparing T_{reg} cell differentiation in spleen. The reagents are intravenously

injected every 3 days (N= 3) in normal mice. The spleen was extracted at day10, and then splenocyte are analyzed B. The dot plot of flow cytometry. The graph indicated that T_{reg} of ST-H_2S lipo is significantly more differentiated than GYY4137 ($P < 0.001$) and saline ($P< 0.01$). ST-H_2S lipo: spleen targeting H_2S lipo, T_{reg}: regulatory T cell, **: $P < 0.01$, ***:$P < 0.001$.

2.3.5 Reflecting properties of PEG in H_2S lipos

The PEG is the most widely used polymer for drug delivery. By adding PEG to nanoparticles, the effects of 1) preventing self-aggregation, 2) enhancing stability, and 3) extending circulation time are brought about. The PEG shapes a steric barrier on the surface of the liposome to inhibit membrane fusion, resulting in preventing self-aggregation and increasing stability. In the size stability test of H_2S lipo, it was confirmed that the size change tends to decrease as the mass ratio of PEG increases (**Figure 2.7**, **Table 5**). Also, PEG extends circulation time because it has excellent water solubility and reduces biological interaction. In in vivo PET images, the circulation half-life of H_2S $lipo_{5k\text{-}2}$ was 4.4 hours, and that of H_2S $lipo_{5k\text{-}12}$ was 14.7 hours, which increased more 3-fold changes (**Table 6**). From this, it can be seen that the circulation time increases as the PEG density of H_2S lipo increases. PEG reduces biological interaction because it has characteristics of a steric barrier and conformational cloud. In the fluorescence images of released H_2S, it was identified that as the PEG density increased, less H_2S was released (**Figure 2.9**). This may be due to the decrease in biological interaction with the increase in PEG.

H_2S lipos reflect the characteristics of PEG, which is non-ionic

hydrophilic polymer. First, in the result of zeta potential study, the non-ionic characteristic of PEG is reflected because the surface net charge becomes neutral as the PEG density of H_2S lipo increases (**Figure 2.6C**). Second, the size changes of H_2S lipo according to the PEG lengths was identified. At the same mass ratio (DSPC : PEG), it was confirmed that the size of H_2S lipos containing PEG; 2 kDa was smaller than that of H_2S lipos containing PEG; 5 kDa (**Table 5**). In addition, it is known that PEG affects drug loading efficiency. As the PEG density increases, the membrane permeability increases, and the loading of water-soluble drugs decreases. Conversely, it prevents the desorption of hydrophobic drugs. In the result of the loading efficiency experiment of H_2S lipo, it was confirmed that there was no significant difference according to PEG density (**Figure 2.6B**). It could be because GYY4137, the H_2S donor, is a water-soluble drug and can be dissolved in an organic solvent. To sum up, H_2S lipos showed different characteristics depending on the type and amount of PEG, reflecting the characteristics of PEG, a non-ionic hydrophilic polymer (74, 76, 84-88).

2.4 Summary

In chapter 2, we developed a simple spleen targeted delivery strategy for H_2S donor using one of the most widely used drug delivery systems, a PEGylated liposome, through functional evaluations by in vitro and in vivo experiments. First, through various characterization methods, H_2S lipos with high stability among PEGylation strategies were identified, and excellent loading ability and no cytotoxicity were confirmed. In in vitro experiments, H_2S lipos showed superior H_2S release ability and inducing anti-inflammatory differentiation of macrophage cell line. In vivo PET imaging quantitatively showed that H_2S $lipo_{5k\text{-}2}$ has excellent spleen targeting ability. In the in vivo studies using normal mouse, we identified a significant uptake of spleen of ST-H_2S lipo and distinctive ability of H_2S release. In addition, ST-H_2S lipo successfully induced T_{reg} differentiation in the spleen compared to the unloaded H_2S donor. These results suggest the potential of the immunomodulatory function of ST-H_2S lipo and lead us to the next experiment.

Chapter 3.

Therapeutic effect of the systemic immune modulator in the colitis model

3.1 Backgrounds

Gasotransmitters are endogenously produced by various enzymes in mammalian cells. NO production is catalyzed from L-arginine by a family of NO synthases (NOSs). CO production is catalyzed by a family of ham oxygenases (HMOXs, also known as HOs) which drives oxidative degradation of ham. H_2S production is catalyzed by CBS, CSE, and MPST (also known as MST) (11, 89, 90). Studies have reported the expression of gasotransmitter related enzymes in UC patients and the colitis model. For H_2S related enzymes, their degree of expression is dissimilarly reported. Kyle et al. reported that CSE expression and H_2S synthase are significantly increased in the colitis model (>12-fold and >7-fold, respectively) (91). Additionally, Hirata et al. reported that the expression of CBS and CSE is significantly increased (92). These studies suggested that the increased H_2S by up-regulated enzymes promotes ulcer healing and ameliorates inflammation as an anti-inflammatory molecule and not pathogenesis. In contrast, Wallace et al. reported that the expression of CBS and CSE is significantly decreased in severe colonic injury of the colitis model (18). De et al. reported that the expression of CBS mRNA and protein in the colitis model is significantly down-regulated and H_2S levels decreased (93). In UC patients, Shanwen et al. reported that CBS expression is decreased

compared to normal sites (94). To sum up, studies have shown that 1) expression of H_2S related enzymes could be increased or decreased, and 2) increased H_2S by up-regulated enzymes drives anti-inflammatory reaction. This evidence could be one of the rationales to use H_2S donor therapeutics in UC. In CO related enzymes, HMOX-1 has been mainly studied. In UC patients, HMOX-1 expression was heterogeneous according to severity. HMOX-1 expression is increased at the site of a mild inflammatory reaction. On the other hand, HMOX-1 expression is decreased at the site of a severe inflammatory reaction (95). These results may explain our observation using transcriptomics data that showed an increased expression of HMOX-1 in the colitis model but decreased the expression in patients with UC. Because CO is decreased in severe UC, it could be a therapeutic material as well. Recently, it has been reported that CO delivery by gas-entrapping materials induced a therapeutic effect in the DSS induced colitis mouse model (96). NO has long been known to be involved in inflammatory reactions in UC. NO especially leads to tissue injury by oxidative metabolism and is produced in activated macrophages and neutrophils. Additionally, the NOS activity in UC patients was 10-fold higher than in the normal group (97, 98), which is a similar finding with our transcriptomics data analysis in the colitis model and patients with UC.

In gastrointestinal systems, the effects of H_2S in immune modulation are well reported in various pathological conditions. Induction of a stomach ulcer in a rat resulted in an increased endogenous H_2S level, and an inhibitor of endogenous H_2S reduced the ulcer healing process (19). In the colitis model, H_2S donors showed notable therapeutic effects. Inhibiting the endogenous synthesis of H_2S resulted in severe mucosal injury and inflammation of the colon. In contrast, H_2S donors significantly reduced the colitis severity and proinflammatory tumor necrosis factor (TNF)-α cytokine (18). Furthermore, delivering H_2S into the colon helps to restore the microbiota biofilm and increases the mucus granules (17). Among immune cells, T_{reg} has an important role in the pathogenesis of IBD (5). In T_{reg} depleted mice, inflammatory cytokine and aggravated inflammation of the intestine were increased. In addition, T_{reg} cells are responsible for inhibiting the interaction between T cell and antigen presenting cells (APCs) (22, 56, 79, 99). Additionally, IBD patients showed apoptosis of T_{reg} at the inflammation site of the colon (100-103). Therefore, we selected T_{reg} differentiation as a key immune modulation marker to assess the protective effect of the ST-H_2S lipo in the DSS induced colitis model in this study.

3.2 Material and Methods

3.2.1 Transcriptomics-level analysis of gasotransmitters

The RNA expression profiles of UC patients (GSE38713) and DSS induced colitis model (GSE31906) were derived from gene expression omnibus (GEO) of national center for biotechnology information (NCBI). Investigated RNA expression of gasotransmitter related enzymes were cystathionine-beta-synthase (CBS), cystathionine-gamma-lyase (CTH), 3-mcaptopyruvate sulfurtransferase (MPST), nitric oxide synthase 1(NOS1), nitric oxide synthase 2 (NOS2), heme Oxygenase 1 (HMOX1), heme oxygenase 2 (HMOX2). The CBS, CTH, and MPST released H_2S. NOS1 and 2 released NO. HMOX1 and 2 released CO. In GSE38713, rectum or sigmoid colon was extracted from UC patients (n = 23) and control group (n = 20) for RNA expression analysis. Subjects which were diagnosed at least 6 months before were selected to UC patients. Subjects which had no lesion or mild symptoms in gastrointestinal tracts were selected to control group. In GSE31906, distal colon (about 8 cm) was extracted from colitis model (n = 27) and control group (n = 9). The raw data of GSE38713 and GSE31906 was analyzed using Bioconductor tool of R software (Parteck Inc, MO, USA) (104, 105).

3.2.2 In vivo biodistribution of fluorescent H_2S lipo in DSS induced colitis model

Fluorescent H_2S lipo was used to compare biodistribution between ST-H_2S lipo and LC-H_2S lipo in DSS induced colitis model. Fluorescence dye, 1,1’-dioctadecyl-3,3,3',3’-tetramethyl-indotricarbocyanine iodide (DiR), was dissolved in organic solvent with H_2S lipo composite before evaporate phase. The 8-week-old C57/BL6 mice were induced colitis model using DSS. The reagents were intravenously injected to colitis model mice at 7 days from giving DSS. Next day, injected mice were sacrificed and dissected organ. The collected organs were heart, muscle, lung, kidney, liver, spleen, small intestine, and colon. Fluorescence images of organs were acquired by IVIS instrument. All fluorescence images of organs were quantified using living image 2.5.

3.2.3 Animals and DSS induced colitis model

The C57BL/6 female mice were purchased from the Institute for Experimental Animals, College of Medicine, Seoul National University. All

experimental protocols were screened and approved by the Institutional Animal Care and Use Committee of Seoul National University. All mice were housed in specific pathogen free (SPF) facility. The colitis model was induced by 3% DSS (36-50 kDa). The mice received 3% DSS water for 7 days. Then normal drinking water were given for 5 days. All animal experimental protocols were approved by the Institutional Animal Care and Use Committee of Seoul National University.

3.2.4 DSS induced colitis model treatment

The 8-week-old C57/BL6 female mice were induced colitis model using DSS. Tap water with 3% DSS was given except for normal group (106). 3% DSS water was given up to 7 days in the study for comparing groups which are normal, saline, GYY 4137 (60 μM and 100 μM), ST-H_2S lipo (60 μM and 100 μM) (107). In comparison test between ST-H_2S lipo and LC-H_2S lipo, 3% DSS water was given up to 6 days in the study. The reagents were intravenously injected every day or every other day (**Figure 3.1**). The weight change (%) was daily recorded for checking disease condition. The colitis models were sacrificed using CO_2 chamber. The spleen and colon were extracted. The red blood cell (RBC) lysis buffer was used when spleen

was extracted. The whole colon length was examined for comparing contraction by inflammation. Distal 3 cm of colon samples were used to colon weight and H&E staining. The colon per length was examined for granular immune cell accumulation. The histological analysis was conducted using H&E images of colon. The method of inflammation score was performed according to the reference (57, 108). The score is marked by 0 to 11. The categories of inflammation score are severity of inflammation (1 to 4), extent of inflammation (1 to 3), presence of epithelial hyperplasia (0 or 1), and presence of ulceration (0 or 3).

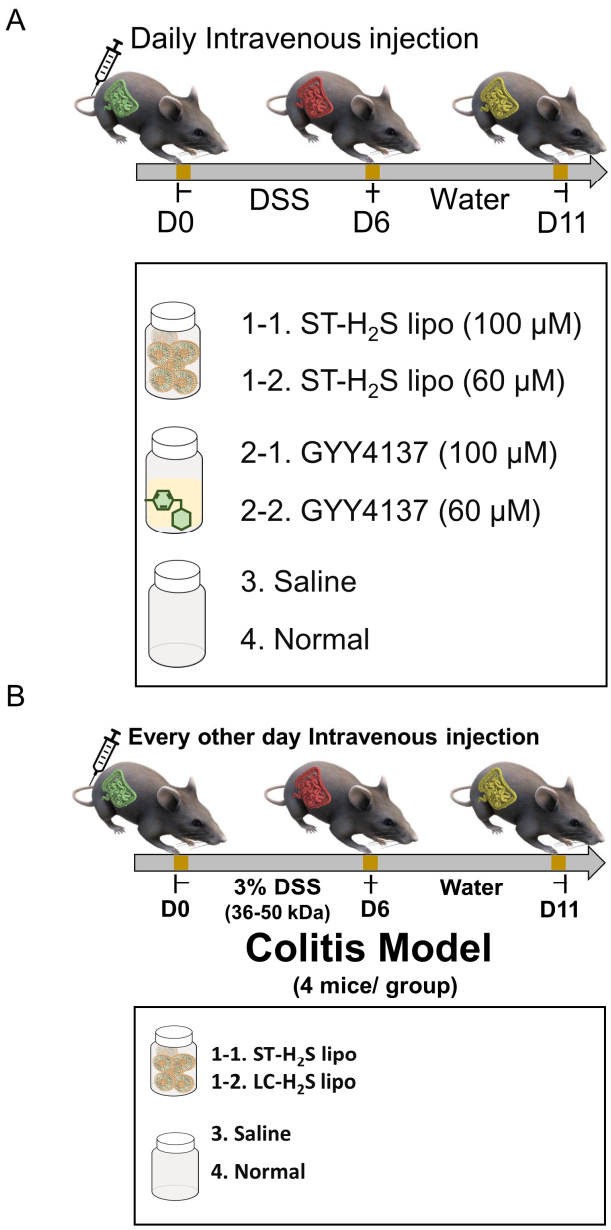

Figure 3.1 The schematic design of therapeutic experiments in colitis model. A. The comparison of therapeutic effect between normal, saline, GYY4137, and H_2S lipo in DSS induced colitis model. B. The comparison of therapeutic effect between normal, saline, ST-H_2S lipo, LC-H_2S lipo in DSS induced colitis model.

3.2.5 Immunofluorescence

The extracted spleen and distal colon were stored in 4% paraformaldehyde solution. After paraffin blocking, the paraffins were sectioned to 4 μm thickness. The sectioned slices were processed by several phase for immunofluorescence. The xylene was used to remove paraffin in tissue and then ethanol with serial concentration was used to remove xylene in tissue. The distilled water was used between each procedure. For antigen retrieval, sectioned tissue was incubated with 0.1% of trypsin for 25 min at 37 ℃. Then 0.1% of Triton X-100 was used to permeabilization for 10 min. The 10% fetal bovine serum was used for blocking. After procedure of antibody incubation overnight at 4 ℃, Hoechst 33342 was used to stain nuclei for 10 min. All Images were acquired using confocal scanning microscope.

3.2.6 Statistical analyses

The statistics were performed using GraphPad Prim 8 statistical analysis. Student's T tests or Mann- Whitney tests were used to compare RNA expression differences from GEO data. One-way analysis of variance

(ANOVA) with Tukey post hoc test was used to compare three or more groups. The differences with $P < 0.05$ were considered significant.

3.2.7 Comparison of H&E-stained images and fluorescent images

It is widely accepted that hematoxylin and eosin (H&E) staining can exhibit histological characteristics in diverse tissues such as lymphoma, breast cancer, and prostate cancer. When identifying spatial clusters from H&E-stained images, various clustering algorithms, including K-means algorithm, Watershed algorithm and Otsu thresholding method, have been proposed. Among them, K-means algorithm is most popular. Spleen tissues are especially characterized by the structure of red pulp, white pulp, and marginal zone, so it is expected that identification of these histological structures through clustering algorithms can be easily performed. K-means clustering was used according to the literature. After defining a patch of 32 × 32 size around each pixel in a H&E staining image, 512 features were extracted for each patch by using the VGG16 pre-trained CNN model. After that, K-means clustering was applied to cluster pixels in the image. K was set as 5 to represent background, border of each tissue, red pulp, marginal zone, and white pulp, and then the border of each tissue was also indicated as the background. Lastly, each defined section of the H&E image was

compared with the corresponding fluorescence image to quantify the amount of fluorescence in each histological region.

3.3 Results and Discussion

3.3.1 Transcriptomics-level evidence for the potential of H_2S based therapeutics in ulcerative colitis

To explore the potential of H_2S based therapeutics in UC, we examined the gene expression of H_2S synthesizing enzymes in patients with ulcerative colitis (UC) and in the mouse model of colitis. H_2S is synthesized by three enzymes, cystathionine-beta-synthase (CBS), cystathionine-gamma-lyase (CTH), and 3-mercaptopyruvate sulfurtransferase (MPST) (109). In both the UC patients and mouse model of colitis, gene expressions of H_2S synthesizing enzymes were significantly reduced compared to those of the normal control (**Figure 3.2**) ($P < 0.0001$, all graphs). This observation could be one of the rationales to use H_2S donor therapeutics in UC patients. Meanwhile, the gene expression of the other gasotransmitters (NO and CO) synthesizing enzymes were not significantly decreased in colitis. In contrast to the H_2S synthesizing enzymes, the CO synthesizing enzymes, HMOX1 and HMOX2, showed a significantly higher expression in the colitis model

compared to the control group ($P < 0.0001$, $P < 0.001$, respectively). In the UC patients, HMOX1 expression was significantly lower than in the control group, and HMOX2 expression was not significantly different compared to normal tissue ($P < 0.0001$) (**Figure 3.3A**). Moreover, the NO related enzymes, NOS1 and NOS2, showed an increased expression in the mouse colitis model compared to the control group (**Figure 3.3B**) ($P < 0.0001$, all graphs). Taken together, H_2S is the only gasotransmitter whose related genes are downregulated in both the mouse model of colitis and patients with UC.

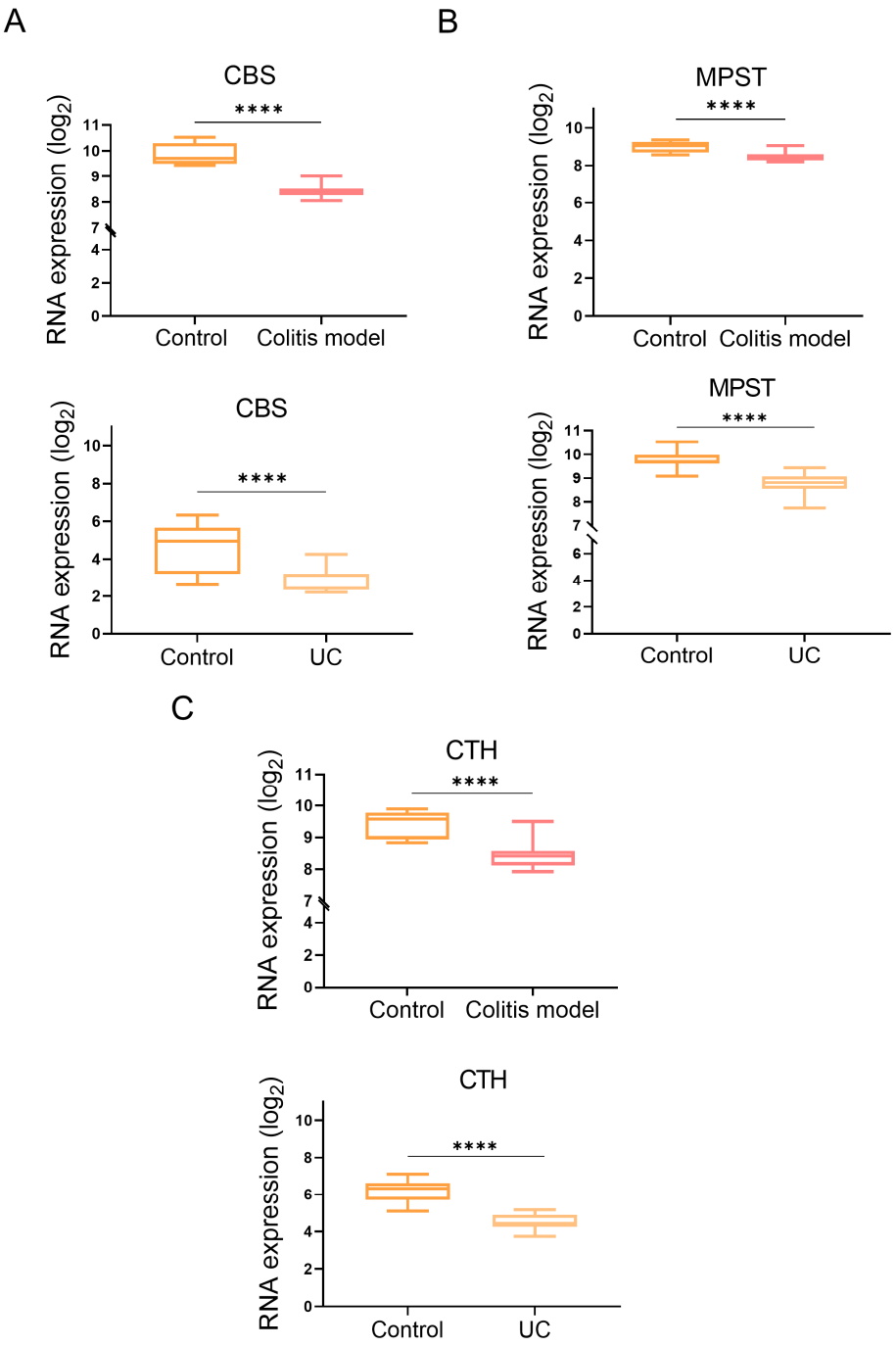

Figure 3.2 The RNA expression analysis of enzymes related with H_2S in both DSS induced colitis model and ulcerative colitis patients. The

comparison of expression of H_2S related enzymes which are CBS, MPST, and CTH. The graphs of DSS colitis model (top) and ulcerative colitis patient (bottom) indicate quantified RNA expression differences.

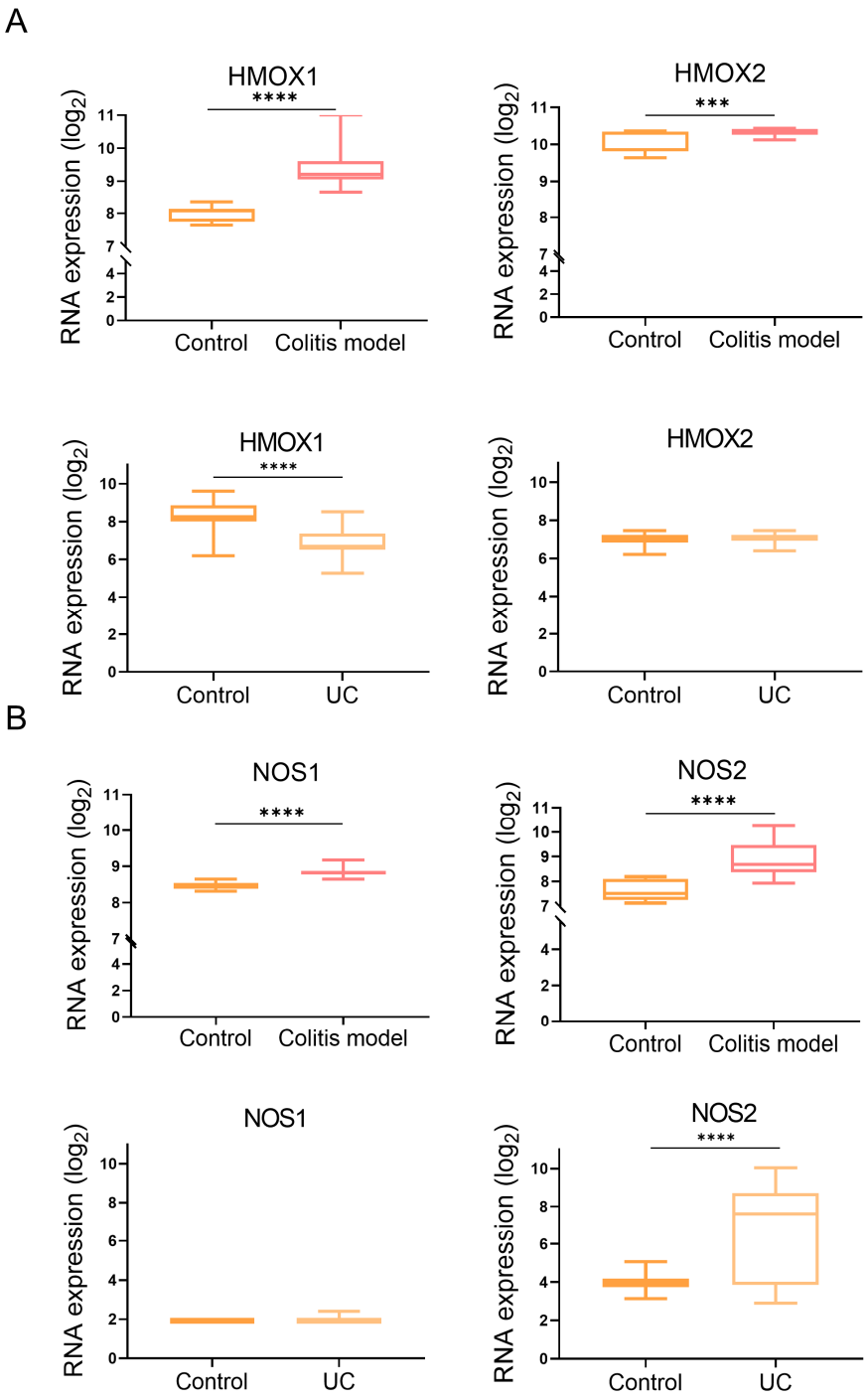

Figure 3.3 The RNA expression analysis of enzymes related with NO and CO. The graphs of DSS induced colitis model (top) and ulcerative colitis

patient (bottom) indicate RNA expression differences compared to control group A. The comparison of expression of NO related enzymes which are HMOX1 and HMOX2. B. The comparison of expression of CO related enzymes which are NOS1 and NOS2. ***: $P < 0.001$. ****: $P < 0.0001$.

3.3.2 In vivo biodistribution of H_2S lipo in a colitis model

Before we moved on to examine the therapeutic effect of H_2S lipo in a DSS-induced colitis model, we evaluated the biodistribution of ST-H_2S lipo and LC-H_2S lipo in the model. H_2S lipo as a versatile platform could signal fluorescence through the intercalation of DiR which is the one of the fluorescent dyes. Saline, DiR, DiR labeled ST-H_2S lipo and DiR labeled LC-H_2S lipo were each systemically administered into the colitis model. Organs were removed after 24 hours, and fluorescence images were obtained. We hypothesized that ST-H_2S lipo accumulates in the spleen, and LC-H_2S lipo accumulates more in the inflamed site of the colon due to a longer circulation time. As expected, ST-H_2S lipo showed prominent uptake in the spleen while LC-H_2S lipo showed minimal uptake ($P < 0.0001$). In the colon, both LC-H_2S lipo and ST-H_2S lipo accumulated in the colon, and the uptake was significantly higher for LC-H_2S lipo compared to ST-H_2S lip ($P < 0.0001$) (**Figure 3.4**). Consequently, we identified that the PEGylation strategies of H_2S lipo could be suitable for systemic or local immunomodulation in the colitis model. ST-H_2S lipo demonstrated an excellent spleen targeting ability and a moderate targeting ability to inflammatory sites which therefore may elicit a systemic and local

immunomodulatory effect. Meanwhile, LC-H_2S lipo may be suitable for delivery of H_2S to an inflamed site due to its long-circulating property.

We further explored the splenic distribution of H_2S lipo through analysis using fluorescent H_2S lipo and H&E images (**Figure 3.5**). We systemically administrated DiD labeld ST-H_2S lipo in normal mice. After 24 hours, spleen was extracted and used for the analysis. As expected, the fluorescence intensity was not shown in the control tissue. Also, the fluorescence signals were well aligned with the histological structures in the spleen. Through evaluating the amount of fluorescent signal in each compartment of the spleen, relatively high uptake of fluorescent nanoparticles in marginal zone and relatively low uptake in white pulp were observed. This suggests that immune cells in the Marginal Zone significantly affect the action of H_2S lipo.

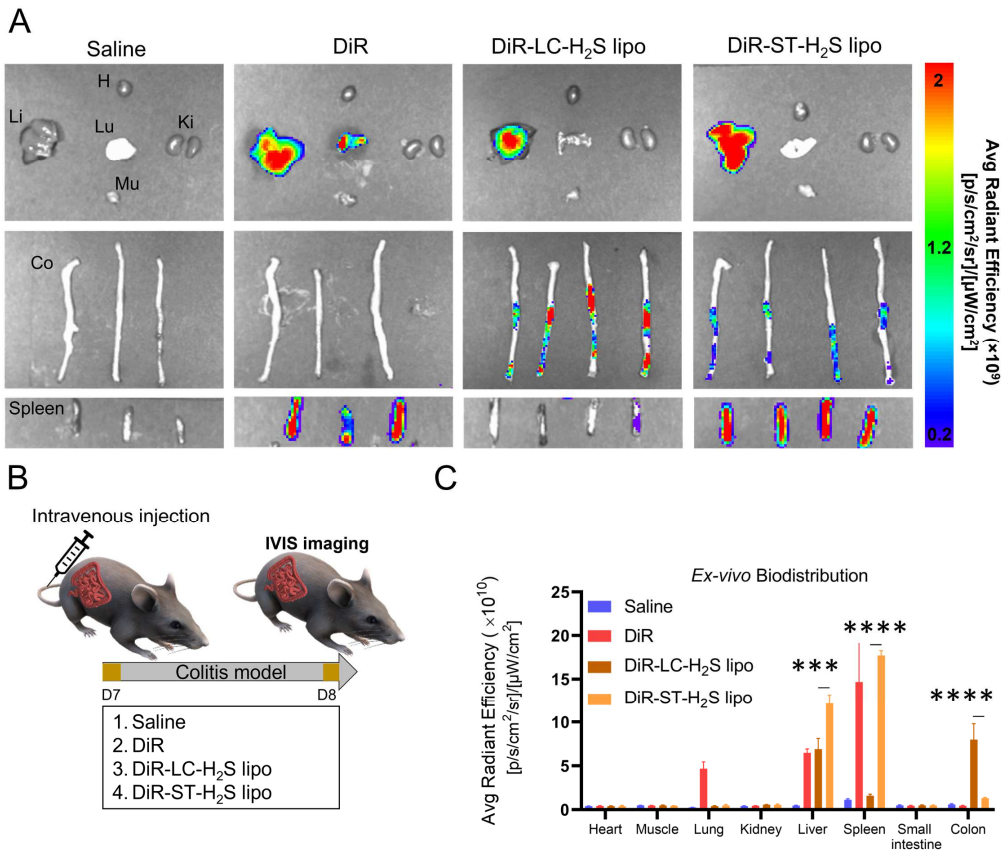

Figure 3.4 The ex vivo biodistribution in DSS induced colitis model. A. Biodistribution of saline injected group, DiR injected group, DiR-LC-H_2S lipo injected group, and DiR-ST-H_2S lipo injected group were compared (n = 3; saline and DiR, n = 4; DiR-LC-H_2S lipo, DiR-ST-H_2S lipo). The ex vivo fluorescence images showed organs which are heart (h), liver (Li), lung (Lu), kidney (Ki), muscle (Mu), colon (Co), and spleen. Organs were collected after 24 hours intravenously injection. Ex vivo fluorescence images were acquired by IVIS. B. The schematic design of ex vivo biodistribution imaging in DSS induced colitis model. C57BL/6 mice were

induced colitis using 3% DSS (36-50 kDa). C. The graph indicates comparison of quantified average radiant efficiency of extracted organs between saline, DiR, DiR-LC-H_2S lipo, and DiR-ST-H_2S lipo. ***: $P < 0.001$. ****: $P < 0$.

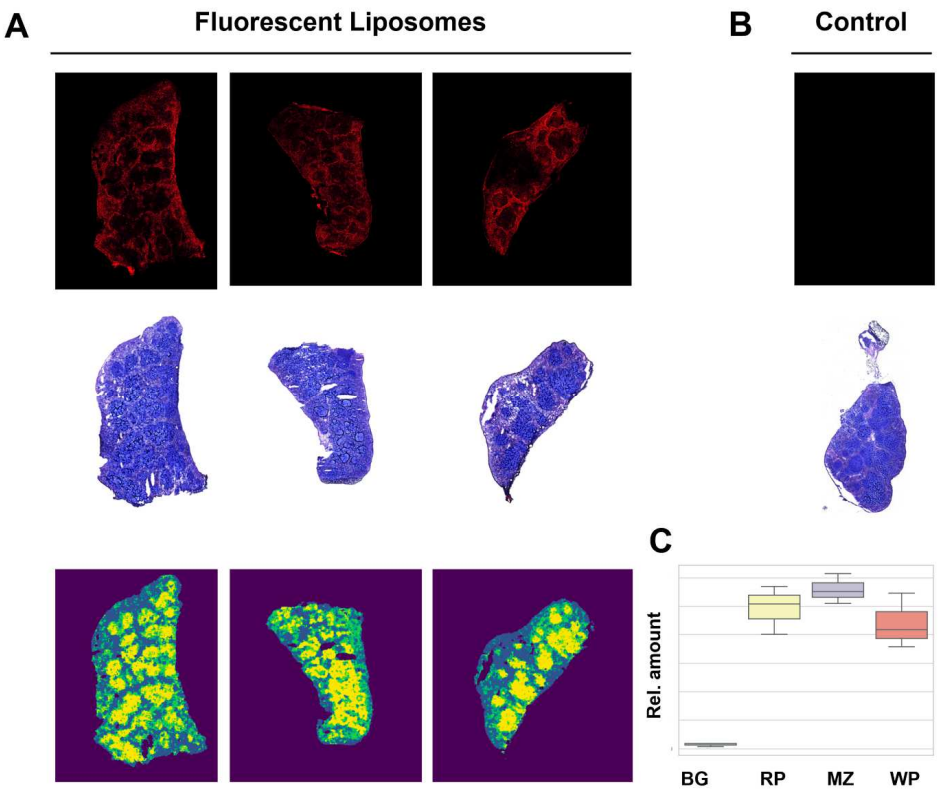

Figure 3.5 Analysis using images of fluorescent H_2S lipo and H&E images (A) Three spleen tissues from mice intravenously injected with DiD ST-H_2S lipo. From top to bottom, fluorescent images, H&E images, and resultant images from K-means clustering with H&E images were represented in order. (B) A spleen tissue from an untreated mouse. A fluorescent image of the same condition with a and a H&E image were represented. (C) Comparison of the amount of fluorescence intensity in each spatial compartment demarcated by background (BG), red pulp (RP), marginal zone (MZ), and WP (white pulp).

3.3.3 Therapeutic effect of H_2S lipo in the colitis model

The therapeutic effect of the H_2S lipo and unloaded H_2S donor was compared in the DSS-induced colitis model (**Figure 3.1A**). We daily intravenously injected GYY4137 (60 μM), GYY4137 (100 μM), ST-H_2S lipo (60 μM), and ST-H_2S lipo (100 μM) each. The weights change (%) between day 0 and day 11 for the normal, saline, GYY4137 (60 μM), GYY4137 (100 μM), ST-H_2S lipo (60 μM), and ST-H_2S lipo (100 μM) treated groups were 104.57 ± 4.3%, 71.84 ± 5.85%, 73.62 ± 3.01%, 73.34 ± 8.41%, 77.80 ± 4.15%, and 82.52 ± 10.28%, respectively. Only the ST-H_2S lipo (100 μM) treated group showed a statistically significant less weight reduction compared to the saline treated DSS colitis model (Repeated Measure Analysis Of Variance, Tuckey post-hoc test, P = 0.032) (**Figure 3.6**). The degree of inflammatory process for each group was observed with H&E stained slides of the colon epithelium. In the saline treated DSS induced colitis models, the epithelial structure was almost entirely destructed, and immune cells were massively infiltrated. In the GYY4137 (100 μM) treated models, although the mucosal structures were slightly more preserved compared to the saline treated model, mucosal ulcerations

were found. Moreover, immune cells were infiltrated into level of the muscularis mucosa. Interestingly, the ST-H_2S lipo (100 μM) treated models showed a preserved mucosa structure with intact goblet cells, and only a small number of immune cells were infiltrated (**Figure 3.8A**). Inflammation scores were measured with the H&E slides and compared between the groups. The GYY4137 treated models showed a significantly lower score than that of the saline treated model ($P < 0.01$). The ST-H_2S lipo (100 μM) treated group showed a significantly lower score than those of the saline and GYY4137 (100 μM) treated groups ($P < 0.0001$ and $P < 0.05$, respectively) (**Figure 3.8B**). Furthermore, alcian blue staining of the colon epithelium was performed to evaluate the mucin component after treatment. The GYY4137 treated models tended to preserve mucin to some extent, unlike the saline treated models in which the mucin component was barely detected ($P = 0.14$). The ST-H_2S lipo (100 μM) treated group showed a significantly higher alcian blue intensity than that of the saline treated group ($P < 0.5$) (**Figure 3.8**). In terms of colon length, only the ST-H_2S lipo group showed significant less contraction of colon compared to the saline group (ST-H_2S lipo (60 μM), $P < 0.05$; ST-H_2S lipo (100 μM), $P < 0.01$). In terms of colon weight and length which reflect the degree of inflammation of the colon, we identified that the ST-H_2S lipo (100 μM) treated model had a significantly

lower value compared to the saline, GYY4137 (60 μM), GYY4137 (100 μM), and ST-H_2S lipo (60 μM) treated models ($P < 0.001$, $P < 0.05$, $P < 0.01$, and $P < 0.05$, respectively) (**Figure 3.9**). To explore the systemic immune modulation effect, the T_{reg} proportion was evaluated in bone marrow and spleen samples after treatment (**Figure 3.11**). The ST-H_2S lipo (100 μM) treated group showed more T_{reg} differentiation than that of the saline treated group in the spleen ($P < 0.05$). Additionally, the ST-H_2S lipo (100 μM) treated group showed more T_{reg} differentiation of bone marrow compared to the saline and GYY4137 (100 μM) treated groups ($P < 0.05$, $P < 0.05$, respectively) (**Figure 3.11**). To sum up, we identified that ST-H_2S lipo showed a higher therapeutic effect than that of the unloaded H_2S donor in the DSS induced colitis model. ST-H_2S lipo was able to induce T_{reg} differentiation in the spleen and bone marrow.

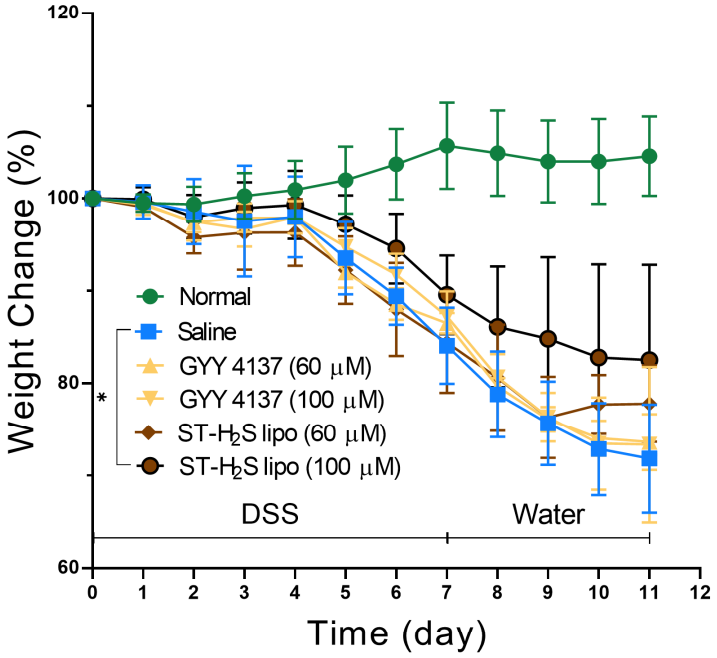

Figure 3.6 The comparison of weight change (%) between normal, saline, GYY4137, and H_2S lipo. The graph indicates comparison of weight change in DSS induced colitis model (n = 5, respectively). Weight change (%) shows the change based on 0 day.

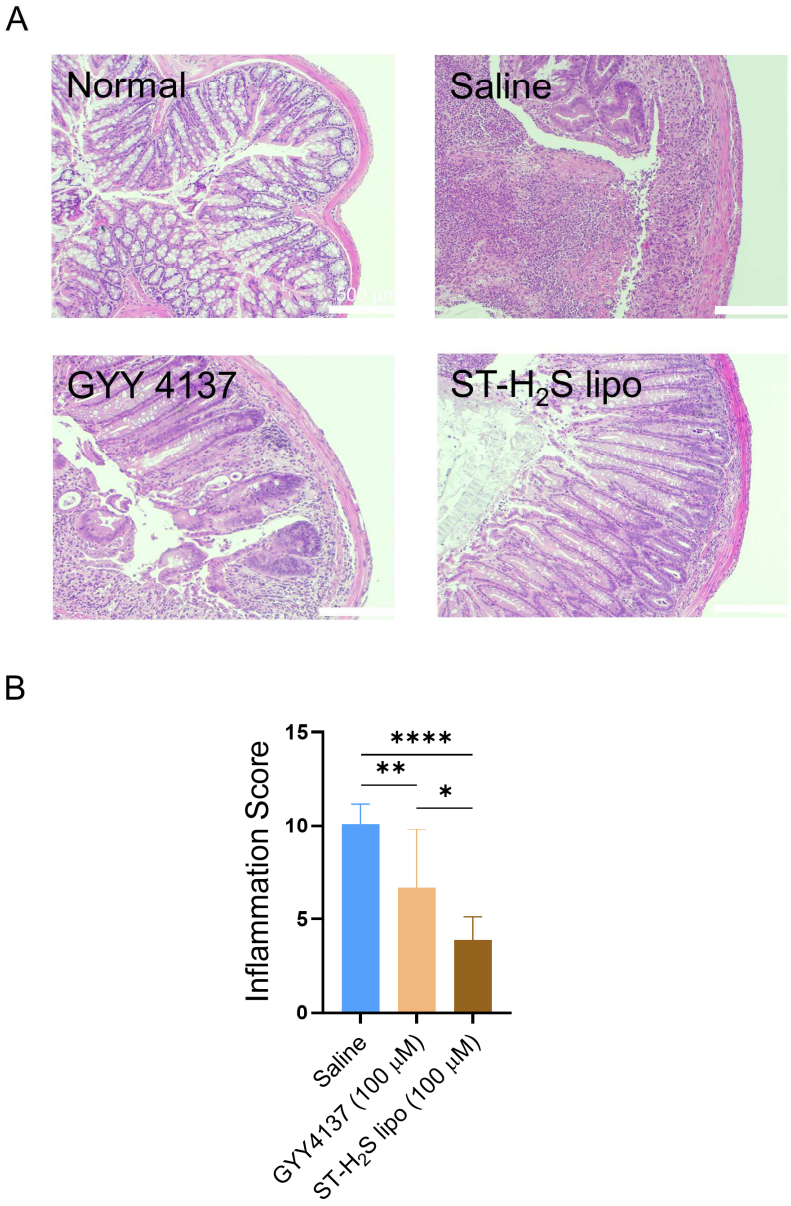

Figure 3.7 The comparison of inflammatory process between normal, saline, GYY4137, and H_2S lipo. A. The H&E images of colon of colitis model. B. The graph indicates comparison of inflammation score (n = 8, respectively). *: P < 0.05, **: P < 0.01, ****: P < 0.0001.

A

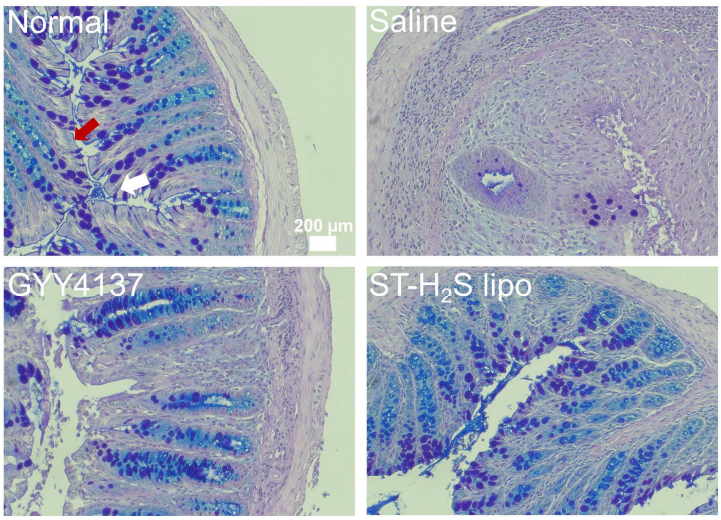

B

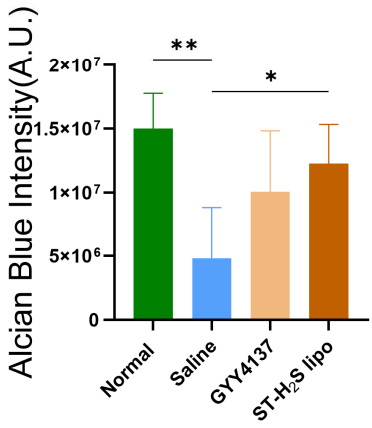

Figure 3.8 Alcian blue colon staining of treatment of DSS induced colitis model. A. mucin was stained by alcian blue. Mucin is included in mucus on the epithelial surface and goblet cells. The red arrow indicates mucus and white arrow indicates goblet cells. B. In the graph of alcian blue intensity, Normal and ST-H_2S lipo group are significantly more stained than saline group ($P < 0.01$ and $P < 0.05$, respectively). ST-H_2S lipo: spleen targeting H_2S lipo, *: $P < 0.05$, **: $P < 0.01$

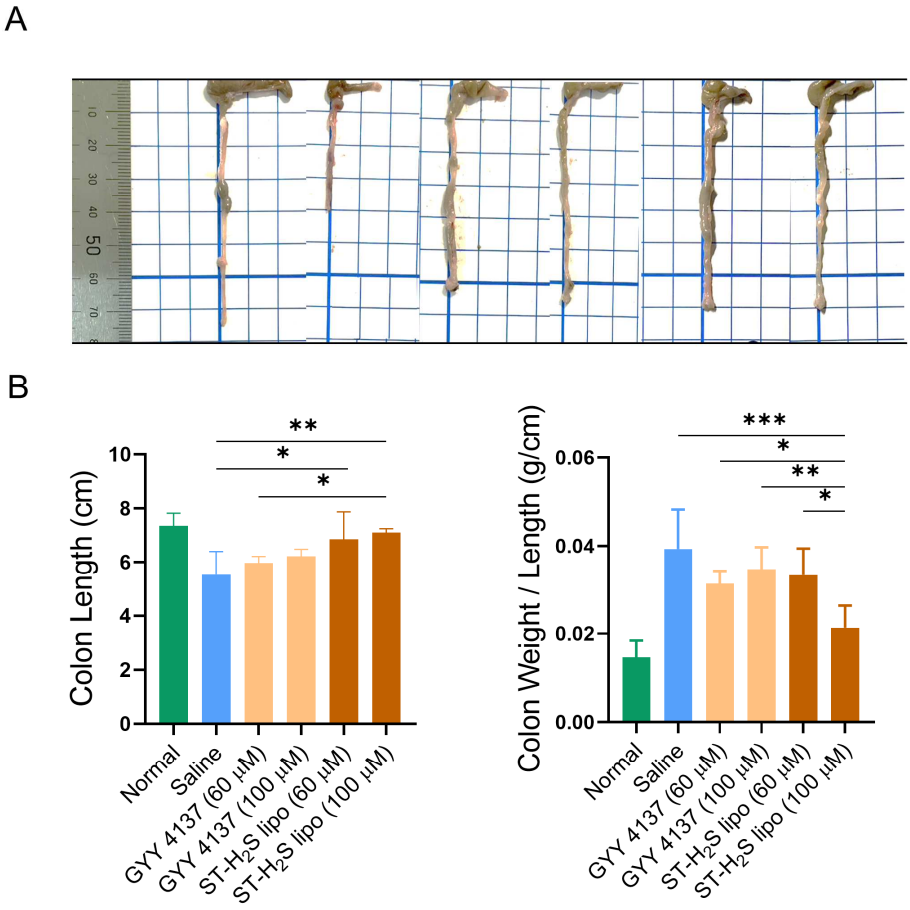

Figure 3.9 The comparison of colon lengths between normal, saline, GYY4137, and H_2S lipo. A. The representative images of extracted colon in colitis model. B. The graph (left) indicates comparison of colon length (n = 5, respectively). The graph (right) indicates comparison of colon weight/length (n = 5, respectively). *: $P < 0.05$, **: $P < 0.01$, ***: $P < 0.001$.

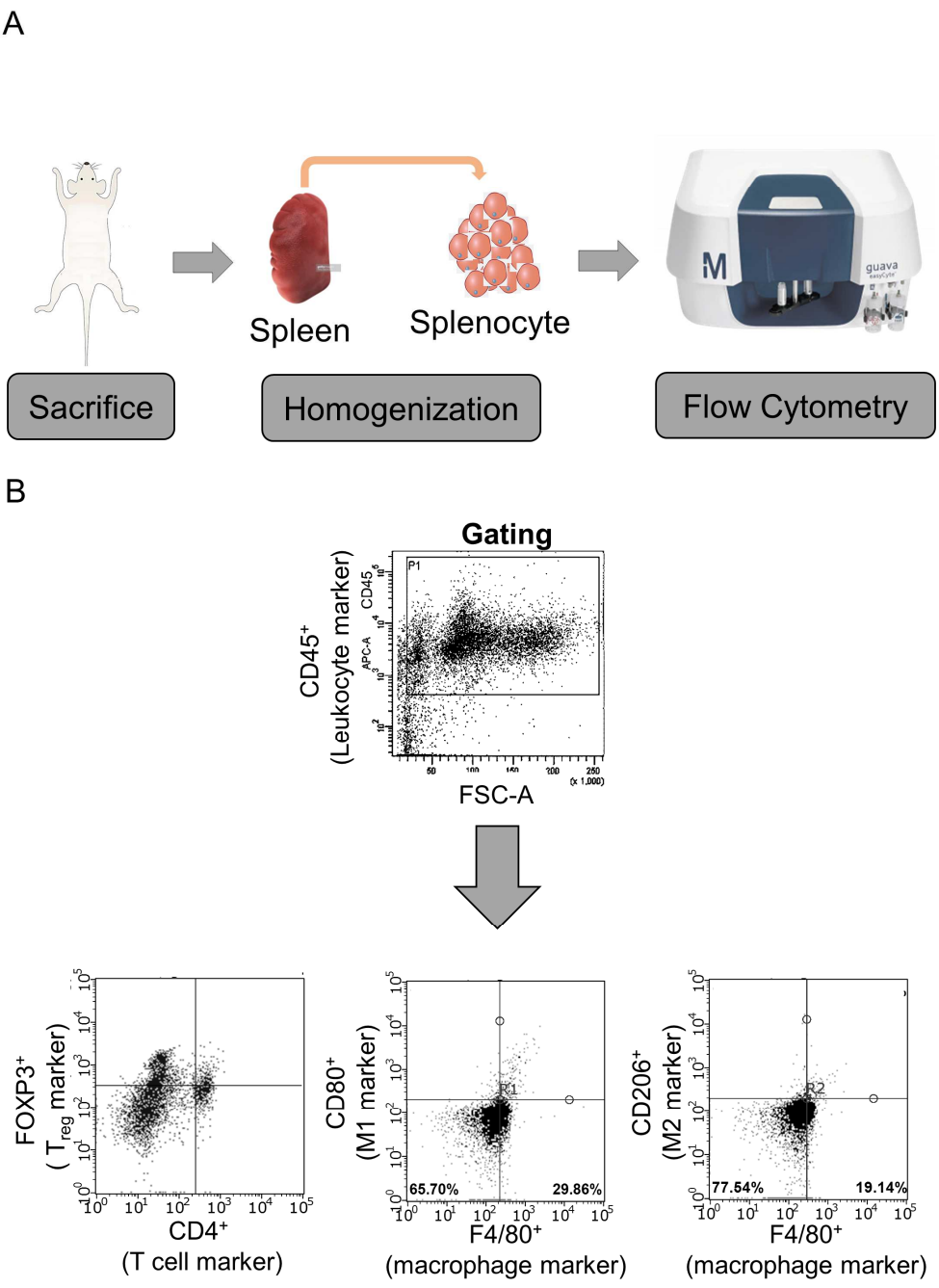

Figure 3.10 Gating Strategy of flow cytometry. A. Procedures of flow cytometry using splenocyte B. Gating strategy of flow cytometry analysis. CD45 antibody was used as leukocyte marker. CD4 and FOXP3 antibodies

were used as regulatory T cell markers. CD80 and F4/80 antibodies were used as M1 macrophage markers. CD206 and F4/80 antibodies were used as M2 macrophage markers.

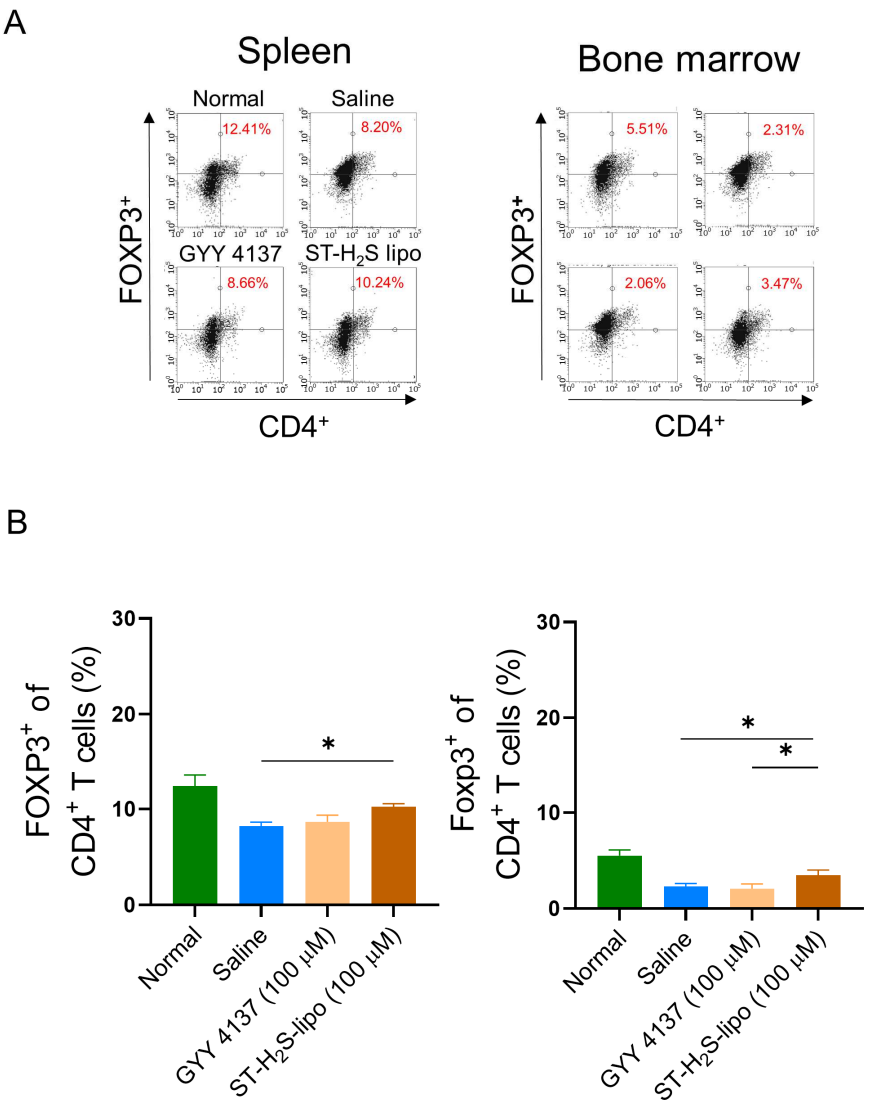

Figure 3.11 The comparison of T_{reg} differentiation between normal, saline, GYY4137, and H_2S lipo in spleen and bone marrow. CD4 and FOXP3 antibodies are used as T_{reg} cell marker. A. Dot plot of flow cytometry B. The graph (left) indicates comparison of quantified $FOXP3^+$ of $CD4^+$ T cells (%) in spleen (n = 3). The graph (right) indicates comparison of $FOXP3^+$ of $CD4^+$ T cells (%) in bone marrow (n = 3). *: $P < 0.05$.

3.3.4 Comparison of therapeutic effect of colitis model between ST-H_2S lipo and LC-H_2S lipo

We further explored the therapeutic effects of ST-H_2S lipo and LC-H_2S lipo in the DSS induced colitis model. The weights change (%) at 10 days for the normal, saline, ST-H_2S lipo, and LC-H_2S lipo groups was 102.61 ± 4.63, 75.62 ± 3.34, 84.16 ± 8.39, and 76.3 3± 7.76, respectively (**Figure 3.1B**, **Figure 3.12**). The ST-H_2S lipo treated group showed a significantly less weight change compared to the saline treated control group (Repeated Measure Analysis Of Variance and Tuckey post-hoc test, P = 0.02). However, the LC-H_2S lipo treated group showed no significant difference in weight change compared to the saline treated control group (P = N.S.) (**Figure 3.12**). In the H&E staining, both the ST-H_2S lipo and LC-H_2S lipo treated groups showed less immune cell infiltration and epithelial destruction compared to the saline treated control group (**Figure 3.14**). Moreover, ST-H_2S lipo had a lower inflammation score compared to the saline and LC-H_2S lipo treated groups ($P < 0.0001$, $P < 0.01$; respectively) (**Figure 3.14**). In the comparison of the colon length, only the ST-H_2S lipo treated group showed significant differences compared to the saline treated group ($P < 0.05$). For the colon weight and length, the ST-H_2S lipo treated group had a

significantly lower colon weight and length compared to the saline treated group ($P < 0.05$) (**Figure 3.15**). To assess the systemic immune modulation effect, differentiation of T_{reg}, M1, and M2 macrophages in the spleen was evaluated using flow cytometry. Unlike LC-H_2S lipo, ST-H_2S lipo significantly induced more T_{reg} differentiation than that of the saline group ($P < 0.05$). The ST-H_2S lipo treated group tended to have less M1 differentiation ($F4/80^+$ $CD80^+$) compared to the saline treated group ($P = 0.053$). Additionally, the ST-H_2S lipo treated group tended to have higher M2 ($F4/80^+$ $CD206^+$) differentiation compared to the saline treated group ($P = 0.15$) (**Figure 3.16**). In spleen and mucosal tissues, T_{reg} differentiation was assessed using T_{reg} immunofluorescence images. In the spleen, the ST-H_2S lipo treated group showed a brighter signal compared to the saline treated group ($P < 0.05$; **Figure 3.17**). In the colon, both ST-H_2S lipo and LC-H_2S lipo induced to a greater degree more T_{reg} differentiation than that of the saline group ($P < 0.001$ and $P < 0.0001$, respectively) (**Figure 3.17**). Lastly, serum markers related to the inflammatory process were compared between the groups (ST-H_2S lipo, LC-H_2S lipo, and saline treated DSS induced colitis model groups and the normal group). While C-reactive protein (CRP), a marker for systemic inflammation, was significantly higher in the saline treated group compared to the normal group ($P < 0.0001$), and only the ST-

H_2S lipo treated group showed a significantly lower CRP concentration compared to the saline treated group ($P < 0.05$), indicating its effect in systemic immune modulation. The ST-H_2S lipo treated group tended to have a lower concentration of CRP compared to the LC-H_2S lipo treated group ($P = 0.18$). Moreover, IL-6, TNF-α, and pro-inflammatory cytokines were significantly higher in the saline treated groups ($P < 0.0001$, $P < 0.0001$, respectively), and their concentrations were significantly lower in both the ST-H_2S lipo and LC-H_2S lipo treated groups compared to the saline treated group (IL-6, $P < 0.0001$ and 0.0001; TNF- α, $P < 0.001$ and $P < 0.0001$, respectively). The ST-H_2S lipo treated group tended to have a lower concentration of IL-6 compared to the LC-H_2S lipo treated group ($P = 0.18$). Furthermore, IL-4, an anti-inflammatory cytokine, was significantly higher in both the ST-H_2S lipo and LC-H_2S lipo treated groups compared to the saline treated group ($P < 0.01$ and $P < 0.05$, respectively) (**Figure 3.18**). Finally, we examined the histology of the major organs after the treatment to assess the potential in vivo toxicity of ST-H_2S lipo. There was no overt organ damage in the ST-H_2S lipo or ST-H_2S lipo treated group (**Figure 3.19**). Taken together, we found that 1) ST-H_2S lipo has a superior protective effect compared to unloaded GYY4137, and 2) ST-H_2S lipo showed a higher protective effect compared to LC-H_2S lipo, potentially due to a higher

systemic immunomodulatory effect (**Figure 1.3**).

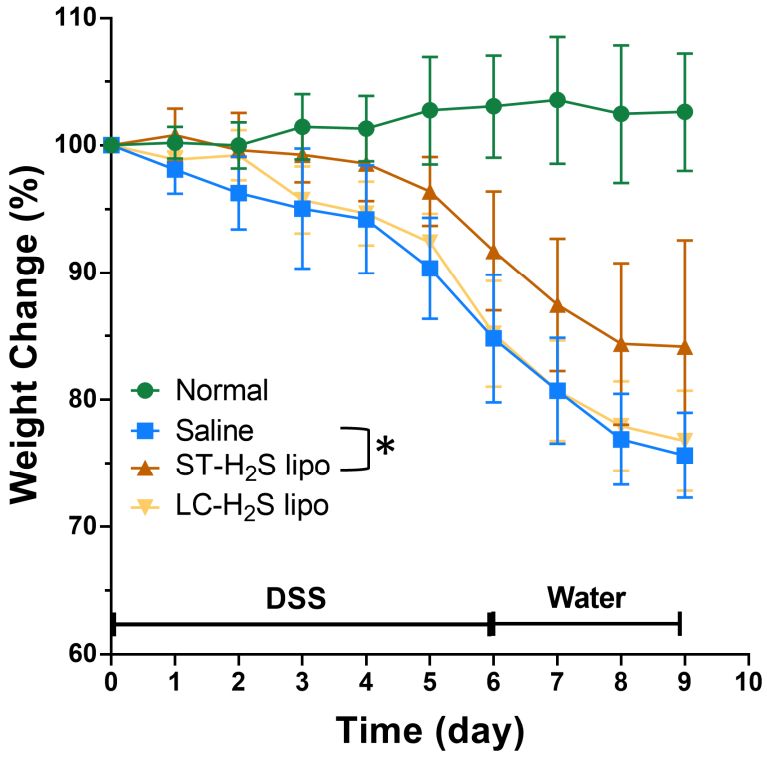

Figure 3.12 The comparison of weight change (%) between normal, saline, ST-H_2S lipo, and LC-H_2S lipo.

A

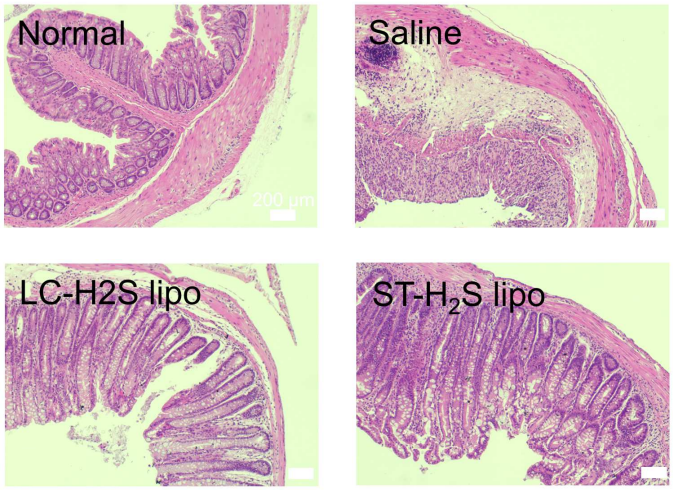

B

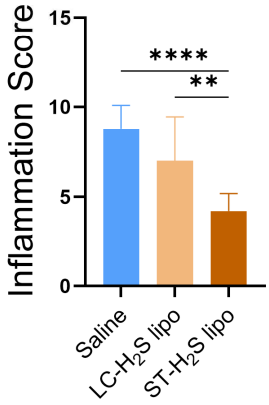

Figure 3.13 The comparison of inflammatory process between normal, saline, LC-H_2S lipo, ST-H_2S lipo. The H&E images of colon of colitis model. (D) The graph indicates comparison of inflammation score between saline, ST-H_2S lipo, and LC-H_2S lipo (n = 8). ST: spleen targeting, LC: long-circulating, **: $P < 0.01$, ***: $P < 0.001$.

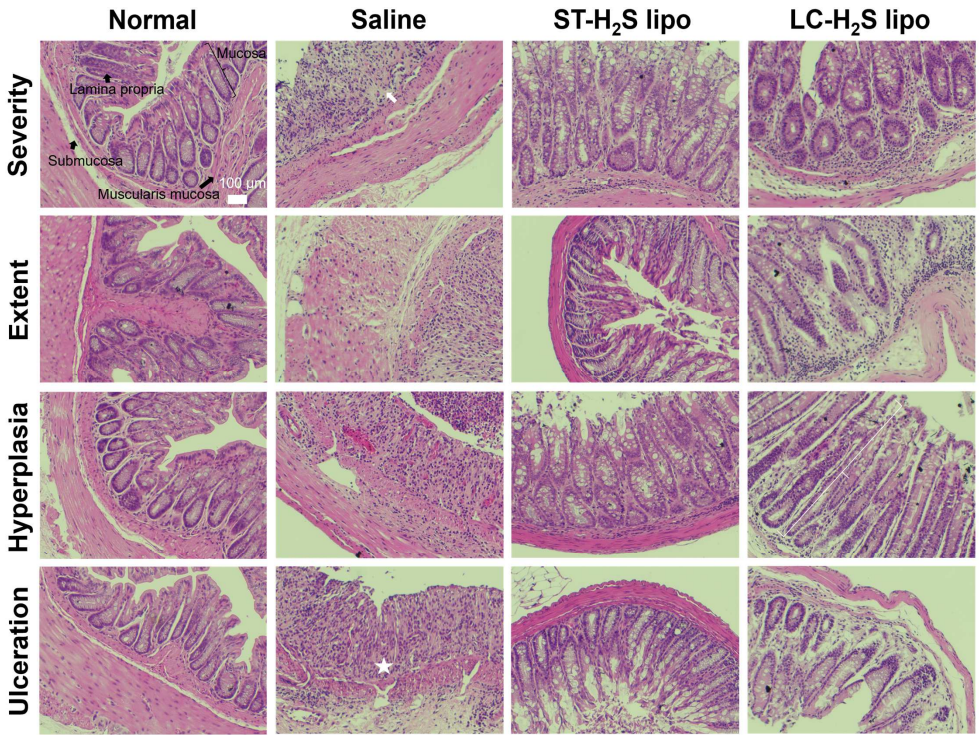

Figure 3.14 Representative H&E images about general criteria of histomorphology scores for colitis model. general criteria are (1) severity, (2) extent, (3) hyperplasia, and (4) ulceration. (1) severity is scoring degree of leukocyte density of lamina propria region. (2) extent is scoring degree of expansion of leukocyte infiltration. Histomorphology score is increased when leukocytes gradually infiltrate from mucosa to transmural. Definition of (3) hyperplasia is increased epithelial cell number in crypts and crypts are elongated. Definition of (4) ulceration is epithelial defect reaching beyond muscularis mucosa. Yellow arrow indicates the loss of villi and crypt's structures. Yellow curly bracket indicates hyperplasia. Yellow star indicates ulceration. According to four different criteria, ST-H_2S lipo treated group demonstrated the lowest score among the four groups shown here.

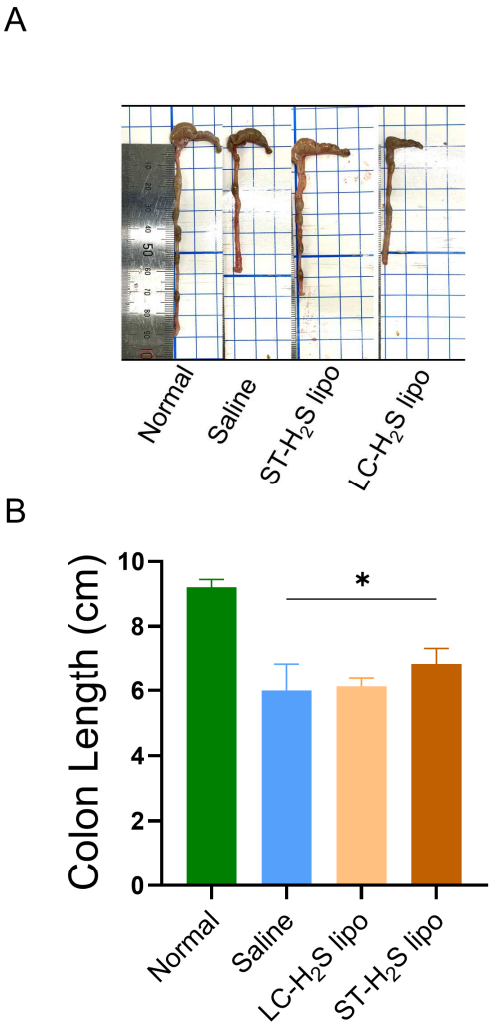

Figure 3.15 The comparison of colon lengths between normal, saline, LC-H_2S lipo, ST-H_2S lipo. A. The extracted images of colon in colitis model. Representative images indicate normal, saline, ST-H_2S lipo, and LC-H_2S lipo from left respectively. B. The graph (left) indicates comparison of colon length (n = 5, respectively). The graph (right) indicates comparison of colon weight/length (n = 5, respectively). *: $P < 0.05$.

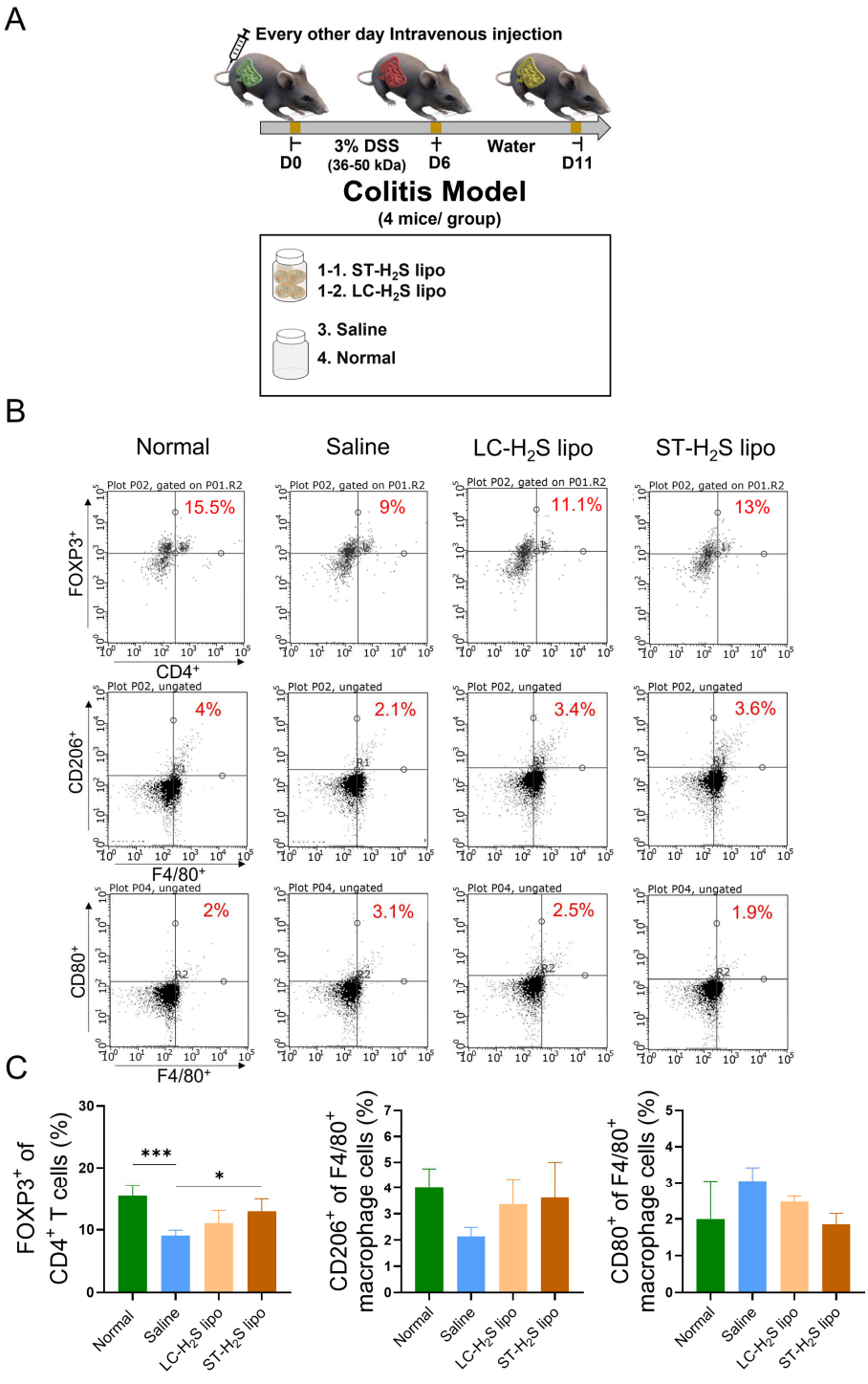

Figure 3.16 Comparison of in vivo immune cell differentiation between ST-H_2S lipo and LC-H_2S lipo in spleen. A. Schematic design of the experiment.

The colitis model was induced by 3% DSS. Mice received 3% DSS water for day7. Reagents were intravenously injected every other day (N= 4 respectively). Mice were sacrificed to extract spleen at day11. B. Dot plot of flow cytometry. CD4 and FOXP3 antibodies were used as regulatory T cell markers. CD80 and F4/80 antibodies were used as M1 macrophage markers. CD206 and F4/80 antibodies were used as M2 macrophage markers. C. Graphs showed that ST-H_2S lipo is significantly more T_{reg} differentiated than saline group. ST-H_2S lipo: spleen targeting H_2S lipo, LC-H_2S lipo: long circulation H_2S lipo, ***: $P< 0.001$, *: $P< 0.05$

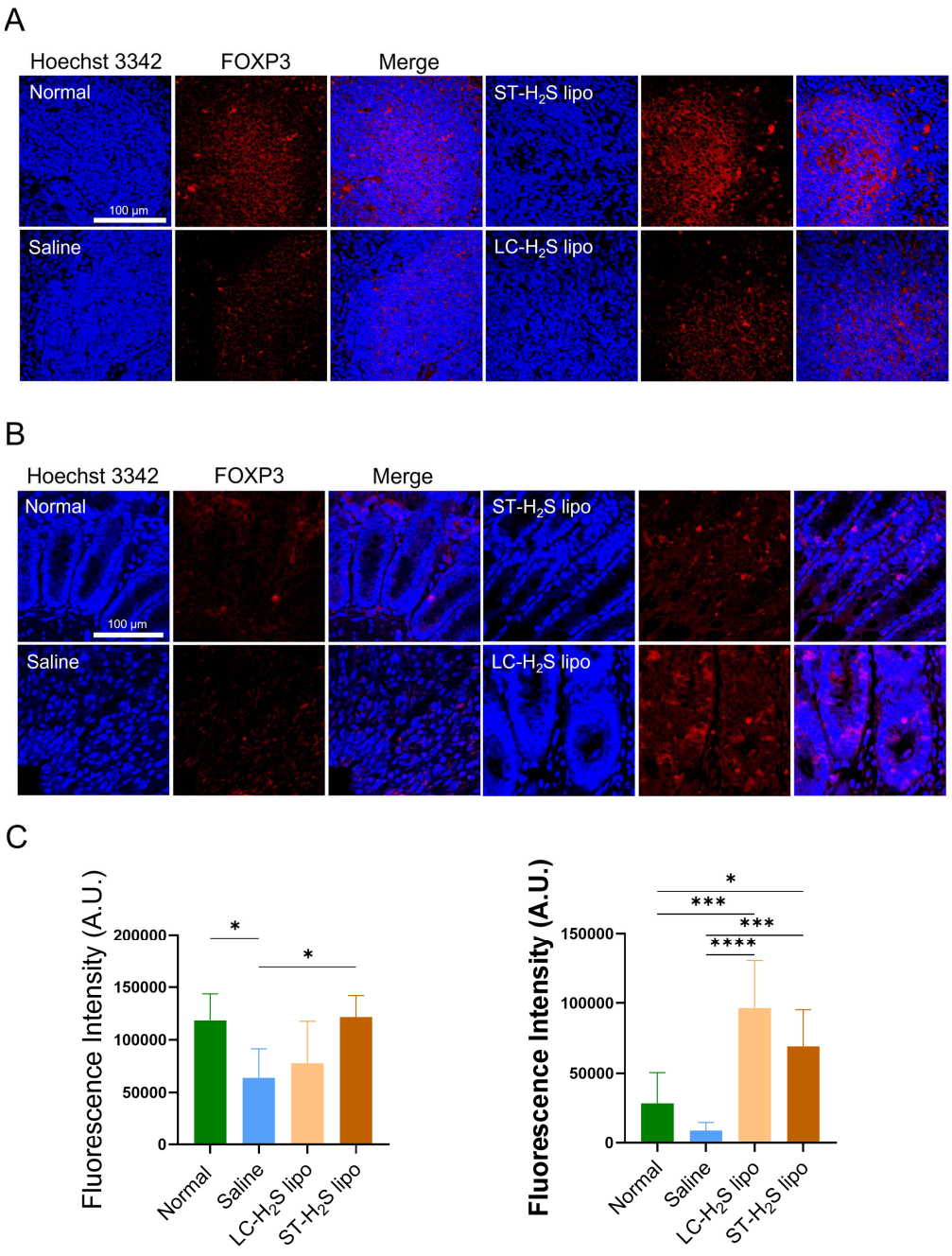

Figure 3.17 Immunofluorescence images of FOXP3 differentiation in spleen and colon. A. Immunofluorescence images in spleen B.

Immunofluorescence images in colon. Red fluorescence by Cyanine5.5 indicates FOXP3 of T_{reg} cells. C. The graph (left) indicates comparison of fluorescence intensity in spleen (n = 5). The graph (right) indicates comparison of fluorescence intensity in colon (n = 5). *: $P < 0.05$, ***: $P < 0.001$, ****: $P < 0.0001$.

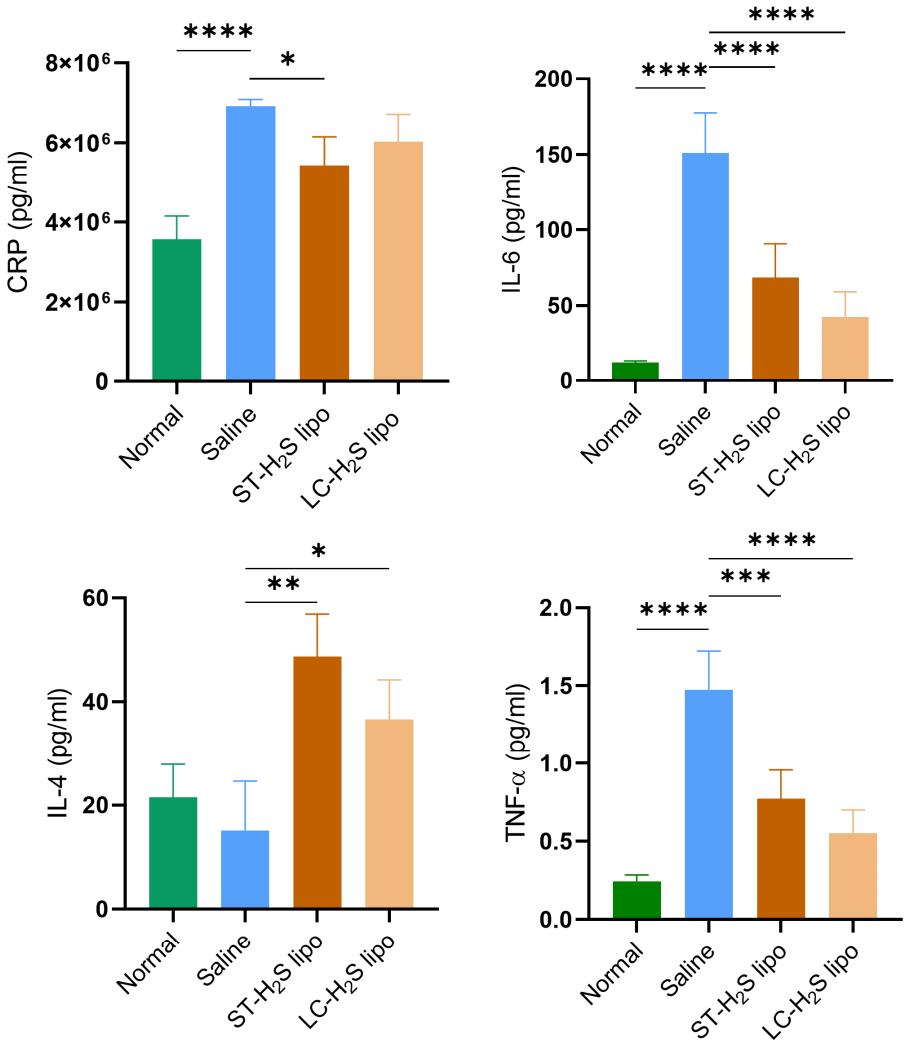

Figure 3.18 Plasma cytokine analysis in the treatment of comparison between ST-H_2S lipo and LC-H_2S lipo. Plasma was collected from blood in EDTA tube after treatment. In CRP analysis, ST-H_2S lipo was significantly

less detected than saline group. In IL-6 analysis, ST-H_2S lipo and LC-H_2S lipo were significantly less detected than saline group. In IL-4 analysis, ST-H_2S lipo and LC-H_2S lipo were significantly less detected than saline group. In TNF-α analysis, ST-H_2S lipo and LC-H_2S lipo were significantly less detected than saline group. ST-H_2S lipo: spleen targeting H_2S lipo, LC-H_2S lipo: long circulating H_2S lipo, *: $P < 0.05$, **: $P< 0.01$, ***: $P< 0.001$, ****: $P< 0.0001$

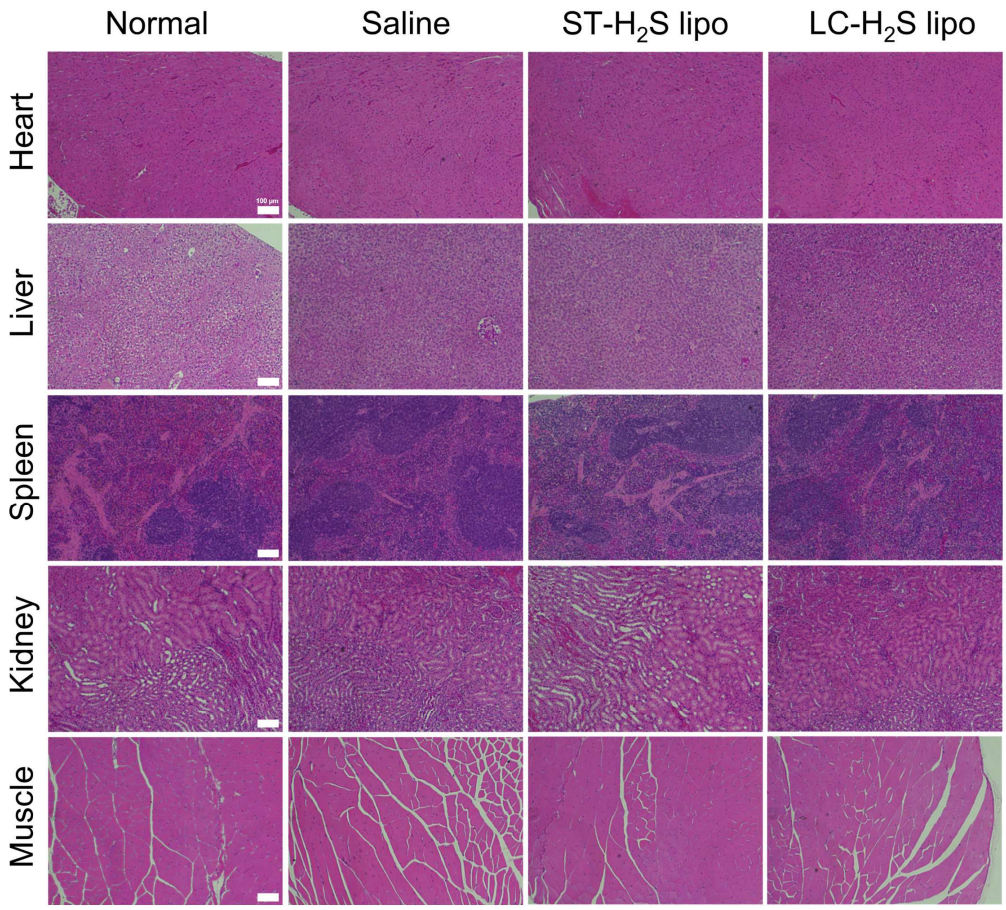

Figure 3.19 H&E staining of extracted organs in the treatment of comparison between ST-H_2S lipo and LC-H_2S lipo. The organs which is heart, liver, spleen, kidney, and muscle were extracted at day10 of treatment. The compared group are normal, saline, ST-H_2S lipo and LC-H_2S lipo. ST-H_2S lipo: spleen targeting H_2S lipo, LC-H_2S lipo: long circulation H_2S lipo

3.3.5 Therapeutic potential of various spleen targeting nanoparticles

Many studies have reported on the therapeutic potential of spleen targeting by various approaches. In a treatment study on experimental autoimmune encephalomyelitis (EAE), antigens linked to syngeneic splenic leukocytes with ethylene carbodiimide (Ag-SP) accumulated in the MZ. Consequently, they induced T_{reg} differentiation (69). In a treatment study using an inflammatory arthritis model, noninvasive ultrasound stimulation into the spleen showed a reduction of the disease severity through the cholinergic anti-inflammatory pathway (70). Especially, many studies have reported on the therapeutic potential of spleen targeting nanoparticles (**Table 5**). Zhai et al. developed induced pluripotent stem cells (iPSCs) encapsulated in coalescent an erythrocyte-liposome (iPSC@RBC-Mlipo). As mentioned above, the spleen has the ability to filter damaged erythrocytes. iPSC@RBC-Mlipo used the characteristic of spleen targeting. In terms of the spleen targeting efficiency, iPSC@RBC-Mlipo was three times higher compared to iPSC encapsulated in liposomes (iPSC@Mlipo). In the treatment of the B16F10 tumor model, iPSC@RBC-Mlipo showed a significantly better antitumor effect and inhibition of metastasis than that of iPSC@Mlipo (29). Shimizu et al. developed an antigen (Ag) encapsulated

PEGylated liposome (PL). As a spleen targeting strategy, the phenomenon when more PL is repeatedly administered, more of it accumulates in the splenic MZ, was used. In the treatment of the EG7-OVA tumor model, the group with pre-injected empty PL prior to Ag encapsulated PL injection induced a more obvious cytotoxic T lymphocyte (CTL) immune response and suppressed tumor growth than the group without pre-injected empty PL (42). Tripathi et al. developed 4-sulfated N-acetyl galactosamine which could specifically target resident macrophages in the liver and spleen conjugated chitosan nanoparticles (SCNPs). In the treatment of leishmaniasis, amphotericin B (AmB) loaded SCNPs (AmB-SCNPs) delivered significantly more AmB to the spleen compared to the AmB-chitosan nanoparticles (AmB-CNPs) ($P < 0.05$). Moreover, AmB-SCNPs showed a significantly more anti-leishmanial activity than that of the AmB-CNPs ($P < 0.05$) (48). Ye et al. developed passively spleen targeted actarit, anti-rheumatic drug, loaded solid lipid nanoparticle (SLN). The actarit-SLN was more accumulated in the spleen than that of the unloaded actarit (6.31% to 16.29%) (39). Yi et al. studied nanostructure morphology suitable for targeting DCs. Among the nanostructures which were all assembled from poly(ethylene glycol)-bl-poly(propylene sulfide) (PEG-bl-PPS), polymersomes (PS) structurally similar to liposomes showed the highest

uptake in the splenic DCs of normal mice. Interestingly, in the spleen of atherosclerotic Ldlr-/- mice, PS uptake by macrophages was significantly reduced ($P < 0.005$), while PS uptake by DCs was barely changed compared to normal mice. As result, PS was predominantly phagocyted by splenic DCs compared to macrophages in atherosclerotic Ldlr-/- mice ($P = 0.006$) (41). Kranz et al. developed RNA-lipoplex (RNA-LPX) with a net charge suitable for DCs targeting. They found that RNA-LPX with about -30 mV was more accumulated in the spleen compared to the positively charged RNA-LPX. In the treatment of several tumor models, the selected RNA-LPX formulation for delivering RNA to the spleen induced strong immune responses and showed an antitumor efficacy due to systemic DC targeting (31). In the present study, we developed a simple spleen targeting strategy by modulating the PEG type and ratio, in arguably the most frequently used nanoparticles for drug delivery, a PEGylated liposome. When comparing the spleen targeting efficiency (%), ST-H_2S lipo showed the highest efficiency among the other spleen targeting nanoparticles (29, 39, 41, 48). We found the ideal composition of PEG to obtain a reasonable loading efficiency, stability and excellent spleen targeting ability (**Table 7**)

Type of disease model	Nanoparticles	Size (nm)	Zeta potential (mV)	Stealth polymer	Spleen targeting strategy	Spleen targeting efficiency* (%)	Ref
Tumor	iPSC@RBC-Mlipo	184	4.7	DSPE-PEG_{2000}	Damaged erythrocyte membrane entrapped by spleen	160	(29)
Tumor	Ag encapsulated PL	Not mentioned	Not mentioned	DSPE-PEG_{2000}	Repeated pre-injection of empty PL for delivering Ag encapsulated PL to splenic marginal zone B cell	N/A	(42)
Leishmaniasis	AmB loaded SCNPs	333±7	−13.9±0.24	N/A	Targeting resident macrophage	50.9	(48)
Rheumatoid arthritis	Actarit loaded SLNs	241±23	−17.14±1.6	N/A	Passive targeting to RES organs	120	(39)
Atherosclerosis	PS	113.7	−0.2±1.68	PEG-bl-PPS	Changing the nanostructure morphology	16.7	(41)
Tumor	RNA-LPX	200-320	Around −30	N/A	Negative charged lipid nanocarrier	N/A	(31)

Type of disease model	Nanoparticles	Size (nm)	Zeta potential (mV)	Stealth polymer	Spleen targeting strategy	Spleen targeting efficiency* (%)	Ref
IBD	ST-H_2S lipo	110.3±42.4	−28.1	DSPE-PEG_{5000}	Ideal PEG size and ratio for spleen targeting	179.9	This study

Table 7 Therapeutic potential of various spleen targeting nanoparticles. *Spleen targeting efficiency (%) is calculated by the (spleen uptake of the nanoparticle/ the liver uptake of the nanoparticle) × 100. N/A: not applicable, iPSCs: induced pluripotent stem cells, iPSC@RBC-Mlipo: iPSCs encapsulated in coalescent erythrocyte-liposome, PL: PEGylated liposome, iPSC@Mlipo: iPSC encapsulated in liposome, DSPE: 1,2- Distearoyl-sn-glycero-3-phosphoethanolamine, PEG: polyethylene glycol, AmB: amphotericin B, SCNPs: 4-sulfated N-acetyl galactosamine conjugated chitosan nanoparticles, SLN: solid lipid nanoparticle, TEC: overall targeting efficiency, PS: polymersome, PEG-bl-PPS: poly(ethylene glycol)-bl-poly(propylene sulfide), RNA-LPX: RNA-lipoplexes, DCs: dendritic cells, IBD: inflammatory bowel dis

3.3.6 Possibility of H_2S lipo as a new clinical immunomodulator in IBD

H_2S lipo should be further studied in order to confirm its therapeutic potential for IBD in clinical. Immunomodulators used in IBD treatment produce anti-inflammatory effects by targeting specific immune processes such as TNF-α, IL-12/23, JAK, and sphigosine-1-phosphate (S1P). However, since the response rate varies from 16 to 70%, the development of immunomodulatory agents with a new mechanism of action is needed (10). Hydrogen sulfide (H_2S) is a lipophilic gas molecule that is rapidly dispersed into the cytoplasm without a specific transporter and is involved in various anti-inflammatory processes. H_2S is involved in anti-inflammatory mechanisms different from those of conventional immunomodulators used in IBD, such as T_{reg} differentiation by promoting TET1 and TET2 expression, M2 macrophage differentiation through PPARɣ and PPARɣ coacticator-1β, and inhibition of the NF-κB signaling pathway. In order for H_2S lipo, which emits anti-inflammatory hydrogen sulfide, to enter the clinical trial of IBD, the safety and effectiveness of H_2S lipo should be evaluated. First, safety data through various dose level measurements are needed. Mirandola et al reported that treatment with 2 mM of H_2S donor resulted in cytotoxicity (110). Although ST-H_2S lipo (60 μM and 100 μM)

had no cytotoxicity in the treatment of the colitis model, additional dose levels need to be evaluated. Second, in order to confirm the effectiveness, the exact mechanism of the treatment effect of the colitis model of H_2S lipo should be identified, and the treatment effect should be compared with conventional immunomodulators used for IBD treatment. Also, a more detailed study on the method of administration is needed. In the case of systemically administered LC-H_2S lipo, the possibility of oral administration, which is much more convenient, should be evaluated as it targets the inflammatory site and relieves symptoms. Currently, clinical trials of H_2S-releasing agents are underway. SG1002 (sodium polythionate) developed by Sulfagenix is designed to improve high fat diet (HFD) induced metabolic and cardiac dysfunction and has completed the phase 1 clinical trial (111). ATB-346 (H_2S-releasing derivative of naproxen) developed by Antibe Therapeutics is designed to prevent gastrointestinal bleeding and ulceration, side effects of the nonsteroidal anti-inflammatory drugs (NSAIDs), by inhibiting the NF-kB pathway. In Phase 2 clinical, ATB-346 relieved the pain of patients with osteoarthritis and effectively reduced the side effects of NSAIDs ($P< 0.001$) (112). In conclusion, based on the involvement of H_2S in various anti-inflammatory reactions, the therapeutic effect of H_2S lipo in colitis model, and the clinical trial of other H_2S-

releasing drugs, it is suggested that H_2S lipo may be a new immunomodulatory agent for IBD, but various studies are needed to move forward it into clinical trials

3.4 Summary

In chapter 3, we identified the therapeutic potential of H_2S for colitis in transcriptomics-level evidence and further the excellent therapeutic effects of ST-H_2S lipo in colitis model. In the gene expression analysis of colon in both UC and colitis model, it was identified that expression of CBS, CTH, and MPST involving H_2S production were significantly reduced. Then, we evaluated the therapeutic effects of H_2S lipo in the colitis model. In the result, ST-H_2S lipo showed superior results than unloaded H_2S donor in several therapeutic indexes including weight changes and inflammation score. In addition, it was identified that ST-H_2S lipo induced more T_{reg} differentiation in bone marrow and spleen as an effective systemic immune modulator. In the comparison of therapeutic effect between ST-H_2S lipo and H_2S donor loaded conventional long circulating liposome (LC-H_2S lipo), ST-H_2S lipo demonstrated an even higher protective effect against inflammation in colon compared to LC-H_2S lipo, which may be attributed to the higher efficiency of ST-H_2S lipo improving systemic immune homeostasis.

Chapter 4.

Conclusion

We developed spleen targeting H_2S donor loaded liposomes (ST-H_2S lipo) for delivering highly reactive H_2S donor to specific organ (i.e., spleen). Our ST-H_2S lipo demonstrated an excellent loading capacity of H_2S donor and stability. Additionally, ST-H_2S lipo induced a M2 phenotypic change in macrophages after efficient cell uptake and H_2S release in the in vitro experiments. The excellent spleen targeting ability of the ST-H_2S lipo was confirmed in both normal mice and colitis model. Through analysis of RNA expression, the expression of H_2S related enzymes were decreased in both colitis patients and colitis model. In the treatment of the DSS induced colitis model, we found that ST-H_2S lipo showed a significantly greater therapeutic effect than that of the unloaded H_2S donor. Moreover, ST-H_2S lipo demonstrated an even higher protective effect against inflammation in colon compared to the H_2S donor loaded conventional long-circulating liposome (LC-H_2S lipo). ST-H_2S lipo treatment showed a higher systemic immune modulative effect compared to the LC-H_2S lipo treatment. These findings demonstrate the potential of the spleen targeting H_2S lipo in the treatment of IBD.

The degree process was a meaningful period in which I was able to lay the groundwork as a researcher and think about the way forward. A wide variety of experiments were conducted to confirm the immunomodulatory

effect of H_2S lipo: synthesis of H_2S lipo, cell works, flow cytometry, confocal imaging, radiolabeling, PET imaging, IVIS imaging, modeling, and RNA seq-analysis using webtools. In in vitro experiments, I cultured cell lines, analyzed the physical and chemical properties of cells through flow cytometry and studied the interaction between nanoparticles and cell through confocal imaging. In the future, I plan to evaluate the efficacy of immunomodulators not only in macrophages, but also in various cell lines such as dendritic cells, T cells, and cancer cells. During the degree process, I performed several mice models including myocardial infarction reperfusion model, arthritis model, Parkinson disease model, cancer model, and colitis model. Various skills including intravenous injection, obtained through this allowed the experimental plan to be carried out without a hitch. In the future, I plan to study other diseases suitable for application of spleen targeting nanoparticles. In particular, I would like to study the bidirectional interaction between post-stroke infection and splenic immune cells and evaluate the immunomodulatory efficacy of spleen targeting nanoparticles in stroke models. In PET imaging research, I learned the radiolabeling of nanoparticles and quantitative analysis skills. Through experiments of colitis model, several biological analyses at the cell level, tissue level, and mouse level were performed and reasonable grounds of therapeutic effects were

presented. In the future, I plan to study whether H_2S lipo is effective in preventing the recurrence of IBD, which is incurable and has a frequent recurrence. Furthermore, I plan to study the correlation between IBD and central nervous system disorders, which are attracting attention these days. In synthesis of nanoparticles, I performed various experiments to synthesize, purify, and characterize liposomes. In the future, I plan to improve efficiency of spleen targeting liposomes through in-depth exploration of spleen targeting strategies. In addition, I will study synthesizing various nanoparticles as well as liposomes.

References

1.Ulcerative colitis. Nat Rev Dis Primers. 2020;6(1):73.

2.Abraham C, Cho JH. Inflammatory bowel disease. N Engl J Med. 2009;361(21):2066-78.

3.Collaborators GBDIBD. The global, regional, and national burden of inflammatory bowel disease in 195 countries and territories, 1990-2017: a systematic analysis for the Global Burden of Disease Study 2017. Lancet Gastroenterol Hepatol. 2020;5(1):17-30.

4.Hindryckx P, Jairath V, D'Haens G. Acute severe ulcerative colitis: from pathophysiology to clinical management. Nat Rev Gastroenterol Hepatol. 2016;13(11):654-64.

5.Chang JT. Pathophysiology of Inflammatory Bowel Diseases. N Engl J Med. 2020;383(27):2652-64.

6.Feuerstein JD, Isaacs KL, Schneider Y, Siddique SM, Falck-Ytter Y, Singh S, et al. AGA Clinical Practice Guidelines on the Management of Moderate to Severe Ulcerative Colitis. Gastroenterology. 2020;158(5):1450-61.

7.Jeuring SFG, Bours PHA, Zeegers MP, Ambergen TW, van den Heuvel TRA, Romberg-Camps MJL, et al. Disease Outcome of Ulcerative Colitis in an Era of Changing Treatment Strategies: Results from the Dutch Population-Based IBDSL Cohort. Journal of Crohn's and Colitis. 2015;9(10):837-45.

8.Kucharzik T, Maaser C. Infections and Chronic Inflammatory Bowel

Disease. Visceral Medicine. 2014;30(5):326-32.

9.Salas A, Hernandez-Rocha C, Duijvestein M, Faubion W, McGovern D, Vermeire S, et al. JAK-STAT pathway targeting for the treatment of inflammatory bowel disease. Nat Rev Gastroenterol Hepatol. 2020;17(6):323-37.

10.Baumgart DC, Le Berre C. Newer Biologic and Small-Molecule Therapies for Inflammatory Bowel Disease. N Engl J Med. 2021;385(14):1302-15.

11.Mustafa AK, Gadalla MM, Snyder SH. Signaling by gasotransmitters. Sci Signal. 2009;2(68):re2.

12.Szabó C. Hydrogen sulphide and its therapeutic potential. Nature Reviews Drug Discovery. 2007;6(11):917-35.

13.Zhao W, Ndisang JF, Wang R. Modulation of endogenous production of H2S in rat tissues. Canadian journal of physiology and pharmacology. 2003;81(9):848-53.

14.Szabo C. Roles of hydrogen sulfide in the pathogenesis of diabetes mellitus and its complications. Antioxidants & redox signaling. 2012;17(1):68-80.

15.Wang Y, Zhao X, Jin H, Wei H, Li W, Bu D, et al. Role of Hydrogen Sulfide in the Development of Atherosclerotic Lesions in Apolipoprotein E Knockout Mice. 2009;29(2):173-9.

16.Fiorucci S, Antonelli E, Distrutti E, Rizzo G, Mencarelli A, Orlandi S, et al. Inhibition of hydrogen sulfide generation contributes to gastric injury

caused by anti-inflammatory nonsteroidal drugs. Gastroenterology. 2005;129(4):1210-24.

17.Motta JP, Flannigan KL, Agbor TA, Beatty JK, Blackler RW, Workentine ML, et al. Hydrogen sulfide protects from colitis and restores intestinal microbiota biofilm and mucus production. Inflamm Bowel Dis. 2015;21(5):1006-17.

18.Wallace JL, Vong L, McKnight W, Dicay M, Martin GR. Endogenous and exogenous hydrogen sulfide promotes resolution of colitis in rats. Gastroenterology. 2009;137(2):569-78, 78 e1.

19.Wallace JL, Dicay M, McKnight W, Martin GR. Hydrogen sulfide enhances ulcer healing in rats. FASEB J. 2007;21(14):4070-6.

20.Li L, Fox B, Keeble J, Salto-Tellez M, Winyard PG, Wood ME, et al. The complex effects of the slow-releasing hydrogen sulfide donor GYY4137 in a model of acute joint inflammation and in human cartilage cells. J Cell Mol Med. 2013;17(3):365-76.

21.Zhang G, Wang P, Yang G, Cao Q, Wang R. The inhibitory role of hydrogen sulfide in airway hyperresponsiveness and inflammation in a mouse model of asthma. Am J Pathol. 2013;182(4):1188-95.

22.Miao L, Shen X, Whiteman M, Xin H, Shen Y, Xin X, et al. Hydrogen Sulfide Mitigates Myocardial Infarction via Promotion of Mitochondrial Biogenesis-Dependent M2 Polarization of Macrophages. Antioxidants & redox signaling. 2016;25(5):268-81.

23.Wu D, Gao B, Li M, Yao L, Wang S, Chen M, et al. Hydrogen Sulfide

Mitigates Kidney Injury in High Fat Diet-Induced Obese Mice. Oxid Med Cell Longev. 2016;2016:2715718.

24.Li T, Zhao B, Wang C, Wang H, Liu Z, Li W, et al. Regulatory effects of hydrogen sulfide on IL-6, IL-8 and IL-10 levels in the plasma and pulmonary tissue of rats with acute lung injury. Exp Biol Med (Maywood). 2008;233(9):1081-7.

25.Zhang GY, Lu D, Duan SF, Gao YR, Liu SY, Hong Y, et al. Hydrogen Sulfide Alleviates Lipopolysaccharide-Induced Diaphragm Dysfunction in Rats by Reducing Apoptosis and Inflammation through ROS/MAPK and TLR4/NF-kappaB Signaling Pathways. Oxid Med Cell Longev. 2018;2018:9647809.

26.Mitchell MJ, Billingsley MM, Haley RM, Wechsler ME, Peppas NA, Langer R. Engineering precision nanoparticles for drug delivery. Nature Reviews Drug Discovery. 2021;20(2):101-24.

27.Cifuentes-Rius A, Desai A, Yuen D, Johnston APR, Voelcker NH. Inducing immune tolerance with dendritic cell-targeting nanomedicines. Nature Nanotechnology. 2021;16(1):37-46.

28.Ramishetti S, Kedmi R, Goldsmith M, Leonard F, Sprague AG, Godin B, et al. Systemic Gene Silencing in Primary T Lymphocytes Using Targeted Lipid Nanoparticles. ACS Nano. 2015;9(7):6706-16.

29.Zhai Y, He X, Li Y, Han R, Ma Y, Gao P, et al. A splenic-targeted versatile antigen courier: iPSC wrapped in coalescent erythrocyte-liposome as tumor nanovaccine. Sci Adv. 2021;7(35).

30.Bronte V, Pittet MJ. The spleen in local and systemic regulation of immunity. Immunity. 2013;39(5):806-18.

31.Kranz LM, Diken M, Haas H, Kreiter S, Loquai C, Reuter KC, et al. Systemic RNA delivery to dendritic cells exploits antiviral defence for cancer immunotherapy. Nature. 2016;534(7607):396-401.

32.LoPresti ST, Arral ML, Chaudhary N, Whitehead KA. The replacement of helper lipids with charged alternatives in lipid nanoparticles facilitates targeted mRNA delivery to the spleen and lungs. J Control Release. 2022;345:819-31.

33.Schmid D, Park CG, Hartl CA, Subedi N, Cartwright AN, Puerto RB, et al. T cell-targeting nanoparticles focus delivery of immunotherapy to improve antitumor immunity. Nature Communications. 2017;8(1):1747.

34.Sago CD, Lokugamage MP, Paunovska K, Vanover DA, Monaco CM, Shah NN, et al. High-throughput in vivo screen of functional mRNA delivery identifies nanoparticles for endothelial cell gene editing. Proc Natl Acad Sci U S A. 2018;115(42):E9944-E52.

35.Kimura S, Khalil IA, Elewa YHA, Harashima H. Novel lipid combination for delivery of plasmid DNA to immune cells in the spleen. J Control Release. 2021;330:753-64.

36.Kimura S, Khalil IA, Elewa YHA, Harashima H. Spleen selective enhancement of transfection activities of plasmid DNA driven by octaarginine and an ionizable lipid and its implications for cancer immunization. J Control Release. 2019;313:70-9.

37.Cheng Q, Wei T, Farbiak L, Johnson LT, Dilliard SA, Siegwart DJ. Selective organ targeting (SORT) nanoparticles for tissue-specific mRNA delivery and CRISPR-Cas gene editing. Nat Nanotechnol. 2020;15(4):313-20.

38.Alvarez-Benedicto E, Farbiak L, Marquez Ramirez M, Wang X, Johnson LT, Mian O, et al. Optimization of phospholipid chemistry for improved lipid nanoparticle (LNP) delivery of messenger RNA (mRNA). Biomater Sci. 2022;10(2):549-59.

39.Ye J, Wang Q, Zhou X, Zhang N. Injectable actarit-loaded solid lipid nanoparticles as passive targeting therapeutic agents for rheumatoid arthritis. Int J Pharm. 2008;352(1-2):273-9.

40.Li S, Wang Y, Wu M, Younis MH, Olson AP, Barnhart TE, et al. Spleen-Targeted Glabridin-Loaded Nanoparticles Regulate Polarization of Monocyte/Macrophage (Mo /Mphi) for the Treatment of Cerebral Ischemia-Reperfusion Injury. Adv Mater. 2022;34(39):e2204976.

41.Yi S, Allen SD, Liu YG, Ouyang BZ, Li X, Augsornworawat P, et al. Tailoring Nanostructure Morphology for Enhanced Targeting of Dendritic Cells in Atherosclerosis. ACS Nano. 2016;10(12):11290-303.

42.Shimizu T, Abu Lila AS, Kawaguchi Y, Shimazaki Y, Watanabe Y, Mima Y, et al. A Novel Platform for Cancer Vaccines: Antigen-Selective Delivery to Splenic Marginal Zone B Cells via Repeated Injections of PEGylated Liposomes. J Immunol. 2018;201(10):2969-76.

43.Fenton OS, Kauffman KJ, Kaczmarek JC, McClellan RL, Jhunjhunwala

S, Tibbitt MW, et al. Synthesis and Biological Evaluation of Ionizable Lipid Materials for the In Vivo Delivery of Messenger RNA to B Lymphocytes. Adv Mater. 2017;29(33).

44.Van der Jeught K, De Koker S, Bialkowski L, Heirman C, Tjok Joe P, Perche F, et al. Dendritic Cell Targeting mRNA Lipopolyplexes Combine Strong Antitumor T-Cell Immunity with Improved Inflammatory Safety. ACS Nano. 2018;12(10):9815-29.

45.Maldonado RA, LaMothe RA, Ferrari JD, Zhang AH, Rossi RJ, Kolte PN, et al. Polymeric synthetic nanoparticles for the induction of antigen-specific immunological tolerance. Proc Natl Acad Sci U S A. 2015;112(2):E156-65.

46.Stead SO, Kireta S, McInnes SJP, Kette FD, Sivanathan KN, Kim J, et al. Murine and Non-Human Primate Dendritic Cell Targeting Nanoparticles for in Vivo Generation of Regulatory T-Cells. ACS Nano. 2018;12(7):6637-47.

47.Leuschner F, Dutta P, Gorbatov R, Novobrantseva TI, Donahoe JS, Courties G, et al. Therapeutic siRNA silencing in inflammatory monocytes in mice. Nat Biotechnol. 2011;29(11):1005-10.

48.Tripathi P, Dwivedi P, Khatik R, Jaiswal AK, Dube A, Shukla P, et al. Development of 4-sulfated N-acetyl galactosamine anchored chitosan nanoparticles: A dual strategy for effective management of Leishmaniasis. Colloids Surf B Biointerfaces. 2015;136:150-9.

49.Jiang Y, Hardie J, Liu Y, Ray M, Luo X, Das R, et al. Nanocapsule-mediated cytosolic siRNA delivery for anti-inflammatory treatment. J

Control Release. 2018;283:235-40.

50.van Leent MMT, Beldman TJ, Toner YC, Lameijer MA, Rother N, Bekkering S, et al. Prosaposin mediates inflammation in atherosclerosis. Sci Transl Med. 2021;13(584).

51.Saito E, Kuo R, Pearson RM, Gohel N, Cheung B, King NJC, et al. Designing drug-free biodegradable nanoparticles to modulate inflammatory monocytes and neutrophils for ameliorating inflammation. J Control Release. 2019;300:185-96.

52.Wallace JL, Ferraz JG, Muscara MN. Hydrogen sulfide: an endogenous mediator of resolution of inflammation and injury. Antioxidants & redox signaling. 2012;17(1):58-67.

53.Benedetti F, Curreli S, Krishnan S, Davinelli S, Cocchi F, Scapagnini G, et al. Anti-inflammatory effects of H2S during acute bacterial infection: a review. J Transl Med. 2017;15(1):100.

54.Li M, Mao J, Zhu Y. New Therapeutic Approaches Using Hydrogen Sulfide Donors in Inflammation and Immune Response. Antioxidants & redox signaling. 2021;35(5):341-56.

55.Dilek N, Papapetropoulos A, Toliver-Kinsky T, Szabo C. Hydrogen sulfide: An endogenous regulator of the immune system. Pharmacol Res. 2020;161:105119.

56.Yang R, Qu C, Zhou Y, Konkel JE, Shi S, Liu Y, et al. Hydrogen Sulfide Promotes Tet1- and Tet2-Mediated Foxp3 Demethylation to Drive Regulatory T Cell Differentiation and Maintain Immune Homeostasis.

Immunity. 2015;43(2):251-63.

57.Erben U, Loddenkemper C, Doerfel K, Spieckermann S, Haller D, Heimesaat MM, et al. A guide to histomorphological evaluation of intestinal inflammation in mouse models. Int J Clin Exp Pathol. 2014;7(8):4557-76.

58.Vignali DA, Collison LW, Workman CJ. How regulatory T cells work. Nat Rev Immunol. 2008;8(7):523-32.

59.Whiteman M, Li L, Rose P, Tan CH, Parkinson DB, Moore PK. The effect of hydrogen sulfide donors on lipopolysaccharide-induced formation of inflammatory mediators in macrophages. Antioxidants & redox signaling. 2010;12(10):1147-54.

60.Xu W, Chen J, Lin J, Liu D, Mo L, Pan W, et al. Exogenous H2S protects H9c2 cardiac cells against high glucose-induced injury and inflammation by inhibiting the activation of the NF-kappaB and IL-1beta pathways. Int J Mol Med. 2015;35(1):177-86.

61.Wallace JL, Wang R. Hydrogen sulfide-based therapeutics: exploiting a unique but ubiquitous gasotransmitter. Nat Rev Drug Discov. 2015;14(5):329-45.

62.Mebius RE, Kraal G. Structure and function of the spleen. Nat Rev Immunol. 2005;5(8):606-16.

63.Humphrey JH, Grennan D. Different macrophage populations distinguished by means of fluorescent polysaccharides. Recognition and properties of marginal-zone macrophages. Eur J Immunol. 1981;11(3):221-8.

64.Yamazaki S, Dudziak D, Heidkamp GF, Fiorese C, Bonito AJ, Inaba K,

et al. CD8+ CD205+ splenic dendritic cells are specialized to induce Foxp3+ regulatory T cells. J Immunol. 2008;181(10):6923-33.

65.Seifert HA, Hall AA, Chapman CB, Collier LA, Willing AE, Pennypacker KR. A transient decrease in spleen size following stroke corresponds to splenocyte release into systemic circulation. J Neuroimmune Pharmacol. 2012;7(4):1017-24.

66.Heusch G. The Spleen in Myocardial Infarction. Circ Res. 2019;124(1):26-8.

67.Feng ZD, B.; Wang, R.; Wang, G.; Wang, C.; Tan, Y.; Liu, L.; Wang, C.; Liu, Y.; Liu, Y.; et al. The Novel Severe Acute Respiratory Syndrome Coronavirus 2 (SARS-CoV-2) Directly Decimates Human Spleens and Lymph Nodes. medRxiv. 2020.

68.Swirski FK, Nahrendorf M, Etzrodt M, Wildgruber M, Cortez-Retamozo V, Panizzi P, et al. Identification of splenic reservoir monocytes and their deployment to inflammatory sites. Science. 2009;325(5940):612-6.

69.Getts DR, Turley DM, Smith CE, Harp CT, McCarthy D, Feeney EM, et al. Tolerance induced by apoptotic antigen-coupled leukocytes is induced by PD-L1+ and IL-10-producing splenic macrophages and maintained by T regulatory cells. J Immunol. 2011;187(5):2405-17.

70.Zachs DP, Offutt SJ, Graham RS, Kim Y, Mueller J, Auger JL, et al. Noninvasive ultrasound stimulation of the spleen to treat inflammatory arthritis. Nat Commun. 2019;10(1):951.

71.Kaur S, Allan SM, Al-Ahmady ZS. Re-directing nanomedicines to the

spleen: A potential technology for peripheral immunomodulation. J Control Release. 2022;350:60-79.

72.Chen KH, Lundy DJ, Toh EK, Chen CH, Shih C, Chen P, et al. Nanoparticle distribution during systemic inflammation is size-dependent and organ-specific. Nanoscale. 2015;7(38):15863-72.

73.Aichele P, Zinke J, Grode L, Schwendener RA, Kaufmann SH, Seiler P. Macrophages of the splenic marginal zone are essential for trapping of blood-borne particulate antigen but dispensable for induction of specific T cell responses. J Immunol. 2003;171(3):1148-55.

74.Harasym TO, Tardi P, Longman SA, Ansell SM, Bally MB, Cullis PR, et al. Poly(ethylene glycol)-modified phospholipids prevent aggregation during covalent conjugation of proteins to liposomes. Bioconjug Chem. 1995;6(2):187-94.

75.Leent MMTv. Regulating trained immunity with nanomedicine. Nature reviews materials. 2022;7(7):465-81.

76.Li L, Whiteman M, Guan YY, Neo KL, Cheng Y, Lee SW, et al. Characterization of a novel, water-soluble hydrogen sulfide-releasing molecule (GYY4137): new insights into the biology of hydrogen sulfide. Circulation. 2008;117(18):2351-60.

77.Lee ZW, Zhou J, Chen CS, Zhao Y, Tan CH, Li L, et al. The slow-releasing hydrogen sulfide donor, GYY4137, exhibits novel anti-cancer effects in vitro and in vivo. PLoS One. 2011;6(6):e21077.

78.Ugliano M, Henschke PA. Comparison of three methods for accurate

quantification of hydrogen sulfide during fermentation. Anal Chim Acta. 2010;660(1-2):87-91.

79.Wu J, Chen A, Zhou Y, Zheng S, Yang Y, An Y, et al. Novel H2S-Releasing hydrogel for wound repair via in situ polarization of M2 macrophages. Biomaterials. 2019;222:119398.

80.Sasakura K, Hanaoka K, Shibuya N, Mikami Y, Kimura Y, Komatsu T, et al. Development of a highly selective fluorescence probe for hydrogen sulfide. J Am Chem Soc. 2011;133(45):18003-5.

81.Sakuma S, Minamino S, Takase M, Ishiyama Y, Hosokura H, Kohda T, et al. Hydrogen sulfide donor GYY4137 suppresses proliferation of human colorectal cancer Caco-2 cells by inducing both cell cycle arrest and cell death. Heliyon. 2019;5(8):e02244.

82.McWhorter FY, Wang T, Nguyen P, Chung T, Liu WF. Modulation of macrophage phenotype by cell shape. Proc Natl Acad Sci U S A. 2013;110(43):17253-8.

83.Welch MJ, Hawker CJ, Wooley KL. The advantages of nanoparticles for PET. J Nucl Med. 2009;50(11):1743-6.

84.Knop K, Hoogenboom R, Fischer D, Schubert US. Poly(ethylene glycol) in drug delivery: pros and cons as well as potential alternatives. Angew Chem Int Ed Engl. 2010;49(36):6288-308.

85.Allen C, Dos Santos N, Gallagher R, Chiu GN, Shu Y, Li WM, et al. Controlling the physical behavior and biological performance of liposome formulations through use of surface grafted poly(ethylene glycol). Biosci

Rep. 2002;22(2):225-50.

86.Che J, Okeke CI, Hu ZB, Xu J. DSPE-PEG: a distinctive component in drug delivery system. Curr Pharm Des. 2015;21(12):1598-605.

87.Shi L, Zhang J, Zhao M, Tang S, Cheng X, Zhang W, et al. Effects of polyethylene glycol on the surface of nanoparticles for targeted drug delivery. Nanoscale. 2021;13(24):10748-64.

88.Labouta HI, Gomez-Garcia MJ, Sarsons CD, Nguyen T, Kennard J, Ngo W, et al. Surface-grafted polyethylene glycol conformation impacts the transport of PEG-functionalized liposomes through a tumour extracellular matrix model. RSC Adv. 2018;8(14):7697-708.

89.Szabo C. Gasotransmitters in cancer: from pathophysiology to experimental therapy. Nat Rev Drug Discov. 2016;15(3):185-203.

90.Wang R. Gasotransmitters: growing pains and joys. Trends Biochem Sci. 2014;39(5):227-32.

91.Flannigan KL, Agbor TA, Blackler RW, Kim JJ, Khan WI, Verdu EF, et al. Impaired hydrogen sulfide synthesis and IL-10 signaling underlie hyperhomocysteinemia-associated exacerbation of colitis. Proc Natl Acad Sci U S A. 2014;111(37):13559-64.

92.Hirata IN, Y.; Takagi, T.; Mizushima, K.; Suzuki, T.; Omatsu, T.; Handa, O.; Ichikawa, H.; Ueda, H.; Yoshikawa, T. Endogenous hydrogen sulfide is an anti-inflammatory molecule in dextran sodium sulfate-induced colitis in mice. Dig Dis Sci. 2011;56 (5):1379-86.

93.De Cicco P, Sanders T, Cirino G, Maloy KJ, Ianaro A. Hydrogen Sulfide

Reduces Myeloid-Derived Suppressor Cell-Mediated Inflammatory Response in a Model of Helicobacter hepaticus-Induced Colitis. Front Immunol. 2018;9:499.

94.Chen S, Zuo S, Zhu J, Yue T, Bu D, Wang X, et al. Decreased Expression of Cystathionine beta-Synthase Exacerbates Intestinal Barrier Injury in Ulcerative Colitis. J Crohns Colitis. 2019;13(8):1067-80.

95.Hegazi RA, Rao KN, Mayle A, Sepulveda AR, Otterbein LE, Plevy SE. Carbon monoxide ameliorates chronic murine colitis through a heme oxygenase 1-dependent pathway. J Exp Med. 2005;202(12):1703-13.

96.Byrne JD, Gallo D, Boyce H, Becker SL, Kezar KM, Cotoia AT, et al. Delivery of therapeutic carbon monoxide by gas-entrapping materials. Sci Transl Med. 2022;14(651):eabl4135.

97.Rachmilewitz D, Stamler JS, Bachwich D, Karmeli F, Ackerman Z, Podolsky DK. Enhanced colonic nitric oxide generation and nitric oxide synthase activity in ulcerative colitis and Crohn's disease. Gut. 1995;36(5):718-23.

98.Middleton SJ, Shorthouse M, Hunter JO. Increased nitric oxide synthesis in ulcerative colitis. Lancet. 1993;341(8843):465-6.

99.de Araujo A, de Lartigue G. Non-canonical cholinergic anti-inflammatory pathway in IBD. Nat Rev Gastroenterol Hepatol. 2020;17(11):651-2.

100.Boehm F, Martin M, Kesselring R, Schiechl G, Geissler EK, Schlitt HJ, et al. Deletion of Foxp3+ regulatory T cells in genetically targeted mice

supports development of intestinal inflammation. BMC Gastroenterol. 2012;12:97.

101.Veltkamp C, Anstaett M, Wahl K, Moller S, Gangl S, Bachmann O, et al. Apoptosis of regulatory T lymphocytes is increased in chronic inflammatory bowel disease and reversed by anti-TNFalpha treatment. Gut. 2011;60(10):1345-53.

102.Teratani T, Mikami Y, Nakamoto N, Suzuki T, Harada Y, Okabayashi K, et al. The liver-brain-gut neural arc maintains the Treg cell niche in the gut. Nature. 2020;585(7826):591-6.

103.Kanamori M, Nakatsukasa H, Okada M, Lu Q, Yoshimura A. Induced Regulatory T Cells: Their Development, Stability, and Applications. Trends Immunol. 2016;37(11):803-11.

104.Ocampo SM, Romero C, Avino A, Burgueno J, Gassull MA, Bermudez J, et al. Functionally enhanced siRNA targeting TNFalpha attenuates DSS-induced colitis and TLR-mediated immunostimulation in mice. Mol Ther. 2012;20(2):382-90.

105.Planell N, Lozano JJ, Mora-Buch R, Masamunt MC, Jimeno M, Ordas I, et al. Transcriptional analysis of the intestinal mucosa of patients with ulcerative colitis in remission reveals lasting epithelial cell alterations. Gut. 2013;62(7):967-76.

106.Wirtz S, Popp V, Kindermann M, Gerlach K, Weigmann B, Fichtner-Feigl S, et al. Chemically induced mouse models of acute and chronic intestinal inflammation. Nat Protoc. 2017;12(7):1295-309.

107.Zhao H, Yan R, Zhou X, Ji F, Zhang B. Hydrogen sulfide improves colonic barrier integrity in DSS-induced inflammation in Caco-2 cells and mice. Int Immunopharmacol. 2016;39:121-7.

108.Perse M, Cerar A. Dextran sodium sulphate colitis mouse model: traps and tricks. J Biomed Biotechnol. 2012;2012:718617.

109.Huang CW, Moore PK. H2S Synthesizing Enzymes: Biochemistry and Molecular Aspects. Handb Exp Pharmacol. 2015;230:3-25.

110.Mirandola P, Gobbi G, Sponzilli I, Pambianco M, Malinverno C, Cacchioli A, et al. Exogenous hydrogen sulfide induces functional inhibition and cell death of cytotoxic lymphocytes subsets. J Cell Physiol. 2007;213(3):826-33.

111.Polhemus DJ, Li Z, Pattillo CB, Gojon G, Sr., Gojon G, Jr., Giordano T, et al. A novel hydrogen sulfide prodrug, SG1002, promotes hydrogen sulfide and nitric oxide bioavailability in heart failure patients. Cardiovasc Ther. 2015;33(4):216-26.

112.Van Dingenen J, Pieters L, Vral A, Lefebvre RA. The H(2)S-Releasing Naproxen Derivative ATB-346 and the Slow-Release H(2)S Donor GYY4137 Reduce Intestinal Inflammation and Restore Transit in Postoperative Ileus. Front Pharmacol. 2019;10:116.

국문 초록

대장염의 치료적 면역조절을 위한 비장 표적 황화수소 공여 리포좀의 개발

오치우
서울대학교
융합과학기술대학원
응용바이오공학과

나노입자는 전신투여 후 대부분 면역 세포에 의해 섭취되기 때문에 면역조절제로서 이상적인 약물 전달체로 여겨지고 있다. 최근 가장 큰 림프 기관인 비장을 표적한 전신 면역조절 약제 개발에 많은 연구가 진행되고 있다. 특히 자가면역 질환과 종양의 면역조절에 효과적인 비장 표적 나노 입자가 활발히 연구되고 있다. 자가면역 질환 중 염증성 장 질환은 위장관의 만성 염증을 보이며 많은 치료 방법이 개발되고 있음에도 불구하고 난치병으로 분류된다. 최근 항염증 기능을 가지는 기체신호전달물질인 황화수소는 염증성 장 질환을 포함한 다양한 염증성 질환에서 뛰어난 면역조절 효과가 입증되어 주목받고 있다. 이 학위 연구에서는 정밀하게 설계된 황화수소 공여체 담지 비장 표적

리포좀 (H_2S donor delivering liposome for spleen targeting; ST-H_2S lipo)을 개발했으며 대장염 모델에서 면역 조절 및 치료 효과를 연구했다. 본 연구에서는 뛰어난 비장 표적을 가지면서 높은 안정성과 담지 효율을 가지는 리포좀의 폴리에틸렌글라이콜 종류와 비율을 확인했다. 덱스트란 설페이트 소듐으로 유도된 대장염 모델에서 담지하지 않은 황화수소 공여체와 달리 ST-H_2S lipo와 기존의 높은 전신 순환 기능을 가지는 리포좀에 담지된 황화수소 공여체 (long-circulating liposome with H_2S donor; LC-H_2S lipo) 모두 염증 증상을 효과적으로 완화시켰다. 더욱이 ST-H_2S lipo는 LC-H_2S lipo 보다 뛰어난 전신 면역조절 효과로 우수한 치료 효과를 보였다. 이 학위 연구는 처음으로 황화수소 공여체 담지 비장 표적 리포좀을 개발하였고 이를 이용한 난치성 염증성 장 질환의 새로운 치료 전략 가능성을 보여주었다.

주요어 : 나노입자, 비장 표적, 황화수소, 염증성 장질환, 항염증, 전신 면역 조절

학번 : 2018-21910